CHEMICAL REVIEWS

REVIEW

pubs.acs.org/CR

Ferroelectric Metal−Organic Frameworks

Wen Zhang* and Ren-Gen Xiong*

Ordered Matter Science Research Center, Southeast University, Nanjing 211189, P. R. China.

CONTENTS

1. INTRODUCTION

1.1. Concepts and History

Ferroelectric compounds are a type of special dielectrics and a subgroup of pyroelectrics and piezoelectrics. They distinguish themselves from others by spontaneous electric polarization whose direction can be reversed by electric field. All ferroelectrics simultaneously show pyroelectricity, piezoelectricity, and second harmonic generation (SHG) properties.[1−4] According to the definition, ferroelectric compounds must adopt space groups belonging to the 10 polar point groups, C_1, C_s, C_2, C_{2v}, C_3, C_{3v}, C_4, C_{4v}, C_6, and C_{6v} (Figure 1). It means only crystalline compounds can give rise to ferroelectricity.

Rochelle salt ($[KNaC_4H_4O_6]\cdot 4H_2O$, potassium sodium tartrate tetrahydrate) is the first compound in the history of ferroelectrics. Its ferroelectricity as an analogy to ferromagnetism was revealed by Valasek in 1920.[5] However, instability, structural complexity, and unique ferroelectricity of Rochelle salt caused difficulties in studies in the early period of ferroelectrics. Fifteen years later, Busch and Scherrer discovered KH_2PO_4 and related compounds as hydrogen-bonded ferroelectrics.[6] Very soon, the first non-hydrogen-bonded ferroelectric $BaTiO_3$ belonging to the perovskite family appeared on the scene in the early 1940s, indicating the spring of the ferroelectrics had come.[7] With the discovery of other oxide compounds, such as lead zirconate titanate ($Pb(Zr,Ti)O_3$) and $LiNbO_3$, a significant progress in applications was made possible. In the period of 1940−1960, the number of known ferroelectric compounds was greatly increased due to contributions from several research groups. Up to now, there are more than 300 pure ferroelectrics and many mixed systems (Figure 2).[8,9] According to chemical compositions and crystal structures, the ferroelectrics cover a wide range of compounds such as inorganic oxides, organic−inorganic hybrids, organic compounds, liquid crystals, and polymers.

A variety of technical applications of ferroelectric materials has been extensively explored because of their excellence in aspects of dielectricity, SHG, piezoelectricity, pyroelectricity, and

Special Issue: 2012 Metal-Organic Frameworks

Received: May 16, 2011
Published: September 23, 2011

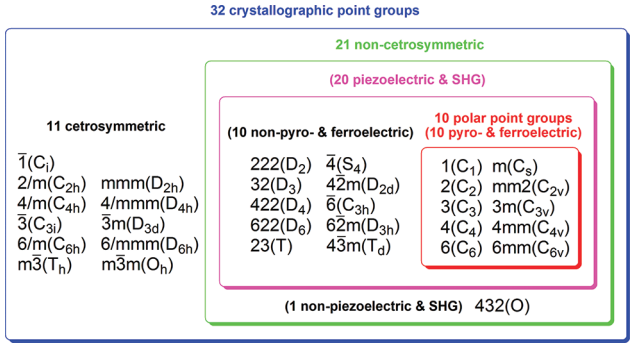

Figure 1. Relationship among ferroelectricity, pyroelectricity, piezoelectricity, and SHG based on symmetry considerations.

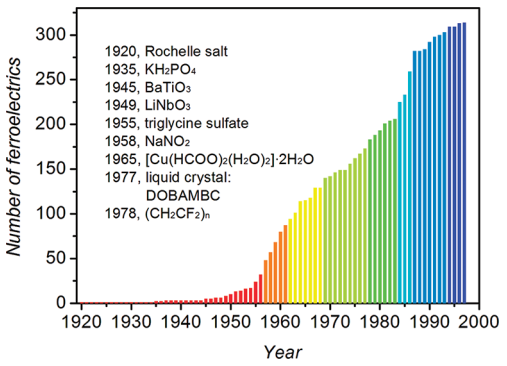

Figure 2. Accumulated number of ferroelectrics during the period 1920−1997 (data from refs 8 and 9). Only pure oxide compounds and each group of homologues for liquid crystals and polymers are taken into account.

ferroelectricity.[10−13] They can be used as ferroelectric random access memories, ferroelectric field-effect transistors, infrared detectors, piezoelectric sensors, nonlinear optical devices, fast displays in electronic equipment, capacitors, and so on.

With the discoveries of ferroelectric systems and broadened applications, ferroelectric theories have been also developed simultaneously in different aspects, i.e., thermodynamic approach such as Landau−Devonshire theory and microscopic theories such as soft-mode theory, pseudospin wave theory, vibronic theory, and first-principles calculations. For detailed information, readers can go to several books and reviews.[14−18]

1.2. Characterization

Properties of ferroelectric compounds are directly linked to the emergence and motions of electric polarization in the structures. The former corresponds to paraelectric−ferroelectric phase transition. It is a structural phase transition. At the vicinity of the transition temperature (T_c), various physical properties exhibit anomalies. The latter are usually recorded as electric hysteresis loops and visualized as electric domain patterns, being direct proofs of ferroelectricity.

1.2.1. Phase Transition and Anomalous Physical Properties. Phase transition is defined as the transformation of a thermodynamic system from one phase of matter to another. In ferroelectric compounds, the characteristic transition is paraelectric−ferroelectric phase transition. This transition usually leads to strong

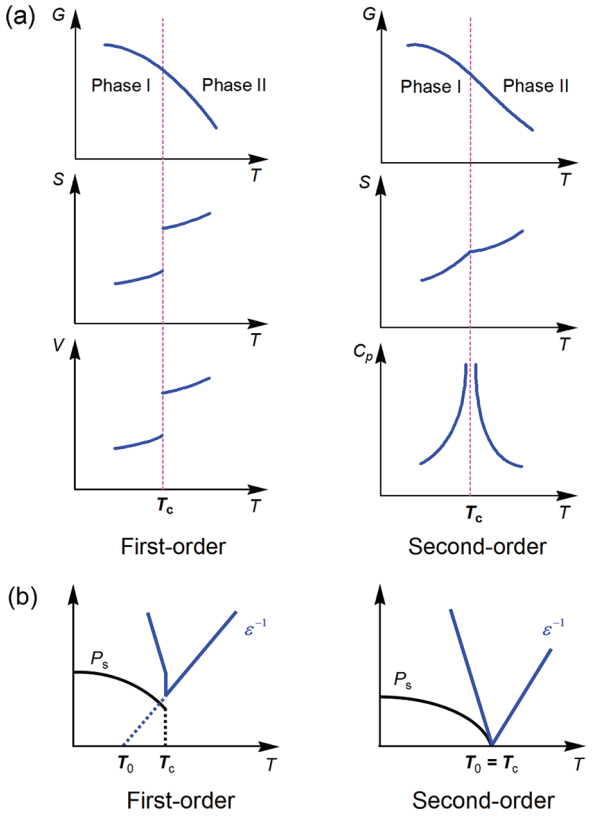

Figure 3. Schematic illustrations for the characteristic temperature dependences of (a) physical properties and (b) dielectric constant and polarization of first- and second-order phase transitions.

anomalies in dielectric, elastic, thermal, and other properties, accompanied with changes in crystal structures.[3,19,20] At the same time, the transition can be affected by pressure, electric field, shock wave, laser, and so on.[21,22] There are several classifications of the phase transitions according to different criteria.

On the basis of the behavior of Gibbs free energy (G) as a function of other thermodynamic variables such as temperature (T) and pressure, phase transitions can be classified as first-order transition and second-order transition (and even higher-order transition). The first-order phase transition is discontinuous in the first derivative of the free energy while the second-order one is continuous in the first derivative such as entropy (S) or volume (V) but discontinuous in a second derivative of the free energy such as specific heat (C_p) (Figure 3a).

For true ferroelectricity, collective alignment of intrinsic dipole moments inside a crystalline compound gives rise to spontaneous polarization (P_s). The occurrence of the polar state leads to a structural transition from a high-temperature, high-symmetry paraelectric phase to a low-temperature, low-symmetry ferroelectric phase. Some symmetry elements of the high-temperature phase are lost below the T_c upon cooling, which is called symmetry breaking. When it happens, one needs to introduce order parameter as a measure of the degree of order in the system. It is zero in one phase (usually above the T_c), and nonzero in the other. For a ferroelectric system undergoing a phase transition, the order parameter is the P_s. Discontinuous change of the P_s corresponds to a first-order phase transition while continuous change of the P_s corresponds to a second-order or continuous one (Figure 3b).

dx.doi.org/10.1021/cr200174w |*Chem. Rev.* 2012, 112, 1163–1195

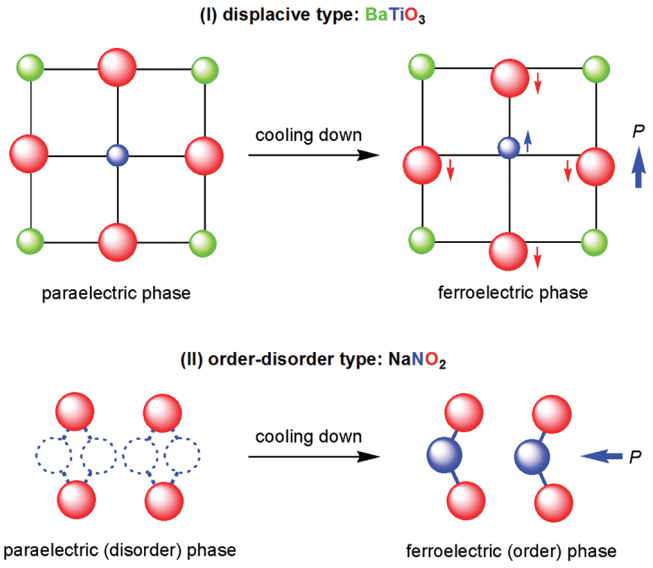

Figure 4. Schematic illustrations for the displacive-type and order–disorder-type ferroelectrics.

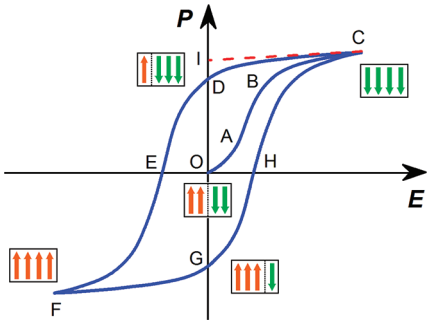

Figure 5. Electric hysteresis loop drawn as polarization vs applied electric field, i.e., P–E curve. Polarization switching is illustrated by arrows that represent polarization in electric domains.

Another classification of the ferroelectric phase transitions is based on the nature of phase change occurring at the T_c, including (I) displacive type and (II) order–disorder type (Figure 4). Many inorganic oxides such as $BaTiO_3$ belong to type I, in which relative displacement of the ions creates spontaneous polarization. $NaNO_2$ is a typical ferroelectric of type II, in which reorientation of the dipolar NO_2^- ions generates ferroelectricity. In fact, the two types are not mutually exclusive. Actual ferroelectric crystals often show both displacive and order–disorder characteristics.

Degree of order in ferroelectric phase transition, together with other detailed information of a ferroelectric, can be determined by various characterization methods such as thermal analysis, dielectric constant measurement, structural determination, and spectroscopic measurements.

Differential scanning calorimetry (DSC) and C_p afford useful information of the degree of order of phase transition. For example, in a DSC curve, a first-order transition shows a peak at the T_c while a second-order one corresponds to a step. In some specific cases undergoing order–disorder-type phase transitions, an estimation of the number of the molecular orientations in the paraelectric phase corresponding to the ordered one in

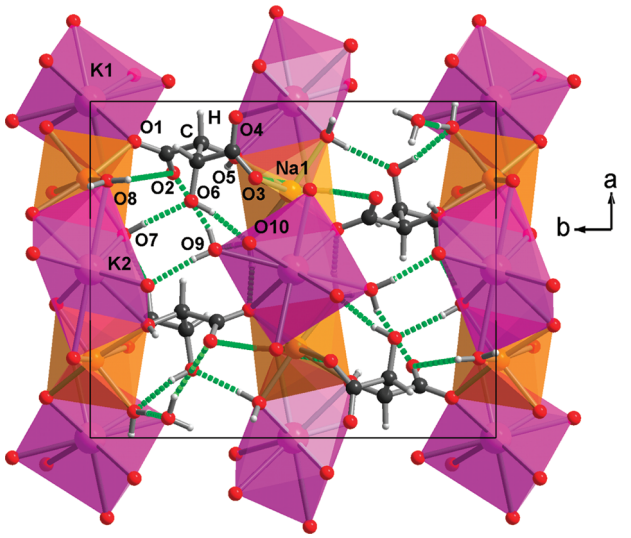

Figure 6. View of the unit cell of Rochelle salt in the paraelectric phase. Green dotted lines represent hydrogen bonds.

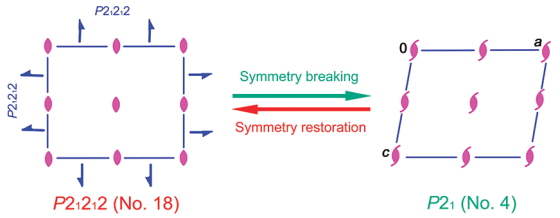

Figure 7. Transformation of the space group of Rochelle salt from paraelectric phase to ferroelectric phase with a change of symmetry elements from 4 (E, C_2, $2C'_2$) to 2 (E, C_2).

the ferroelectric phase from the calorimetric data is made from the Boltzmann equation, $\Delta S = nR\ln(N)$, where ΔS is the entropy change extracted from the C_p data, n is the number of guest molecules per mole, R is the gas constant, and N is the number of possible orientations for the disordered system.

In the vicinity of the T_c, the temperature dependence of the dielectric constant generally shows a noticeable anomaly. Peak values of the dielectric constant vary from tens to even 10^6. It is an effective indicator of the occurrence of phase transition. According to the Curie–Weiss law, $\varepsilon = C/(T - T_0)$ where ε is the dielectric constant, C is the Curie constant, T is the temperature, and T_0 is the Curie–Weiss temperature; the C in both paraelectric and ferroelectric phases (C_{para} and C_{ferro}) can be fitted to give a ratio of C_{para}/C_{ferro} (Figure 3b). If the ratio is close to 8, the phase transition is most probably of first order with $T_0 < T_c$, whereas if the ratio is close to 2, the phase transition is most probably of second order with $T_0 = T_c$. It is notable that, at optical frequencies, refractive index (n) instead of the dielectric constant shows anomalies around the T_c because $n^2 \approx \varepsilon$.

According to the value of C, there are three types of ferroelectric compounds. Type I ferroelectrics show values of $C \approx 10^5$ K, most of them undergoing displacive-type transitions. Type II ferroelectrics have $C \approx 10^3$ K, belonging to order–disorder-type phase transitions. Type III ferroelectrics have $C \approx 10$ K. They are also called improper or extrinsic ferroelectrics in which the ferroelectric phase is caused by some physical quantities instead of the polarization.

dx.doi.org/10.1021/cr200174w |Chem. Rev. 2012, 112, 1163–1195

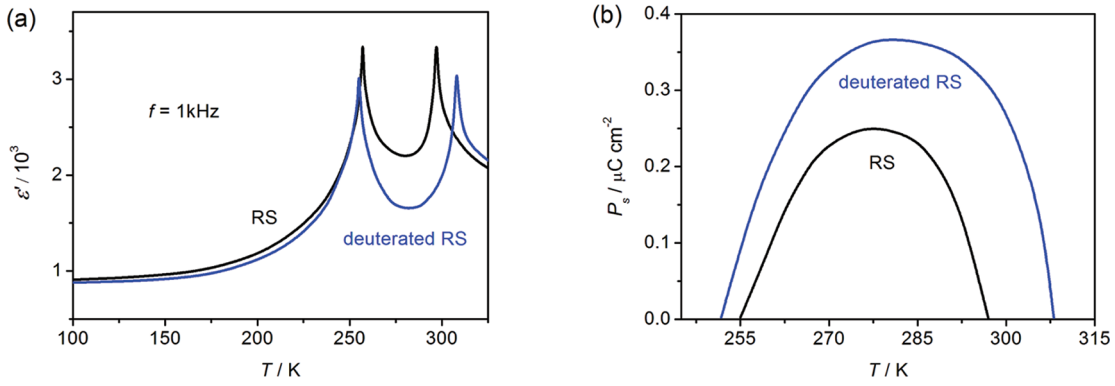

Figure 8. (a) Temperature dependence of dielectric constant, and (b) P_s versus T curve of Rochelle salt.

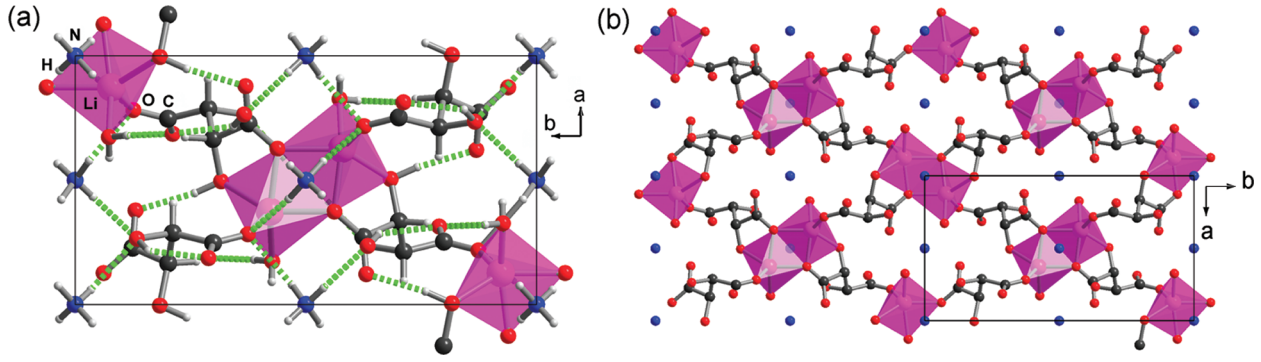

Figure 9. Structures of $[(NH_4)Li(C_4H_4O_6)]\cdot H_2O$ in the paraelectric phase (293 K): (a) unit cell along the *c* axis and (b) layer structure in the *ab* plane. Green dotted lines represent hydrogen bonds.

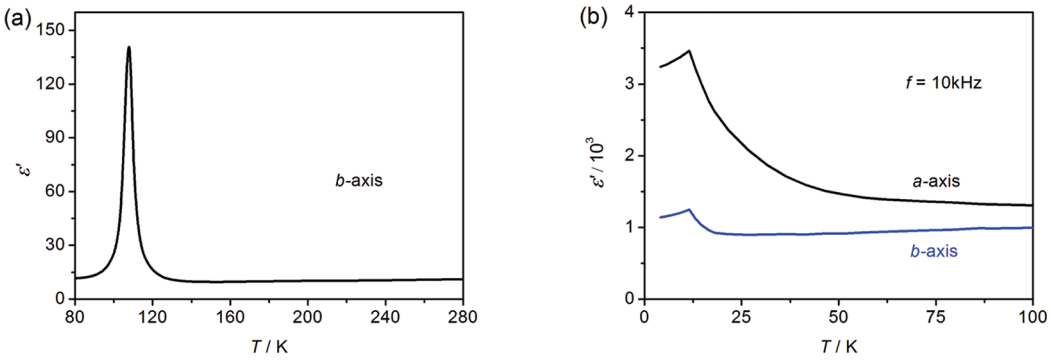

Figure 10. Temperature dependence of dielectric constant of (a) $[(NH_4)Li(C_4H_4O_6)]\cdot H_2O$ and (b) $[LiTl(C_4H_4O_6)]\cdot H_2O$.

Because the paraelectric−ferroelectric phase transition is a structural phase transition, a detailed structure analysis is indispensable for understanding of the origin of ferroelectricity, which may be the displacement of ions or the order−disorder transitions of electrically active groups in the crystal lattice. As mentioned above, a symmetry breaking occurs below the T_c of a ferroelectric phase transition. In the paraelectric phase, the crystal can adopt any of 32 point groups, whereas in the ferroelectric phase, the crystal should belong to one of 10 polar point groups that include 68 polar space groups (Figure 1). According to the Curie symmetry principle, the space group of the ferroelectric phase should be a subgroup of the paraelectric one, although there are exceptional examples. Structural determinations, especially variable-temperature single-crystal X-ray diffraction and neutron diffraction, act as direct methods to show these structural symmetry changes to reveal microscopic mechanisms of polarization.

However, structural analysis of the paraelectric and ferroelectric phases of a crystal compound is often difficult because small displacements of the ions are highly correlated with each other and with thermal parameters, which can result in inaccurate refined values and multiple solutions. As an aid, SHG technique is a useful tool to probe the occurrence of ferroelectricity. Response of SHG is very sensitive to the occurrence of symmetry breaking and time-resolved symmetry breaking. Changes of SHG signal can be found in the vicinity of the transition point when undergoing a

dx.doi.org/10.1021/cr200174w |*Chem. Rev.* 2012, 112, 1163–1195

transition from the centrosymmetric paraelectric phase to the noncentrosymmetric ferroelectric one. The temperature-dependent SHG curve is similar to that of the P_s according to the Landau theory.[14]

Deeper insight of the ferroelectric phase transition can be further explored by various spectroscopic techniques. Infrared spectroscopy and Raman and neutron scattering experiments have provided detailed information on soft modes and lattice-vibrational properties of ferroelectric crystals. Solid-state NMR techniques are particularly suitable in evaluation of dynamic processes in ferroelectric compounds. Quantitative analysis of line shape and relaxation experiments provides a detailed insight into the motional and structural characteristics on a molecular level in the vicinity of the phase transitions, which affords rich information about the individual ionic contributions to ferroelectricity. Meanwhile, local dynamics and characteristics of the electron-density distribution of a particular sort of atoms in solid matrix can be probed by electron spin resonance (ESR) and Mössbauer spectroscopies especially in the cases of phase transitions.[23,24]

1.2.2. Polarization and Electric Domain. In ferroelectric phase, electric displacement or polarization versus electric field ($P-E$) measurements afford electric hysteresis loops (Figure 5). As a direct sign of ferroelectricity, it is actually a macroscopic reflection of the motions of electric domains or polarization switching below the dielectric breakdown field of the ferroelectrics. Electric domains are the regions of a crystal where the spontaneous polarization is uniformly oriented. From the hysteresis loop, one can extract some characteristic parameters to describe the ferroelectricity, such as P_s (OI), remanent polarization (P_r, OD or OG), and coercive field (E_c, OE or OH). The E_c is often defined as a minimum field that is required to switch the full P_r. Ferroelectric switching is an activated process that depends both on temperature and applied field strength.

From a microscopic point of view, a ferroelectric crystal initially consists of an equal number of positive and negative electric domains in which the P_s points in the same direction, so there is no net polarization in the whole crystal. At low field applied in the positive direction, a linear relationship between the P and E is shown (OA) and the crystal behaves like a normal dielectric. It is because the electric field applied is not large enough and cannot affect the ferroelectric polarization, corresponding to the process that none of the domains is switched. When the field strength is close to the E_c, a number of the negative domains are switched over in the positive direction and the polarization increases rapidly (AB). At high fields all the domains are aligned in the positive direction as a single domain, meaning a saturation state is reached (BC). When the field strength is reversed to zero, the polarization follows the path CD because some of the domains remain aligned in the positive direction. The intersection of the polarization curve with the y-axis gives the P_r (OD). The polarization is annihilated to zero when the E_c (OE) is applied in the negative direction. Further increase of the field in the negative direction and following reversal completes a loop (CDEFGHC). This electric hysteresis loop is a typical characteristic of ferroelectric crystals. The bistability feature is very similar to ferromagnetic compounds, which also exhibit a similar hysteresis loop depicted as a magnetization versus magnetic field curve. It is the reason that the term "ferroelectric" is coined from "ferromagnetic".

The $P-E$ loop, in fact, also includes relatively small contributions from dielectric displacement and electric conductivity. When the contribution of the electric conductivity becomes

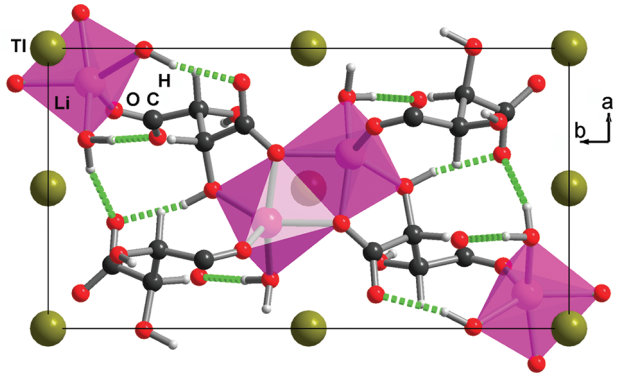

Figure 11. View of the unit cell content of $[LiTl(C_4H_4O_6)]\cdot H_2O$ in the paraelectric phase (293 K). Green dotted lines represent hydrogen bonds.

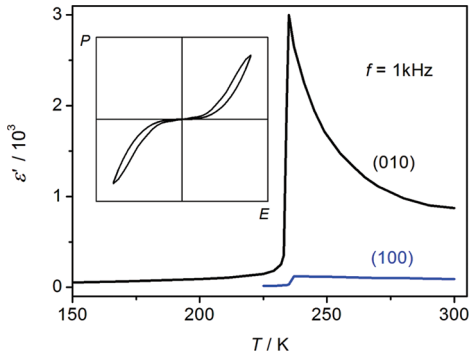

Figure 13. Temperature dependence of dielectric constant of $[Cu(HCOO)_2(H_2O)_2]\cdot 2H_2O$. Inset: Double hysteresis loop at 232 K.

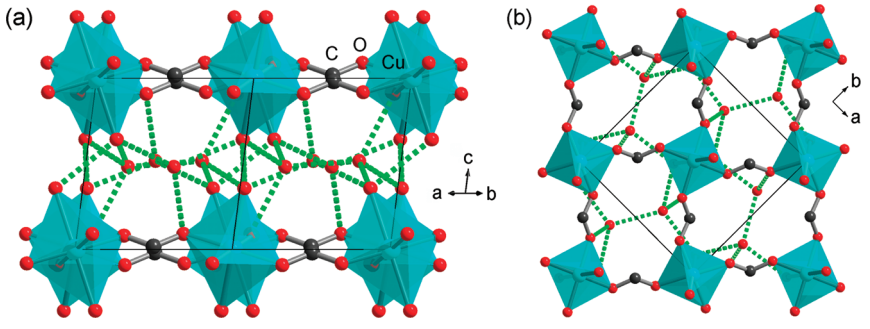

Figure 12. Views of the crystal structure of $[Cu(HCOO)_2(H_2O)_2]\cdot 2H_2O$ at 293 K. Green dotted lines represent hydrogen bonds.

dx.doi.org/10.1021/cr200174w |*Chem. Rev.* 2012, 112, 1163–1195

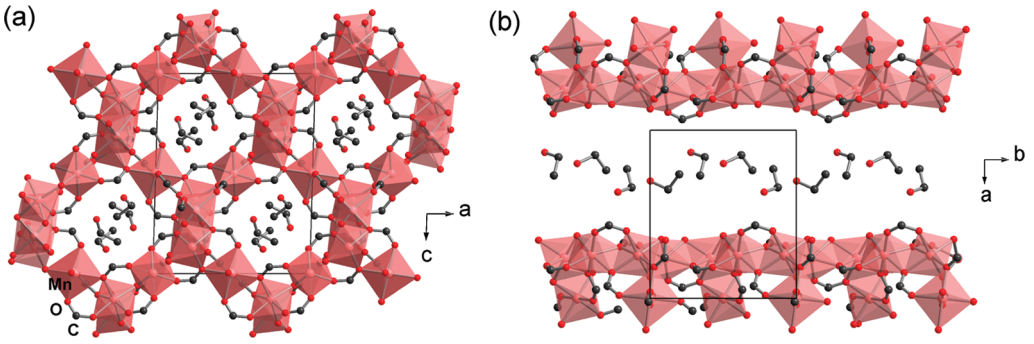

Figure 14. (a) Crystal structure of $[Mn_3(HCOO)_6]\cdot C_2H_5OH$, and (b) schematic illustration of the arrangement of ethanol molecules in the channel along the *b* axis at 190 K.

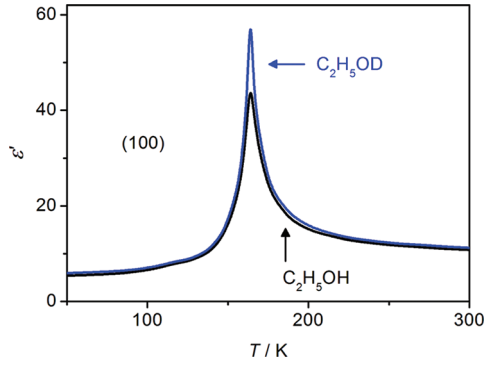

Figure 15. Dielectric constants of $[Mn_3(HCOO)_6]\cdot C_2H_5OH$ and $[Mn_3(HCOO)_6]\cdot C_2H_5OD$ measured along the *a* axis.

evident, a rounded loop appears. It is not unusual that apparent hysteresis curves are partially or not at all related to ferroelectricity. In these cases, the loops cannot be used to estimate the E_c and P_r. Solid evidence of ferroelectricity must be provided by other independent methods, such as piezoelectric, pyroelectric, or temperature-dependent SHG measurement.

Because the most important characteristic of ferroelectric compounds is polarization switching or reversal by an electric field, knowledge of the electric domain structures is essential for a better understanding of ferroelectricity. The polarization switching generally involves the growth of existing antiparallel domains, domain-wall motion, and nucleation and growth of new antiparallel domains (Figure 5). As a direct proof of the existence of ferroelectricity, domain patterns can be visualized by imaging techniques that are classified into surface modification methods, optical methods, scanning microscopy methods, and scanning probe microscopy methods.[25] Progress in visualization and manipulation of domain patterns is crucial for a wide range of applications of the controlled, nanosized structuring of ferroelectric domains.

1.3. Coverage

In this review, we would like to focus on ferroelectric metal−organic frameworks (MOFs). Ferroelectric MOFs fill the gap between pure inorganic and organic ferroelectrics. As hybrid systems, they benefit from structural variability and tunability of the assemblies constructed from both inorganic and organic building blocks such as metal ions, ligands, templates, and solvents. Meanwhile, they are usually synthesized by simple methods at relatively low temperatures. These advantages could help break through one of the bottlenecks of the fundamental study of ferroelectrics, that is, serendipitous synthesis and limited number of ferroelectrics.

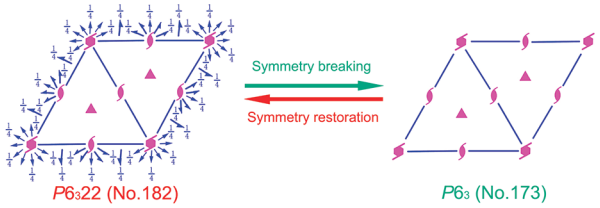

Figure 16. Transformation of the space group of $(NH_4)[Zn(HCOO)_3]$ from paraelectric phase to ferroelectric phase with a change of symmetry elements from 12 (E, $2C_6$, $2C_3$, C_2, $3C'_2$, $3C''_2$) to 6 (E, $2C_6$, $2C_3$, C_2).

The MOFs discussed here cover a wide range of compounds, including conventional MOFs in which the metal ions or clusters are coordinately bridged by different organic linkers to form one-, two-, or three-dimensional (1D, 2D, or 3D) structures and zero-dimensional ionic compounds in which the organic and inorganic components are linked through hydrogen bonds. The reason why we classify the hydrogen-bonded ionic compounds into MOFs is that the hydrogen bond bears features of covalent bond and van der Waals, ionic, and even cation−π interactions, which make it unique among supramolecular interactions.[26] Particularly, dynamics of proton transfer through hydrogen bonds can trigger ferroelectric phase transitions in so-called hydrogen-bond ferroelectrics.[2,27]

The ferroelectric MOFs are organized by anionic or organic parts. Emphases are put on their synthesis, structural analysis, and dielectric and ferroelectric properties. We do avoid covering various aspects of the ferroelectrics. Dielectric behaviors of the ferroelectric MOFs are restricted in the low frequency range of applied electric field (<10 MHz), and only the real part of the dielectric constant (ε') is described in detail. Relaxation properties are not discussed.

2. TARTRATE FAMILY

2.1. $[MNa(C_4H_4O_6)]\cdot 4H_2O$ (M = K, NH_4)

Potassium sodium tartrate tetrahydrate, $[KNa(C_4H_4O_6)]\cdot 4H_2O$, usually called Rochelle salt (RS), is a typical MOF constructed by hydrogen bonds. Its significance in ferroelectrics relies on its historical breakthrough of the field of ferroelectrics as the first ferroelectric.[5]

RS was synthesized from potassium hydrotartrate and sodium carbonate in aqueous solution. Crystal structure analysis reveals

dx.doi.org/10.1021/cr200174w |*Chem. Rev.* 2012, 112, 1163–1195

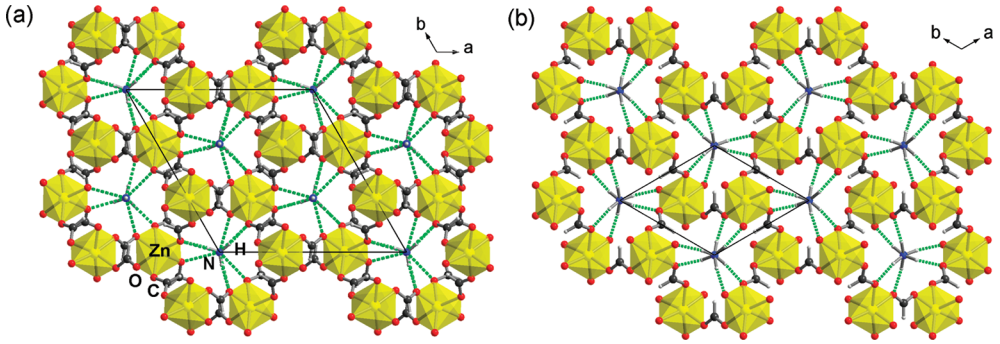

Figure 17. Crystal structures of $(NH_4)[Zn(HCOO)_3]$ at (a) 110 K showing the ordered $[NH_4]^+$ ions and (b) 290 K showing the disordered $[NH_4]^+$ ions. Green dotted lines represent hydrogen bonds.

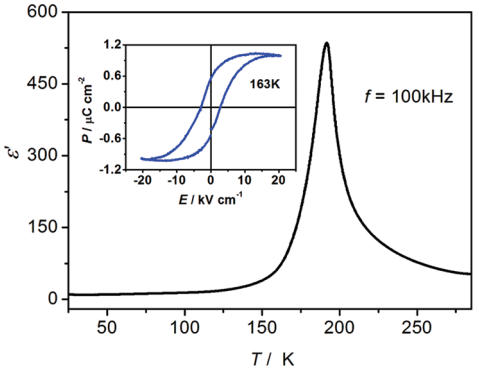

Figure 18. Temperature dependence of dielectric constant of $(NH_4)[Zn(HCOO)_3]$ along the *c* axis. Inset: Hysteresis loop at 163 K.

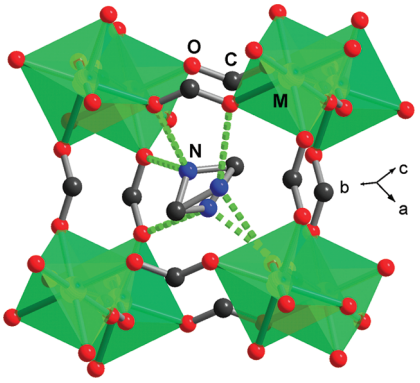

Figure 19. Cage structure of $[(CH_3)_2NH_2][M(HCOO)_3]$ at 293 K. Green dotted lines represent hydrogen bonds.

that the asymmetric unit cell includes one tartrate, four water molecules, one Na cation, and one-half of K(1) and K(2) cations (Figure 6).[28,29] The K and Na ions are surrounded by oxygen atoms of the tartrate and water molecules, adopting geometries of bicapped trigonal prism and distorted octahedron, respectively. The K(1) and Na(1) ions act as bridges between two tartrate ions, and the K(2) ion acts as a bridge between four tartrate ions. Every tartrate is surrounded by six tartrates. The tartrates are tightly connected through O(8) atom of water molecules along the *b* axis. The tartrates, O(8) atoms, and potassium ions constitute a tight sheet parallel to the *bc* plane. There are rows of tartrate ions parallel to the *a* axis, linked by rows of alternating K and Na ions along the *b* axis. The crystal structure of RS is a combination of two kinds of different chains along the *a* axis.

RS exhibits two Curie points at 255 and 297 K. Below 255 K and above 297 K, it crystallizes in the orthorhombic $P2_12_12$, corresponding to the paraelectric phase, whereas between the two temperatures it crystallizes in the monoclinic $P2_1$, corresponding to the ferroelectric phase. The two phase transitions are of second-order type. From a symmetry-breaking viewpoint, the maximal nonisomorphic subgroups of the space group $P2_12_12$ in the upper paraelectric phase are $P2_1$ and $P2$. This is just the case in the spatial symmetry breaking of RS (Figure 7).

Detailed structural analysis reveals that there are two kinds of polarized chain in the ferroelectric phase (274 K). One is similar to those in the high-temperature paraelectric phase (323 K), and the other is similar to those in the low-temperature paraelectric phase (213 K). The main difference among the ferroelectric and the two paraelectric structures is the orientation of each tartrate ion with respect to the crystallographic axes. Pepinsky and co-workers proposed an order−disorder transition of RS.[30] However, it is not justified by thermal parameters obtained in the two paraelectric phases. It is assumed by Solans and co-workers that the ferroelectricity is produced by two nonequivalent chains along the *a* axis, each with a different polarization vector parallel to the *a* axis.

The dielectric constant of RS shows two anomalies at 255 and 297 K (Figure 8a). Above the upper Curie point (297 K), the T_0 is 297 K and the C_{para} is 2.24×10^3 K by fitting the Curie−Weiss law. The P_s is 0.25 $\mu C \cdot cm^{-2}$ at 278 K (Figure 8b). For deuterated RS, $[NaK(C_4H_2D_2O_6)] \cdot 4D_2O$, the two Curie points are 251 and 308 K and the P_s is 0.35 $\mu C \cdot cm^{-2}$ at 278 K. Little difference between the deuterated and nondeuterated RS suggests an order−disorder nature of the ferroelectric phase transitions.

$[(NH_4)Na(C_4H_4O_6)] \cdot 4H_2O$ is an analogue compound to RS. Its dielectric anomaly was observed by Jona and Pepinsky in 1953.[31] It crystallizes in orthorhombic $P2_12_12$ above 109 K and monoclinic $P2_1$ below 109 K.

2.2. $[MLi(C_4H_4O_6)] \cdot H_2O$ Family (M = NH_4, Tl, K)

$[MLi(C_4H_4O_6)] \cdot H_2O$ (M = NH_4, Tl, K) constitutes a family related to RS. Ferroelectricity of ammonium lithium tartrate monohydrate, $[(NH_4)Li(C_4H_4O_6)] \cdot H_2O$, was discovered by Matthias and Hulm and independently by Merz in 1951.[32,33] It undergoes a second-order ferroelectric phase transition from the paraelectric orthorhombic phase ($P2_12_12$) to the ferroelectric monoclinic phase ($P2_1$) at T_c = 106 K.[34]

dx.doi.org/10.1021/cr200174w |*Chem. Rev.* 2012, 112, 1163–1195

In the crystal structure at 293 K, each lithium center is five-coordinated by one water molecule and three carboxyl and one hydroxyl oxygens from the tartrate ligand (Figure 9a). Two of these carboxyl oxygen atoms are related by a 2-fold rotation axis and bridge adjacent lithium centers to form a Li_2O_2 ring. The structure of $[(NH_4)Li(C_4H_4O_6)]\cdot H_2O$ can be described as a packing of 2D $[Li(C_4H_4O_6)(H_2O)]_n$ layers propagating in the *ab* plane (Figure 9b). The isolated NH_4^+ ions reside in the voids formed by the planes, which are connected to each other by hydrogen bonds between the NH_4^+ ions and the oxygen atoms of the tartrate ligands.

The dielectric constant of $[(NH_4)Li(C_4H_4O_6)]\cdot H_2O$ shows an anomaly at 106 K with a peak value of 140 (Figure 10a). Fitting the Curie–Weiss law gives a T_0 of 93.8 K and a C_{para} of 37 K. In the ferroelectric phase, the P_s appears parallel to the *b* axis. Abe and Matsuda suggested that the ferroelectricity came from motions of the hydroxyl groups of the tartrate, similar to the situation in RS.[35,36] An ESR experiment on $[(NH_4)Li(C_4H_4O_6)]\cdot H_2O$ found that the P_s can be reversed by both electric field and shear stress, indicating the coexistence of both ferroelectricity and ferroelasticity below the T_c.[37,38]

$[LiTl(C_4H_4O_6)]\cdot H_2O$ undergoes a second-order phase transition at T_c = 11 K from the paraelectric phase ($P2_12_12$) to the ferroelectric phase with an unknown symmetry.[32] The P_s of $[LiTl(C_4H_4O_6)]\cdot H_2O$ appears parallel to the *a* axis. Crystal structure of $[LiTl(C_4H_4O_6)]\cdot H_2O$ is isomorphous with $[(NH_4)Li(C_4H_4O_6)]\cdot H_2O$ in the paraelectric phase (Figure 11). Spatial symmetry breaking in $[LiTl(C_4H_4O_6)]\cdot H_2O$ is similar to that found in RS, abiding by the Curie symmetry principle.

The dielectric constant of $[LiTl(C_4H_4O_6)]\cdot H_2O$ along the *a* axis shows a large value of 5000 near the T_c, followed with only a slight decreasing tendency down to liquid helium temperature

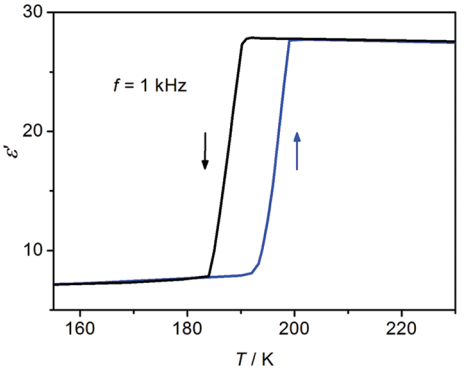

Figure 20. Temperature dependence of dielectric constant of $[(CH_3)_2NH_2][Mn(HCOO)_3]$.

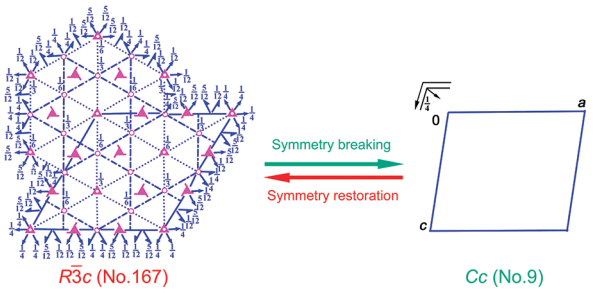

Figure 22. Transformation of the space group of $[(CH_3)_2NH_2][M(HCOO)_3]$ from paraelectric phase to ferroelectric phase with a change of symmetry elements from 12 (E, $2C_3$, $3C_2$, i, $2S_6$, $3\sigma_v$) to 2 (E, σ_h).

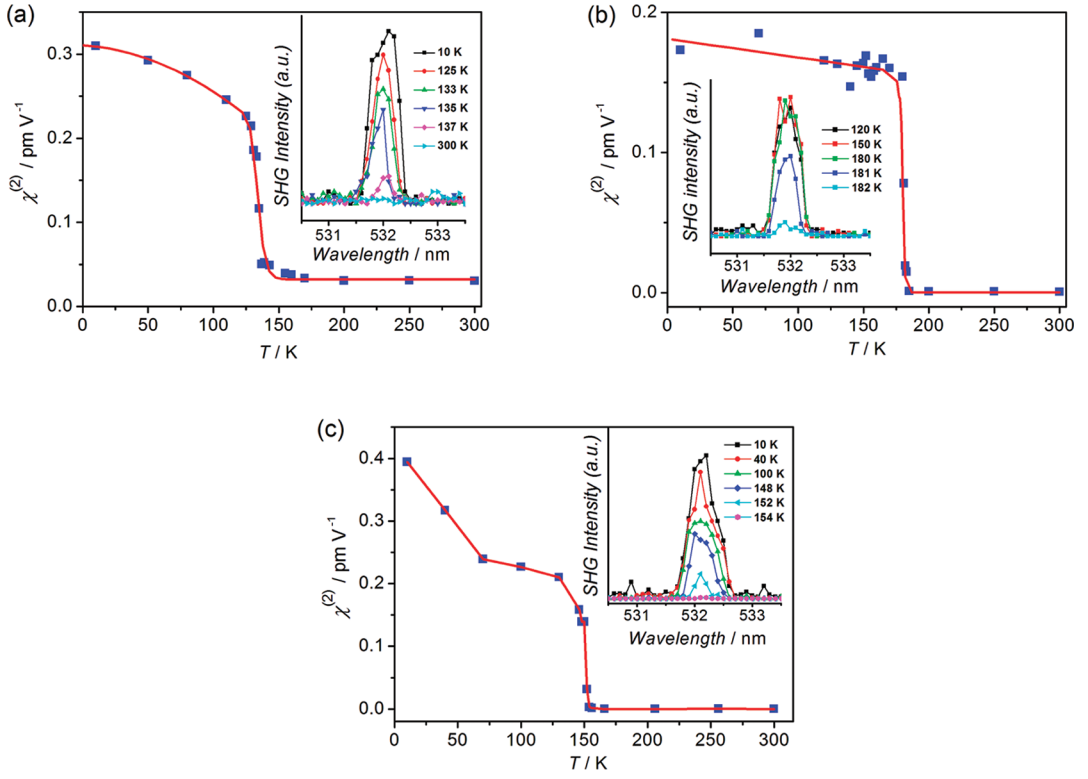

Figure 21. Temperature dependence of second-order nonlinear effective coefficient of (a) $[(CH_3)_2NH_2][Co(HCOO)_3]$, (b) $[(CH_3)_2NH_2][Mn(HCOO)_3]$, and (c) $[(CH_3)_2NH_2][Zn(HCOO)_3]$. Inset: Intensity of SHG as a function of wavelength at different temperatures.[61]

dx.doi.org/10.1021/cr200174w |*Chem. Rev.* 2012, 112, 1163–1195

(Figure 10b). It is a contrast to the behaviors of usual ferroelectrics and explained by the contribution of domain-wall motions.[39] The permittivity was found to be very sensitive to mechanical boundary conditions.[40] The clamped dielectric constant is ~30, much smaller than the free one.[41] A study of deuteration effects on the phase transition has shown that the decreasing and vanishing of the T_c with a finite C in deuterated $[LiTl(C_4H_4O_6)]\cdot H_2O$ is attributed to a displacive-type phase transition.[42]

3. FORMATE FAMILY

Metal formate compounds constitute an interesting family of MOFs exhibiting rich properties varying from magnetism and porosity to ferroelectricity.[43,44] The formate ($HCOO^-$) is an anionic ligand and shows several coordination modes: monodentate, bidentate, tridentate, and tetradentate. As the simplest carboxylate ligand, the formate has found its role in constructing coordination framework materials with interesting magnetic and porous properties due to small stereo effect and short OCO bridge.

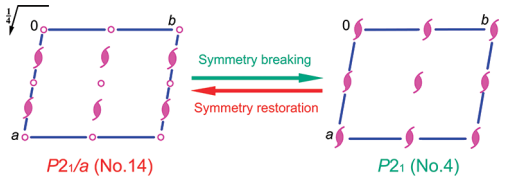

Figure 23. Transformation of the space group of $[Ag(NH_3CH_2COO)(NO_3)]$ from paraelectric phase to ferroelectric phase with a change of symmetry elements from 4 (E, C_2, i, σ_h) to 2 (E, C_2).

3.1. $[Cu(HCOO)_2(H_2O)_2]\cdot 2H_2O$

Copper(II) formate tetrahydrate, $[Cu(HCOO)_2(H_2O)_2]\cdot 2H_2O$, was reported to be antiferroelectric below the T_c = 235.5 K.[45] $[Cu(HCOO)_2(H_2O)_2]\cdot 2H_2O$ crystallizes from aqueous solution as large transparent blue crystals, but easily effloresces in the air. It adopts a space group $P2_1/a$ in the paraelectric phase and $P2_1/n$ in the antiferroelectric phase where the length of the c axis is doubled.[46,47] Such a doubling of the unit cell is characteristic for an antiferroelectric phase transition. $[Cu(HCOO)_2(H_2O)_2]\cdot 2H_2O$ exhibits a layered structure along the ab plane (Figure 12). The 2D layers of copper formate are interleaved with layers of water molecules. Each Cu(II) ion adopts an elongated octahedral geometry, coordinating with O atoms from four bridging formate ligands and two water molecules. There are hydrogen-bonding networks in the water layers, together with the coordinated water molecules to the Cu(II) ions. In the high-temperature phase, the water molecules are disordered. It is believed that the ordering of the water molecules arouses the phase transition. The ferroelectrically ordered water molecules alternate the directions of polarization from layer to layer, so the whole structure is antiferroelectric.

The temperature dependence of the dielectric constant of $[Cu(HCOO)_2(H_2O)_2]\cdot 2H_2O$ shows behaviors of a first-order transition at ~235 K (Figure 12).[48] A sharp anomaly occurs along

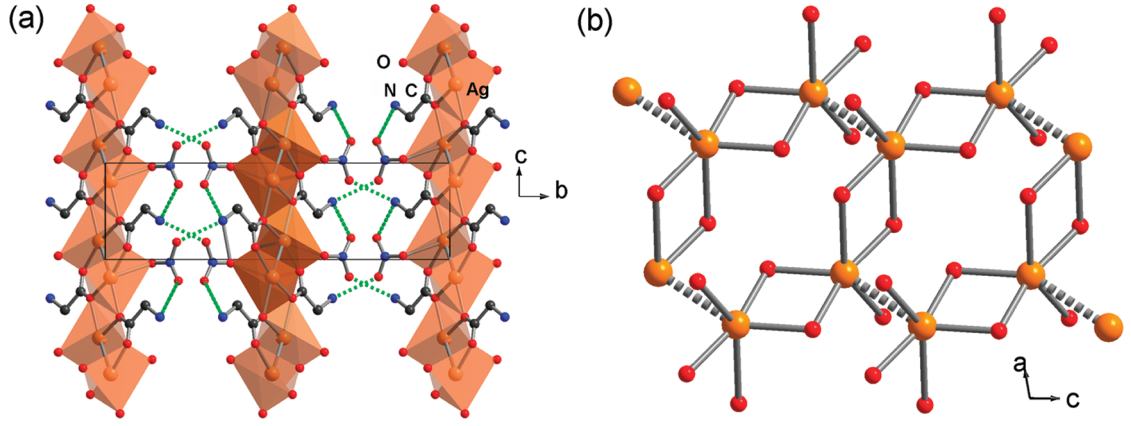

Figure 24. (a) Crystal structure of $[Ag(NH_3CH_2COO)(NO_3)]$ in the paraelectric phase. Green dotted lines represent hydrogen bonds. (b) Coordination structure of the AgO network. Gray dotted lines represent Ag−Ag bonds.

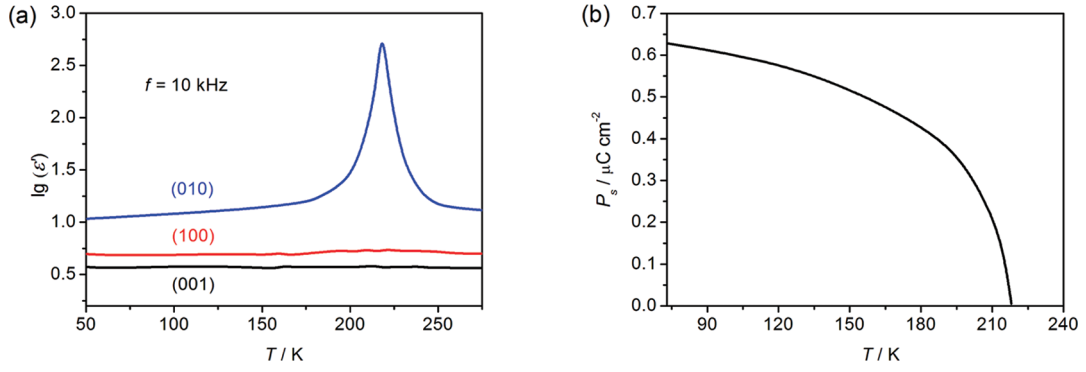

Figure 25. (a) Temperature dependence of dielectric constant, and (b) P_s versus T curve of $[Ag(NH_3CH_2COO)(NO_3)]$.

dx.doi.org/10.1021/cr200174w |Chem. Rev. 2012, 112, 1163–1195

the b axis. Fitting the Curie−Weiss law affords a T_0 of 217 K and a C_{para} of 3.2 × 10^4 K. The deuterated counterpart, $[Cu(HCOO)_2(D_2O)_2]\cdot 2D_2O$, shows a noticeable isotope effect with a shift to a higher temperature of 245 K, revealing the role of hydrogen bonds in the phase transition. A typical antiferroelectric behavior is observed at 232 K (Figure 13). It appears in a narrow range of 231−235 K. Later studies of the antiferroelectricity reveal its complexity below the Curie point. A newly found phase below 227 K is considered to be approximately ferroelectric.

Meanwhile, this compound exhibits an antiferromagnetic transition at 17 K.[49,50] Below this temperature, the magnetic and electric orderings coexist. Thus, it can be called a multiferroic MOF, though there is no direct magnetoelectric coupling.

3.2. $[Mn_3(HCOO)_6]\cdot C_2H_5OH$

A 3D MOF, $[Mn^{III}(HCOO)_3]\cdot$(guest), was reported in 1999.[51] It adopts a NaCl-type structure with guest molecules in cavities.

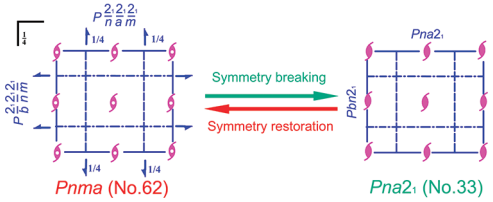

Figure 26. Transformation of the space group of $[Ca(CH_3NH_2CH_2COO)_3Cl_2]$ from paraelectric phase to ferroelectric phase with a change of symmetry elements from 8 (E, C_2, 2C'_2, i, σ_h, 2σ_v) to 4 (E, C_2, 2σ_v).

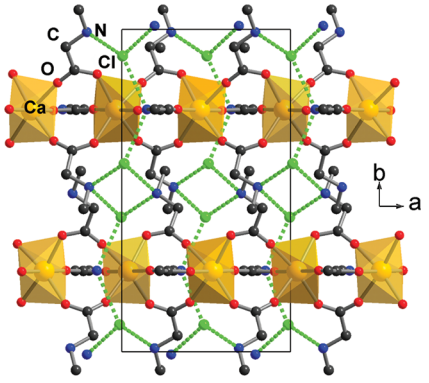

Figure 27. Crystal structure of $[Ca(CH_3NH_2CH_2COO)_3Cl_2]$ at 118 K in the ferroelectric phase. Green dotted lines represent hydrogen bonds.

This compound sheds light on various metal formate compounds as shown below.

$[Mn_3(HCOO)_6]\cdot$(guest) is a well-studied 3D porous magnet.[52] It contains a flexible diamondoid framework based on Mn-centered $MnMn_4$ tetrahedral nodes through bridging formates (Figure 14). In the structure there are porous channels containing many kinds of guests that modulate 3D long-range magnetic orderings. The magnetic properties come from the Mn^{2+} ions (S = 5/2) incorporated in the host lattice.

Guest-free crystal $[Mn_3(HCOO)_6]$ shows a very small and almost temperature-independent dielectric constant (ε' = 5) irrespective of the direction of the electric field.[53] When polar solvents are compatible with the channel, the host−guest compounds are expected to be electrically active, such as $[Mn_3(HCOO)_6]\cdot C_2H_5OH$, which exhibits a surprisingly steep increase in the dielectric constant around 165 K, indicating the possibility of collective freezing of the guest molecules within the 1D channels.[54]

$[Mn_3(HCOO)_6]\cdot C_2H_5OH$ was obtained by keeping $[Mn_3(HCOO)_6]$ crystals in ethanol vapor. It is isostructural to $[Mn_3(HCOO)_6]\cdot H_2O\cdot CH_3OH$ and crystallizes in the monoclinic $P2_1/n$ or $P2_1/c$. There are 1D channels along the b axis where the ethanol molecules reside. Variable-temperature crystal structure analyses reveal a significant change in the arrangement of the guest ethanol molecules between 90 and 190 K. Below the T_c, X-ray diffraction data collected at 90 K discloses an absence of screw (2_1) and glide (n) symmetries. However, the assumed space group $P\bar{1}$ gives almost the same structure with the space group $P2_1/n$.

The dielectric constant of $[Mn_3(HCOO)_6]\cdot C_2H_5OH$ exhibits a very sharp peak at 165 K with a value of ∼45 along the a axis while there are only small anomalies along the b and c axes (Figure 15). Fitting the Curie−Weiss law gives the T_0 of ∼150 K and the C_{para}/C_{ferro} of 4.1. It is therefore a first-order phase transition, which is also confirmed by DSC measurement.

Hysteresis loop was only recorded in a narrow temperature range of 145−166 K. The ferroelectric properties are supposed to come mainly from the guest ethanol molecules. Interaction between the host lattice and C_2H_5OH molecules plays an important role in the ferroelectric phase transition. Deuterated compound $[Mn_3(HCOO)_6]\cdot C_2H_5OD$ shows very similar dielectric behaviors with a sharp peak of 57 at 164 K (Figure 15).

As a porous magnet, $[Mn_3(HCOO)_6]\cdot C_2H_5OH$ undergoes a ferrimagnetic transition at 8.5 K, slightly higher than the ferromagnetic transition temperatures of $[Mn_3(HCOO)_6]\cdot H_2O\cdot CH_3OH$ (T_c = 8.1 K) and $[Mn_3(HCOO)_6]$ (T_c = 8.0 K).

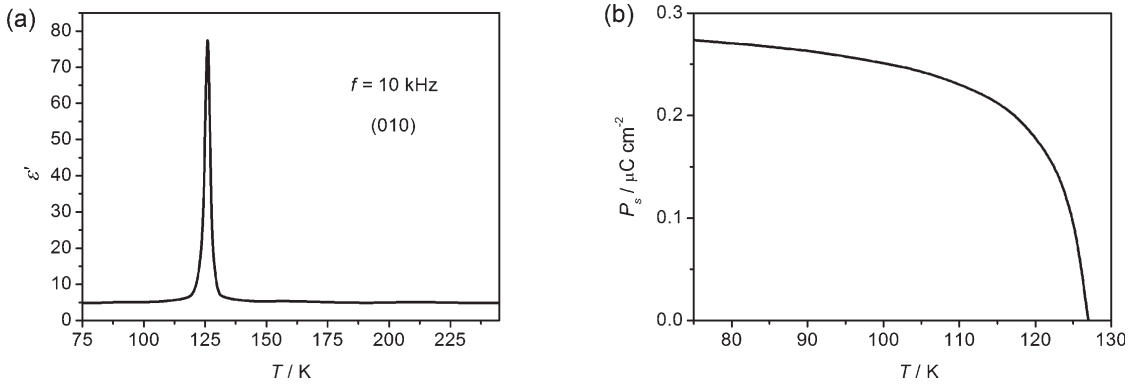

Figure 28. (a) Temperature dependence of dielectric constant, and (b) P_s versus T curve of $[Ca(CH_3NH_2CH_2COO)_3Cl_2]$.

dx.doi.org/10.1021/cr200174w |Chem. Rev. 2012, 112, 1163–1195

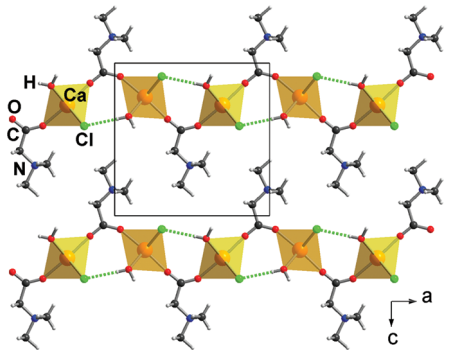

Figure 29. Crystal structure of $[Ca\{(CH_3)_3NCH_2COO\}(H_2O)_2Cl_2]$ at 293 K in the paraelectric phase. Green dotted lines represent hydrogen bonds.

3.3. $(NH_4)[Zn(HCOO)_3]$

Various MOFs based on $[M^{II}(HCOO)_3]^-$ have been successfully obtained. In this series of compounds, cationic amines exert strong template effects on topologies of the frameworks.[55,56] If the smallest ammonium NH_4^+ is employed, the corresponding $(NH_4)[M(HCOO)_3]$ shows a framework with a rarely observed $4_9 \cdot 6_6$ topology. When the cation is $CH_3NH_3^+$, $(CH_3)_2NH_2^+$, $CH_3CH_2NH_3^+$, or $(CH_3)_3NH^+$, a series of perovskite-type compounds is obtained, one of which will be discussed in the next section. If bulky amines such as $(CH_3CH_2)_3NH^+$, $(CH_3CH_2)_2NH_2^+$, or $CH_3CH_2CH_2NH_3^+$ are used, porous MOFs $[M_3(HCOO)_6] \cdot (guest)$ are evolved as mentioned above.

Recently, Wang, Gao, and co-workers reported ferroelectric properties of $(NH_4)[Zn(HCOO)_3]$.[57] The 3D MOF was synthesized from ammonium formate, formic acid, and $Zn(ClO_4)_2 \cdot 6H_2O$ in methanol. It crystallizes in the hexagonal chiral space group $P6_322$ at 290 K and the polar space group $P6_3$ at 110 K. It is in good agreement with the Curie symmetry principle that the ferroelectric space group $P6_3$ is a subgroup of the paraelectric one (minimal nonisomorphic supergroups of $P6_3$ include $P6_3/m$, $P6_322$, $P6_3cm$, and $P6_3mc$) (Figure 16). A tripling of the unit cell at 110 K is evidenced. The structure consists of octahedral metal centers connected by the anti−anti formate to form a 3D chiral anionic $[Zn(HCOO)_3]$ framework with a $4_9 \cdot 6_6$ topology (Figure 17). It can be considered to be built by interpenetration of three sets of 2D cubic nets resulting to hexagonal channels where the ammonium cation arrays locate. The chirality is derived from the handedness imposed by the formate ligands around the metals and the presence of units with only one handedness.

Origin of the ferroelectricity of $(NH_4)[Zn(HCOO)_3]$ may be explained by variable-temperature X-ray diffraction analysis. It shows that the ammonium cations take changes from a disordered state in the high-temperature phase to an ordered state in the low-temperature phase (Figure 17). The NH_4^+ ions form hydrogen bonds to the O atoms of the metal formate framework with N···O distances of 2.972 Å at 290 K and 2.830−3.120 Å at 110 K. It is notable that the NH_4^+ cations in the channels exhibit displacive shifts of about 0.40 Å along the c direction at 110 K compared to the structure at 290 K, which is thought to be closely related to the low-temperature polar structure and the ferroelectricity.

The temperature dependence of the dielectric constant of $(NH_4)[Zn(HCOO)_3]$ shows a big dielectric anomaly along the c axis at T_c = 191 K (Figure 18), indicating a phase transition.

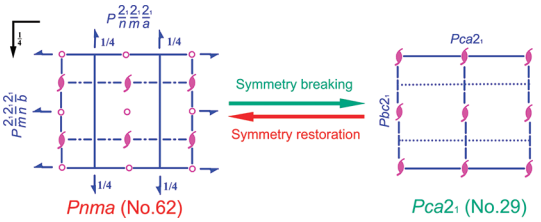

Figure 30. Transformation of the space group of $[Ca\{(CH_3)_3NCH_2COO\}(H_2O)_2Cl_2]$ from paraelectric phase to ferroelectric phase with a change of symmetry elements from 8 (E, C_2, $2C'_2$, i, σ_h, $2\sigma_v$) to 4 (E, C_2, $2\sigma_v$).

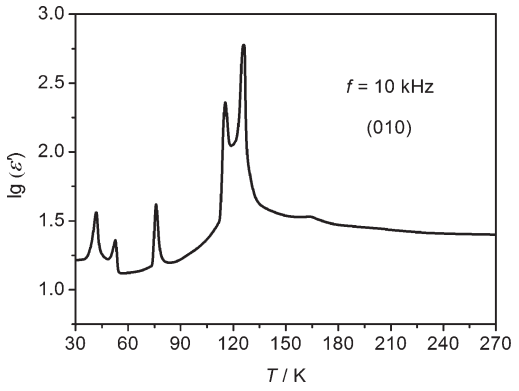

Figure 31. Temperature dependence of dielectric constant of $[Ca\{(CH_3)_3NCH_2COO\}(H_2O)_2Cl_2]$ along the b axis at 10 kHz.

The T_0 is 181 K and the C_{para} is 5.4 × 10^3 K by fitting the Curie−Weiss law, suggesting a typical order−disorder type ferroelectric phase transition. A measurable dielectric hysteresis loop has been obtained with the P_s of 1.0 $\mu C \cdot cm^{-2}$.

It is expected that similar ferroelectric properties of $(NH_4)[M(HCOO)_3]$ where M is divalent Mn, Fe, Co, or Ni will be reported soon. Magnetic properties of these compounds were reported by Wang and co-workers earlier. The Mn formate is an antiferromagnet, exhibiting a spin-flop field at very low field, whereas both the Co formate and Ni formate are weak ferromagnets, and the Co formate displays possible spin-reorientation after antiferromagnetic ordering. These compounds would constitute an attracting family of multiferroic MOFs where the ferromagnetism and ferroelectricity coexist.

3.4. $[(CH_3)_2NH_2][M(HCOO)_3]$ (M = Mn, Fe, Co, Ni, Zn)

Dielectric properties of the metal formate compounds, $[(CH_3)_2NH_2][M(HCOO)_3]$ (M = divalent Mn, Fe, Co, Ni, Zn), were reported by Cheetham and co-workers recently.[58,59] This series of MOFs exhibits perovskite-type structures. They were synthesized from metal chloride and water in dimethylformamide under solvothermal conditions. The dimethylammonium guest comes from in situ hydrolysis of the dimethylformamide.[60]

$[(CH_3)_2NH_2][M(HCOO)_3]$ crystallizes in a central space group $R\bar{3}c$ in the paraelectric phase. The M^{2+} center is octahedrally coordinated by six oxygen atoms from six formates and interconnected by formates to form a 3D framework (Figure 19). The dimethylammonium cation locates in the cage of the framework and is disordered with three different orientations. It undergoes an order−disorder change in the measured temperature range. Structures in the low-temperature phase were not well solved but undoubtedly monoclinic.

dx.doi.org/10.1021/cr200174w |Chem. Rev. 2012, 112, 1163–1195

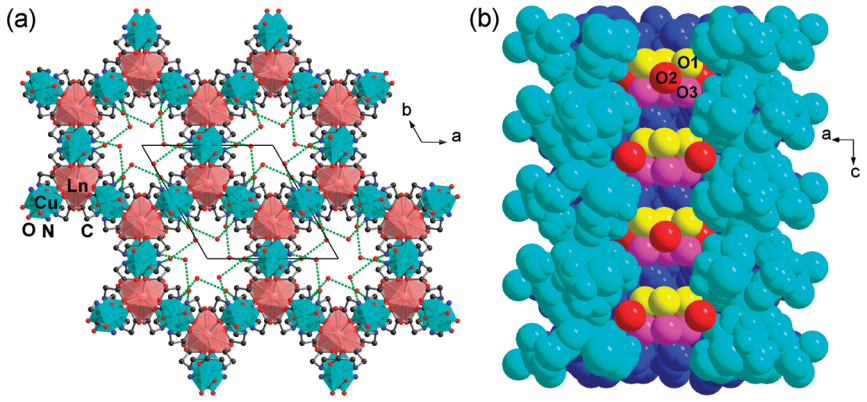

Figure 32. (a) Crystal structure of $[Ln_2Cu_3\{NH(CH_2COO)_2\}_6]\cdot 9H_2O$ at 273 K. Green dotted lines represent hydrogen bonds. (b) Guest water molecules classified into three groups in the channel along the *c* axis.

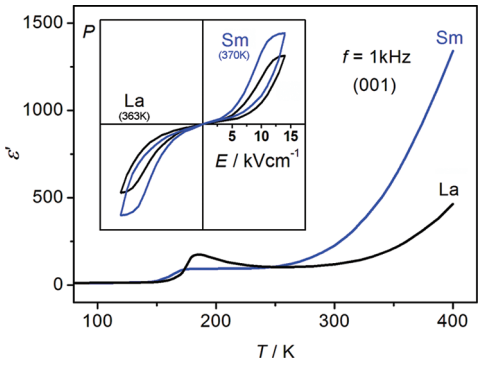

Figure 33. Temperature dependence of dielectric constants of $[Ln_2Cu_3\{NH(CH_2COO)_2\}_6]\cdot 9H_2O$. Inset: Double hysteresis loops.

Dielectric anomalies were found at 185, 160, 165, 180, and 156 K upon cooling for the Mn, Fe, Co, Ni, and Zn compounds, respectively. There is clearly a thermal hysteresis of ~10 K for these metal formates. The dielectric constant curves show steplike shapes with values > 15 in the paraelectric phases, corresponding to a category of high dielectric constant materials (Figure 20). This type of electric ordering associates with an order−disorder phase transition. Below the transition points, antiferroelectric phases were suggested but without direct proof.

In our opinion, the temperature dependence of the dielectric constant of $[(CH_3)_2NH_2][M(HCOO)_3]$ may be associated with improper ferroelectric characteristics. There is one way to testify if the space group is ferroelectric in the low-temperature phase. As mentioned in the Introduction, the temperature dependence of SHG may indicate the occurrence of a paraelectric-to-ferroelectric phase transition.[62] According to the phenomenological Landau theory, if ignoring high-order terms, we get $\chi^{(2)} = 6\varepsilon_0\beta P_s$ where $\chi^{(2)}$ is the second-order nonlinear coefficient and β is almost independent of temperature. It means that the behavior of the temperature dependence of $\chi^{(2)}$ is consistent with that of the P_s. To $[(CH_3)_2NH_2][M(HCOO)_3]$ where M is divalent Co, Mn or Zn, the SHG signal clearly shows a rapid increase to a saturation value below the T_c, indicating the occurrence of a symmetry breaking (Figure 21). These facts strongly support such an idea that below the T_c the space groups of the metal formates should be noncentrosymmetric, which is in good agreement with the case of Co formate reported by Señarís-Rodríguez and co-workers.[63] Thus, the assumed antiferroelectric phase should be a ferroelectric one. The ferroelectric space group *Cc* is a subgroup of the paraelectric one $R\bar{3}c$ (No. 167) because the maximal nonisomorphic subgroups of $R\bar{3}c$ include *R*3*c*, *R*32, $R\bar{3}1$, and *C*2/*c* whereas *Cc* is a subgroup of *C*2/*c*, together with *C*2 and $P\bar{1}$ (Figure 22).

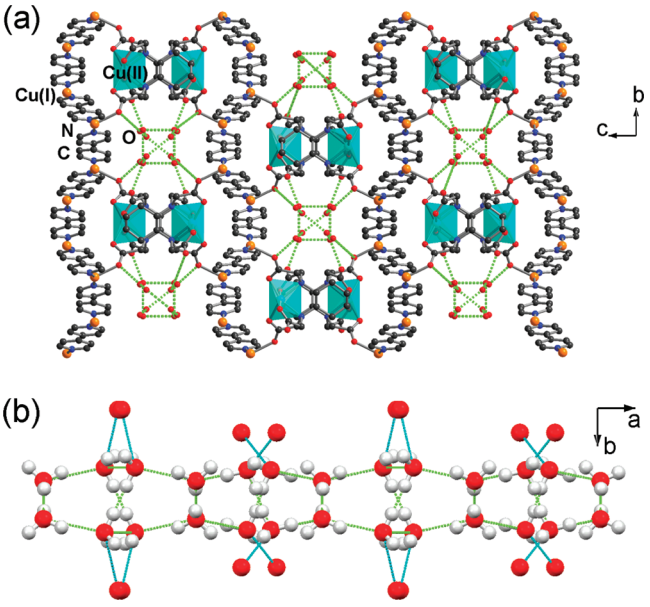

Figure 34. (a) Crystal structure of $[Cu^I_2Cu^{II}(CDTA)(4,4'\text{-bpy})_2]\cdot 6H_2O$ at 250 K. (b) Chain of guest water molecules in the channel along the *a* axis. Green and cyan dotted lines represent hydrogen bonds in the 1D water wire and between the 1D water wire and the framework, respectively.

These metal formates are magnetically ordered below 36 K, as reported by Wang and co-workers.[43,55,56] The Mn, Fe, Co, and Ni formates are canted weak ferromagnets with T_c values of 8.5, 20, 14.9, and 35.6 K, respectively. For the Co and Ni formates, spin reorientations take place at 13.1 and 14.3 K, respectively. All of the samples show hysteresis loops below the critical temperatures. The dominant superexchange mechanism is antiferromagnetic. This series of metal formates are potentially another type of multiferroic MOFs.

dx.doi.org/10.1021/cr200174w |*Chem. Rev.* 2012, 112, 1163–1195

4. AMINO ACID FAMILY

4.1. [Ag(NH$_3$CH$_2$COO)(NO$_3$)]

There are several glycine-containing compounds exhibiting good ferroelectricities, such as triglycine sulfate, triglycine selenate, triglycine fluoroberylate, diglycine nitrate, and glycine phosphite.[11,64−66] The origin of their ferroelectricities is mainly attributed to the nonrigid glycine zwitterions, which can easily transform among numerous rotational conformers due to three internal rotational degrees of freedom. However, it is not the case in glycine silver nitrate, [Ag(NH$_3$CH$_2$COO)(NO$_3$)].

The ferroelectricity of [Ag(NH$_3$CH$_2$COO)(NO$_3$)] was discovered by Pepinsky and co-workers in 1957.[65] Crystals of [Ag(NH$_3$CH$_2$COO)(NO$_3$)] were grown from the aqueous solution of glycine and silver nitrate with 1:1 molar ratio in the dark by slow evaporation. The space group of [Ag(NH$_3$CH$_2$COO)(NO$_3$)] changes from $P2_1/a$ in the paraelectric phase to $P2_1$ in the ferroelectric phase at T_c = 218 K. The symmetry-breaking process abides by the Curie principle, i.e., the maximal nonisomorphic subgroups of the paraelectric space group include Pa, $P2_1$, and $P\bar{1}$ (Figure 23).

In the crystal structure, the Ag ions are coordinated by oxygen atoms of the glycines to form 2D layers in the ac plane (Figure 24). These layers are held together by intercalated nitrates through a network of hydrogen bonds. In the low-temperature ferroelectric phase, the asymmetric unit of [Ag(NH$_3$CH$_2$COO)(NO$_3$)] has two independent molecules. They are related to each other by an inversion center in the high-temperature paraelectric phase. The most significant structural change between the two phases is the movement of the Ag+ ions away from the plane of the oxygen atoms of the glycine zwitterions that leads to the lowering of the crystal symmetry at the T_c.[67]

Therefore, the paraelectric-to-ferroelectric phase transition of [Ag(NH$_3$CH$_2$COO)(NO$_3$)] is of displacive type.[68] Thermal anomaly at the T_c is very small. Temperature dependence of dielectric constant shows a large peak along the b direction at 218 K (Figure 25). Fitting the Curie−Weiss law gives a T_0 of 218 K and a C_{para} of 446 K. The P_s is along the b axis and reaches 0.60 μC·cm^{-2} at 100 K. To the deuterated analogue, [Ag(ND$_3$CH$_2$COO)(NO$_3$)], the T_c is 230 K.

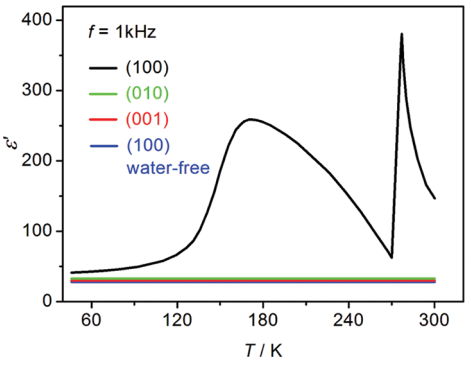

Figure 35. Temperature dependence of dielectric constant of [Cu$^{I}_2$Cu^{II}(CDTA)(4,4′-bpy)$_2$]·6H$_2$O.

4.2. (NH$_3$CH$_2$COO)$_2$·MnCl$_2$·2H$_2$O

(NH$_3$CH$_2$COO)$_2$·MnCl$_2$·2H$_2$O was reported as a room-temperature ferroelectric by Pepinsky and co-workers in 1958.[69] It crystallizes in space group $P2_1$ with two formula units per uint cell. However, there have been only crystallographical structural parameters available without atomic coordinates.[70]

Dielectric constants of (NH$_3$CH$_2$COO)$_2$·MnCl$_2$·2H$_2$O at room temperature are 6.6, 8.1, and 7.4 along the a, b, and c axis, respectively, and they are nearly constant as the temperature decreases. The compound shows polarization up to 328 K before being destroyed by dehydration. Thermal measurement reveals onset of water loss above 308 K, so no Curie temperature can be observed. At room temperature, the P_s is 1.3 μC·cm^{-2} along the b axis and the E_c is 5.6 kV·cm^{-1}. No analogue compounds were found.

4.3. [Ca(CH$_3$NH$_2$CH$_2$COO)$_3$X$_2$] (X = Cl, Br)

Trissarcosine calcium chloride, [Ca(CH$_3$NH$_2$CH$_2$COO)$_3$Cl$_2$], is a uniaxial ferroelectric with a second-order phase transition at 127 K from the orthorhombic $Pnma$ in the paraelectric phase to the orthorhombic $Pn2_1a$ in the ferroelectric phase.[71] The symmetry-breaking process involves a change from the paraelectric $Pnma$ to the ferroelectric $Pn2_1a$, whose minimal nonisomorphic supergroups include $Pnna$, $Pccn$, $Pbcn$, and $Pnma$ (Figure 26).

The compound was grown by slow evaporation from the aqueous solution of calcium chloride and sarcosine in a stoichiometric proportion. The Ca^{2+} ion is octahedrally coordinated by six oxygen atoms from six sarcosines (Figure 27).[72] Each sarcosine connects two Ca^{2+} ions, forming 1D chains along the a axis.

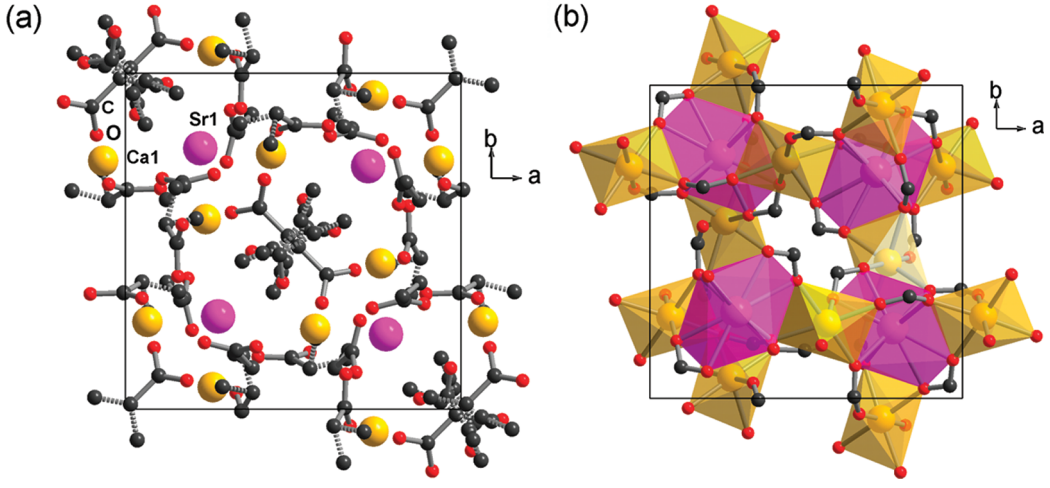

Figure 36. (a) Crystal structure of Ca$_2$Sr(CH$_3$CH$_2$COO)$_6$ in the paraelectric phase. Disordered bonds are depicted as gray dotted lines. (b) Coordination geometry of the metal ions. The ethyl group of the propionate is omitted for clarity.

dx.doi.org/10.1021/cr200174w |Chem. Rev. 2012, 112, 1163–1195

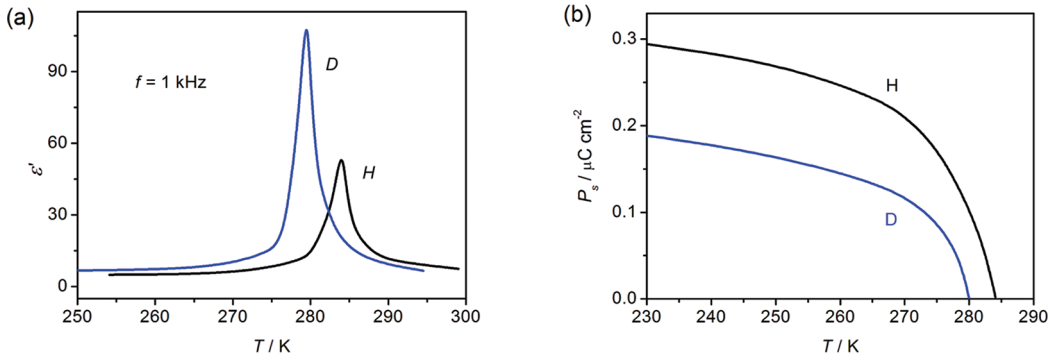

Figure 37. (a) Temperature dependence of dielectric constant, and (b) P_s versus T curve of $Ca_2Sr(CH_3CH_2COO)_6$ (H) and it deuterated form (D).

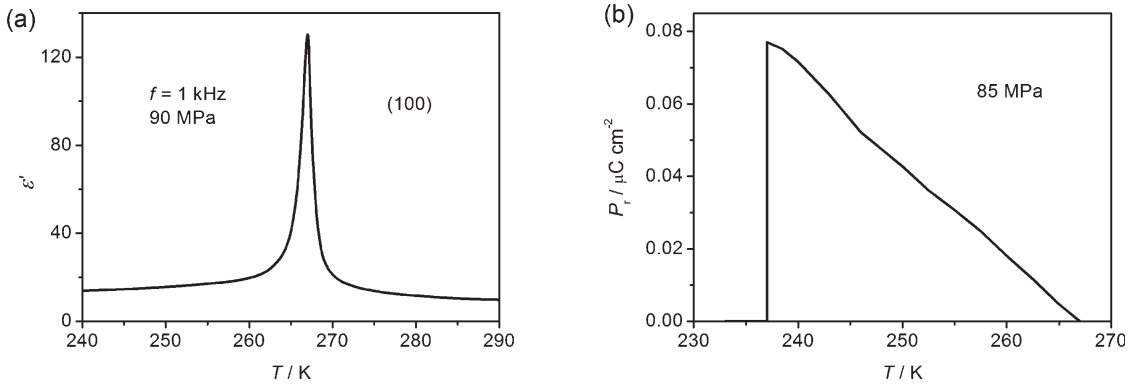

Figure 38. (a) Temperature dependence of dielectric constant, and (b) P_s versus T curve of $Ca_2Ba(CH_3CH_2COO)_6$.

The Cl^- ions are stabilized in the voids formed by the chains. Each Cl^- ion develops three hydrogen bonds with three neighboring N atoms while each N atom involves two hydrogen bonds. One of the three asymmetric sarcosines is perpendicular to the b axis. Below the T_c, the P_s develops along this direction.

Compared with typical ferroelectrics, $[Ca(CH_3NH_2CH_2COO)_3Cl_2]$ shows peculiar properties such as small C_{para} (~58 K), small P_s (0.27 $\mu C \cdot cm^{-2}$ at 78 K), and relatively large entropy change ΔS (2.51 $J \cdot K^{-1} \cdot mol^{-1}$) (Figure 28).[73,74] These observations reveal that the phase transition of $(CH_3NH_2CH_2COO)_3 \cdot CaCl_2$ is of order−disorder type. However, later studies confirm that the phase transition is of displacive type.[75−77]

Ferroelectric transition temperature of the deuterated $[Ca(CH_3ND_2CH_2COO)_3Cl_2]$ is found to be nearly equal to that of $[Ca(CH_3NH_2CH_2COO)_3Cl_2]$.[78] Pressure exerts great influence on the dielectric and ferroelectric properties of the compound. A new phase appears at 5 kbar.[79]

Replacement of the Cl^- ion by Br^- or I^- ion greatly changes the phase transitions of the corresponding compounds. For brominated trissarcosine calcium chloride, $[Ca(CH_3NH_2CH_2COO)_3Cl_{2(1-x)}Br_{2x}]$ ($x \leq 1$), the T_c and P_s decrease rapidly with increasing the molar fraction x of bromide. Meanwhile, the T_c increases greatly with pressure, and the P_s is almost independent of pressure. The mixed crystal shows a ferroelectric phase transition in the range $x \leq 0.66$. For $[Ca(CH_3NH_2CH_2COO)_3Br_2]$, it shows no ferroelectric phase transition down to liquid helium temperature. But the ferroelectric transition appears on application of pressure of 7 kbar at 107 K.[80] The dielectric anomaly increases together with the T_c when the pressure increases. The results indicate that $[Ca(CH_3NH_2CH_2COO)_3Br_2]$ is an incipient ferroelectric and becomes a quantum ferroelectric under hydrostatic pressure.[81]

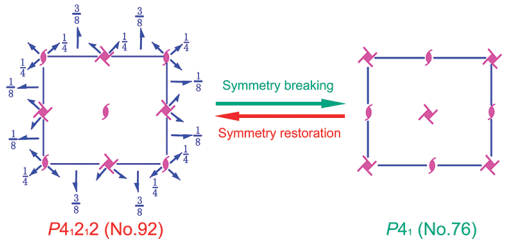

Figure 39. Transformation of the space group of $Ca_2M(CH_3CH_2COO)_6$ from paraelectric phase to ferroelectric phase with a change of symmetry elements from 8 (E, $2C_4$, C_2, $2C'_2$, $2C''_2$) to 4 (E, $2C_4$, C_2).

Dielectric and ferroelectric properties of iodinated trissarcosine calcium chloride were measured at various pressures up to 9 kbar. With an increase of the concentration of the I^- ion, both the peak value of ε' and P_s decrease rapidly. The T_c decreases with increasing the concentration of I^- ion. The effect of substitution of I^- for Cl^- on the dielectric properties is more remarkable than that of Br^- for Cl^-.[82]

4.4. $[Ca\{(CH_3)_3NCH_2COO\}(H_2O)_2Cl_2]$

Betaine calcium chloride dihydrate, $[Ca\{(CH_3)_3NCH_2COO\}(H_2O)_2Cl_2]$, discovered by Rother and co-workers, is an interesting compound exhibiting sequential structural phase transitions.[83] The compound is water-soluble and grown from the aqueous

dx.doi.org/10.1021/cr200174w |Chem. Rev. 2012, 112, 1163–1195

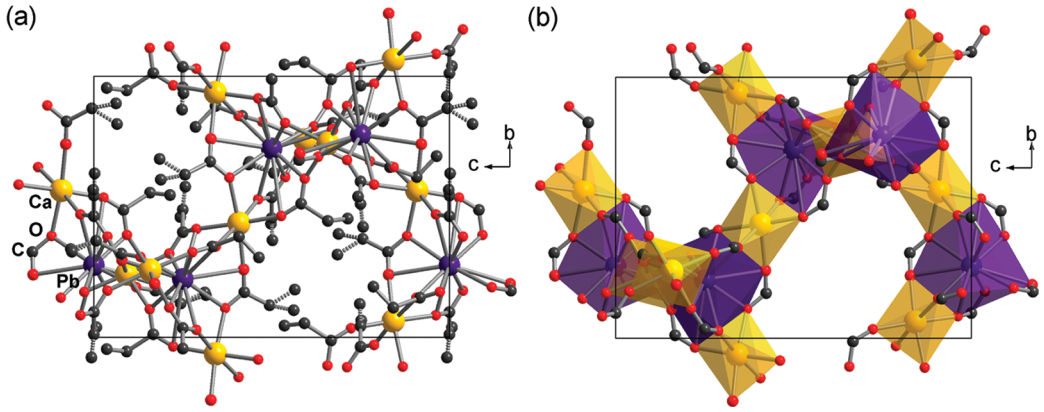

Figure 40. (a) Crystal structure of $Ca_2Pb(CH_3CH_2COO)_6$ in the paraelectric phase. Disorder bonds are depicted as gray dotted lines. (b) Polyhedra of the metal ions. The ethyl group of the propionate is omitted for clarity.

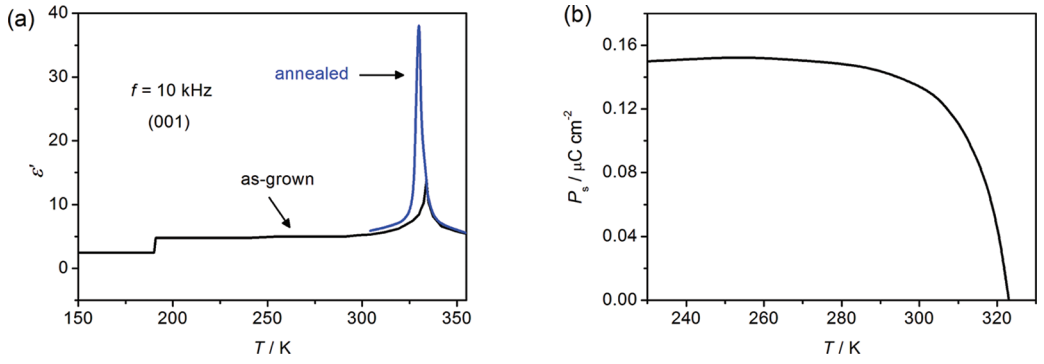

Figure 41. (a) Temperature dependence of dielectric constant of annealed and as-grown crystal, and (b) P_s versus T curve of $Ca_2Pb(CH_3CH_2COO)_6$.

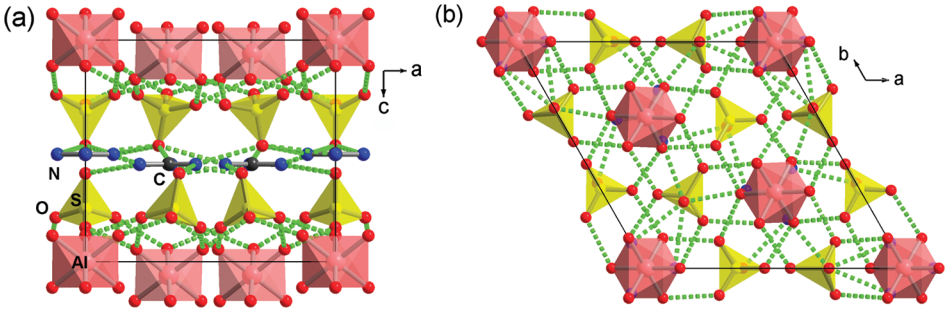

Figure 42. Crystal structure of $[C(NH_2)_3][Al(H_2O)_6](SO_4)_2$ in the ferroelectric phase. Green dotted lines represent hydrogen bonds.

solution containing betaine and inorganic salt in a molar ratio of 1:1. It crystallizes in an orthorhombic space group *Pnma* in the high-temperature phase (>164 K) with four molecular units in the unit cell.[84] The Ca^{2+} ion coordinates with two Cl^- ions, two water molecules, and two oxygen atoms of betaines to form a distorted octahedron (Figure 29). Hydrogen bonds between the Cl and O atoms are very weak with a bond length of ~3.2 Å. The betaine ligands connect neighboring Ca^{2+} ions to result in 1D chains along the *a* axis. At 90 K, a $P2_1ca$ space group was solved.[85]

Interestingly, the symmetry-breaking process in this case involves a change from the paraelectric *Pnma* to the ferroelectric $P2_1ca$, whose minimal nonisomorphic supergroups cover *Pcca*, *Pbcm*, *Pbcn*, and *Pbca*. The ferroelectric space group does not fall in the subgroups of the paraelectric space group (Figure 30), suggesting this phase transition is complex or a mixture of first- and partially second-order characteristics.

Numerous incommensurate and commensurate phases of the compound were reported between 164 and 46 K.[86,87] X-ray diffraction analysis revealed a 1D modulation with a wave vector appearing below T_{c1} = 164 K. The modulation wave vector decreases continuously on cooling in the incommensurate phases and locks at different rational values of the commensurate phases. Below T_{c8} = 46 K, the system undergoes a phase transition into the proper ferroelectric phase.

Dielectric measurements reveal eight anomalies between T_{c1} and T_{c8}.[83] The highest peak of the dielectric constant is at T_{c3} =125 K with a value of ~1 × 10^3 (Figure 31). Below this temperature

dx.doi.org/10.1021/cr200174w |*Chem. Rev.* 2012, 112, 1163–1195

there exist complex hysteresis loops. A ferroelectric single loop appears below the T_{c8} with a P_s value up to 2.5 $\mu C \cdot cm^{-2}$. Isotope effects in $[Ca\{(CH_3)_3NCH_2COO\}(D_2O)_2Cl_2]$ are negligible.

4.5. $[Ln_2Cu_3\{NH(CH_2COO)_2\}_6]\cdot 9H_2O$

Kobayashi and co-workers reported a series of porous MOFs, $[Ln_2Cu_3\{NH(CH_2COO)_2\}_6]_3\cdot nH_2O$, where Ln = trivalent La, Nd, Sm, Gd, Ho, or Er, and $n \approx 9$. Large dielectric constants and antiferroelectric behaviors at high temperatures were observed in these compounds.[88,89]

$[Ln_2Cu_3\{NH(CH_2COO)_2\}_6]\cdot 9H_2O$ were prepared by reaction of $LnCl_3\cdot 9H_2O$ with the mixture of iminodiacetic acid and $Cu(NO_3)_2\cdot 3H_2O$ in a 2:6:3 molar ratio in an aqueous solution with a pH value of 5−6. By evaporation of the resulting mixture at room temperature for one week, blue hexagonal column-shaped crystals were obtained.[90]

All the compounds are isostructural and belong to the trigonal space group $P\bar{3}c1$. In the crystal structures, the copper^{II} ion is six-coordinated in a distorted octahedral geometry by four O atoms and two N atoms from two iminodiacetate ligands to form a tetradentate metalloligand $[Cu\{NH(CH_2COO)_2\}_2]^{2-}$. A 3D honeycomb structure is formed through the assembly of the nine-coordinated Ln^{III} ions and metalloligands (Figure 32a). Chair-shaped hexagonal channels develop along the *c* axis with a diameter of ∼17 Å. Guest water clusters locate in the channel, like a string of pearls. The nine water molecules in the cluster are classified into three groups, occupying different sites in the channels (Figure 32b). The temperature dependence of the lattice constant of the Ln crystals reveals distinct anomalies at ∼350 K, suggesting structural changes of the guest water molecules confined in the channels. The water molecules are gradually lost during 50−130 °C, and the host lattice is stable up to 300 °C.

Dielectric constants for $[Ln_2Cu_3\{NH(CH_2COO)_2\}_6]\cdot 9H_2O$ were measured in the temperature range 80−400 K (Figure 33). They show broad dielectric peaks at ∼150−190 K with a drop from ∼200 to 10 due to freezing of thermal motions of the water molecules. The dielectric behaviors are consistent with the results of molecular dynamics simulations. Above 300 K, the dielectric constants exhibit rapid increases, which are ascribed to

Table 1. Properties of $[C(NH_2)_3]M(RO_4)_2\cdot 12H_2O$

M/R	symmetry at 293 K	$P_s/\mu C\cdot m^{-2}$	$E_c/kV\cdot cm^{-1}$	ref
Al/S	*P*31*m*	0.35 (293 K)	1.7 (293 K)	106, 109
V/S	*P*31*m*	0.38 (293 K)	6 (293 K)	107
Cr/S	*P*31*m*	0.37 (293 K)	?	106
Ga/S	*P*31*m*	0.36 (293 K)	3.6 (293 K)	106, 109
Al/Se	*P*31*m*	0.45 (293 K)	?	106, 109
Cr/Se	*P*31*m*	0.47 (293 K)	?	106, 109
Ga/Se	*P*31*m*	0.47 (293 K)	?	106, 109

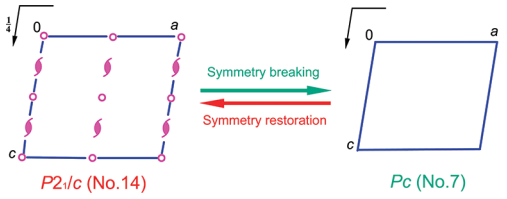

Figure 43. Transformation of the space group of $[(CH_3)_2NH_2][M(H_2O)_6](SO_4)_2$ from paraelectric phase to ferroelectric phase with a change of symmetry elements from 4 [E, C_2, i, σ_h] to 2 [E, σ_h].

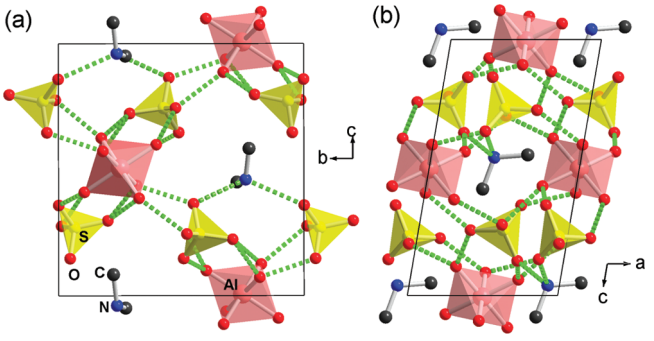

Figure 44. Crystal structure of $[(CH_3)_2NH_2][Al(H_2O)_6](SO_4)_2$ in the ferroelectric phase. Green dotted lines represent hydrogen bonds.

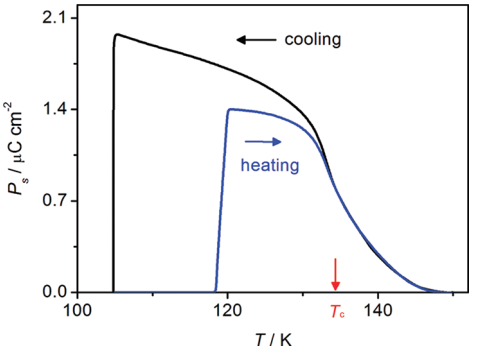

Figure 46. Saturated polarization of $[(CH_3)_2NH_2][Ga(H_2O)_6](SO_4)_2$.

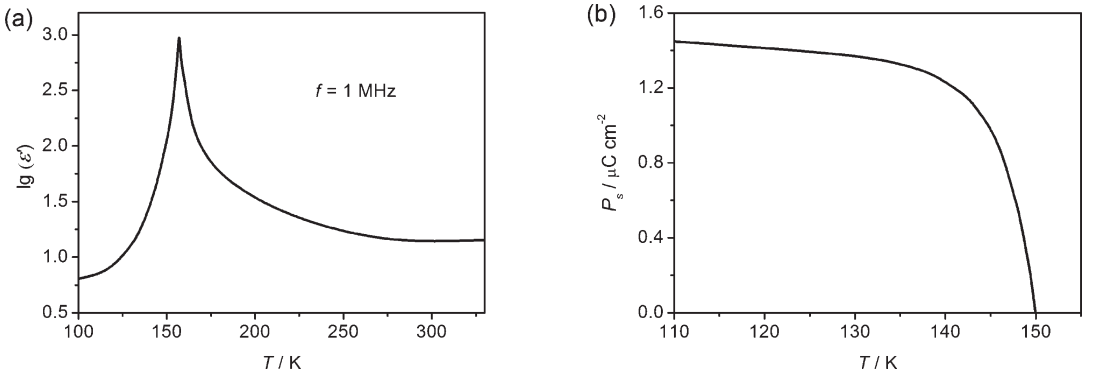

Figure 45. (a) Temperature dependence of dielectric constant, and (b) P_s versus T curve of $[(CH_3)_2NH_2][Al(H_2O)_6](SO_4)_2$.

dx.doi.org/10.1021/cr200174w |*Chem. Rev.* 2012, 112, 1163–1195

approaching antiferroelectric transitions near 400 K. At 400 K, the Sm and La compounds show maximum values of the dielectric constants of ~1300 and 350, respectively. The La compound shows a considerable isotope effect, revealing the essential role of the hydrogen bonds in its dielectric properties. The hysteresis loops of La, Sm, and Gd crystals show typical double hysteresis curves, indicating their antiferroelectricities at high temperatures (Figure 33).

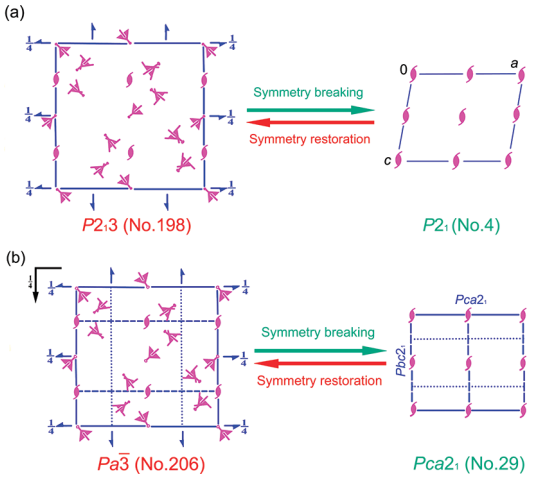

Figure 47. Transformations of the space group of $[CH_3NH_3][M(H_2O)_6](SO_4)_2\cdot 6H_2O$ from paraelectric phase to ferroelectric phase with a change of symmetry elements from (a) 12 (E, $8C_3$, $3C_2$) to 2 (E, C_2) or (b) 24 [E, $8C_3$, $3C_2$, i, $3\sigma_h$, $8S_6$] to 4 [E, C_2, $2\sigma_v$].

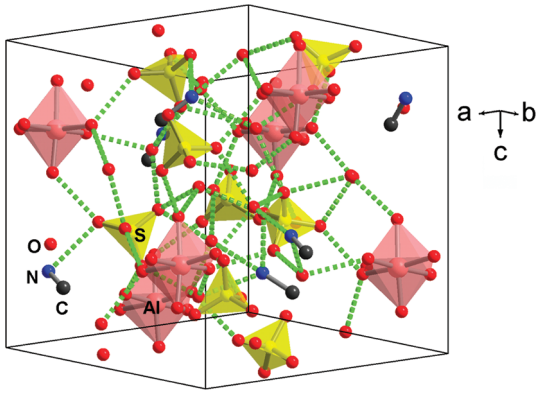

Figure 48. Unit cell of $[CH_3NH_3][Al(H_2O)_6](SO_4)_2\cdot 6H_2O$ in the paraelectric phase. Green dotted lines represent hydrogen bonds.

4.6. $[Cu^I_2Cu^{II}(CDTA)(4,4'\text{-bpy})_2]\cdot 6H_2O$

Very recently, Long and co-workers reported another porous MOF with guest water molecules, $[Cu^I_2Cu^{II}(CDTA)(4,4'\text{-bpy})_2]\cdot 6H_2O$, where H_4CDTA is *trans*-1,2-diaminocyclohexane-*N*,*N*,*N*′,*N*′-tetraacetic acid and 4,4′-bpy is 4,4′-bipyridine.[91] In this compound, the confined 1D water wire in the nanochannel exhibits striking dielectric anomalies at ~175 and 277 K. At the latter temperature, a spontaneous transition occurs between 1D liquid and 1D ferroelectric ice.

$[Cu^I_2Cu^{II}(CDTA)(4,4'\text{-bpy})_2]\cdot 6H_2O$ was prepared from the mixture of H_4CDTA, $Cu(CH_3COO)_2\cdot H_2O$, 4,4′-bpy, and water under hydrothermal conditions. In the crystal structure, the Cu^{II} ion is octahedrally coordinated by two N and four O atoms from one $CDTA^{4-}$ ligand to form a metalloligand $[Cu^{II}(CDTA)]^{2-}$. The Cu^I ion is coordinated by two N atoms from two 4, 4′-bpy ligands and one O atom from the metalloligand, showing a T-shaped geometry (Figure 34a). The resulting $[Cu^I_2Cu^{II}(CDTA)(4,4'\text{-bpy})_2]$ network is a 3-fold interpenetration 2D layer parallel to the *ab* plane. In the 3D supramolecular architecture of the compound, the guest water molecules occupy the channel along the *a* axis. They are held together as a periodic 1D water wire $(H_2O)_{12n}$ by hydrogen-bonding interactions between them and the metalloligands (Figure 34b). The $(H_2O)_{12}$ unit can be viewed as a complex of a water tetramer and a boatlike water octamer acting as proton acceptor and donor, respectively.

The temperature dependence of the dielectric constant of $[Cu^I_2Cu^{II}(CDTA)(4,4'\text{-bpy})_2]\cdot 6H_2O$ shows a very broad peak at ~170 K and a sharp peak at ~277 K measured along the *a* axis, which is significantly different from that of bulk water (Figure 35). The two dielectric anomalies are attributed to the water wire because the dielectric constants along the *b* and *c* axes and for the water-free sample along the *a* axis are almost temperature-independent over the entire temperature range. With the increase of the frequency from 1 kHz to 10 MHz, the broad dielectric peak at ~170 K shifts to a higher temperature and its value decreases from 293 to 82. This behavior does not represent a phase transition but a dielectric relaxation phenomenon. The sharp dielectric peak at 277 K clearly indicates a phase transition. The *P*−*E* loop is obtained at ~250 K. The deuterated compound shows an isotope effect with an ~8 K shift to higher temperature.

However, crystal structure analysis reveals that the compound adopts a centrosymmetric space group *Fddd*, which violates the symmetric requirement for a ferroelectric. A possible explanation

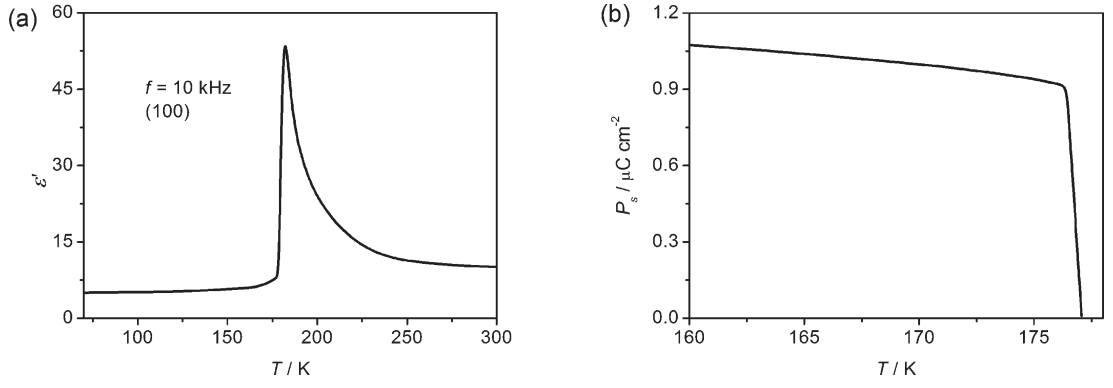

Figure 49. (a) Temperature dependence of dielectric constant, and (b) P_s versus T curve of $[CH_3NH_3][Al(H_2O)_6](SO_4)_2\cdot 6H_2O$.

dx.doi.org/10.1021/cr200174w |*Chem. Rev.* 2012, 112, 1163–1195

is that the exact positions of hydrogen atoms cannot be fully determined. Molecular dynamics simulations disclose that hydrogen-bonding interactions are of critical importance to the ferroelectricity of the 1D ice below 277 K, including both dynamic hydrogen-bonding interactions among water molecules in the water wire and static interactions between water molecules and the host. We think that temperature-dependent SHG measurement would be helpful to provide some insight into whether the low-temperature space group is a noncentrosymmetric one.

5. PROPIONATE FAMILY

The dicalcium metal propionates, $Ca_2M(C_2H_5COO)_6$ where M is divalent Sr, Ba, or Pb cation, exhibit ferroelectricities in some of their phases. In this family, the propionate resembles glycine and its derivatives. Order−disorder changes of the terminal methyl group of the propionate play a key role in the ferroelectric phase transitions.

Table 2. Properties of $[CH_3NH_3][M(H_2O)_6](RO_4)_2\cdot 6H_2O$

M/R	symmetry change	T_c/K	P_s/ $\mu C\cdot cm^{-2}$	E_c/ $kV\cdot cm^{-1}$	ref
Al/S	$P2_13 \leftrightarrow P2_1$ or $Pa\bar{3} \leftrightarrow Pca2_1$	177	1.0 (175 K)	6 (175 K)	2, 118, 119
V/S	cubic ↔ ?	157	0.9 (155 K)	6 (155 K)	2
Cr/S	$Pa\bar{3} \leftrightarrow Pca2_1$	164	1.0 (162 K)	6 (162 K)	2
Fe/S	cubic ↔ ?	169	1.3 (167 K)	6 (167 K)	2
Ga/S	cubic ↔ ?	171	0.4 (just below T_c)	?	9
In/S	cubic ↔ ?	164	1.2 (162 K)	6 (162 K)	2
Al/Se	cubic ↔ ?	216	1.2 (165 K)	1.0 (165 K)	2, 9
Cr/Se	$Pa\bar{3}$ ↔ ?	201.3	0.43 (191 K)	3.3 (191 K)	9
Ga/Se	$Pa\bar{3}$ ↔ ?	207.5	0.42 (191 K)	2.7 (191 K)	9

5.1. $Ca_2Sr(CH_3CH_2COO)_6$

Ferroelectricity of $Ca_2Sr(CH_3CH_2COO)_6$ was found in 1957 by Matthias and Remeika.[92] It undergoes a phase transition from $P4_12_12$ in the paraelectric phase to $P4_1$ in the ferroelectric phase with T_c = 282.6 K.

Crystal structures of $Ca_2Sr(CH_3CH_2COO)_6$ at several temperatures between 113 and 423 K were determined.[93] At room temperature, structure analysis reveals that four of the methyl groups together with one of the α-carbons in a formula unit are in a disordered state occupying respectively two equilibrium atomic positions with the same probability (Figure 36).[94] Occupancies of the three disordered methyl groups, together with the displacements of Sr, Ca and O atoms, vary with temperature in the same manner as the P_s, which takes a saturation value at 113 K. In contrast, one of the other methyl groups is in a state of partial disorder even at 113 K.

The temperature dependence of the dielectric constant of $Ca_2Sr(CH_3CH_2COO)_6$ at 1 kHz shows an anomaly at 283.9 K along the c axis (Figure 37). The fitted T_0 and C_{para} are 278 and 73 K, respectively. The magnitude and temperature dependence of the P_s are explainable by the displacement of CaO_6 octahedra relative to Sr ions. Deuterated $Ca_2Sr(CD_3CD_2COO)_6$ was synthesized to investigate the role of motion of the methyl groups of the propionate in the ferroelectric phase transition. The dielectric constant of the deuterated compound shows an

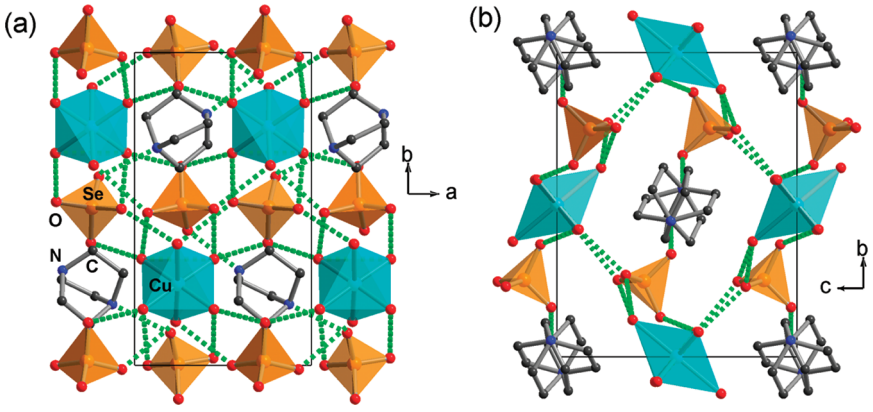

Figure 50. Unit cell of $[H_2dbco][Cu(H_2O)_6](SeO_4)_2$ in (a) the ferroelectric phase and (b) the paraelectric phase. Green dotted lines represent hydrogen bonds.

Table 3. Properties of $[(CH_3)_4N]_2[MX_4]$ (F = Ferroelectric Phase)

M/X	no. of phase transitions	T range of the incommensurate phase/K	symmetry change upon cooling	phase transition temperature/K	$P_s/\mu C\cdot cm^{-2}$	ref
Mn/Cl	5	291.7−292.3	$Pmcn \rightarrow ? \rightarrow P2_1/c11 \rightarrow P112_1/n \rightarrow P12_1/c1 \rightarrow ?$	292.3, 291.7, 266.7, 172.2, 90,	?	125
Fe/Cl	5	280.1−270.7	$Pmcn \rightarrow ? \rightarrow P2_12_12_1 \rightarrow P112_1/n \rightarrow P12_1/c1 \rightarrow ?$	280.1, 270.7, 266.3, 241.2, ?	?	122
Co/Cl	6	293.8−281.2	$Pmcn \rightarrow ? \rightarrow P2_1cn$ (F) $\rightarrow ? \rightarrow P112_1/n \rightarrow P12_1/c1 \rightarrow P2_12_12_1$	293.8, 281.2, 279.5, 277.7, 192.2, 122.2	0.0025 (280 K)	126
Cu/Br	3	270.7−240,	$Pmcn \rightarrow ? \rightarrow Pbc2_1$ (F) $\rightarrow P12_1/c1$	270.7, 240, 235.9	0.07 (239 K)	127
Zn/Cl	5	296.8−280.2	$Pmcn \rightarrow ? \rightarrow P2_1cn$ (F) $\rightarrow P112_1/n \rightarrow P12_1/c1 \rightarrow P2_12_12_1$	296.8, 280.2, 275.5, 168.2, 155.2	0.006 (277 K)	128
Zn/I	2		$Pmcn \rightarrow P12_1/c1 \rightarrow Pbc2_1$ (F)	254, 210	0.13 (150 K)	129

dx.doi.org/10.1021/cr200174w |Chem. Rev. 2012, 112, 1163–1195

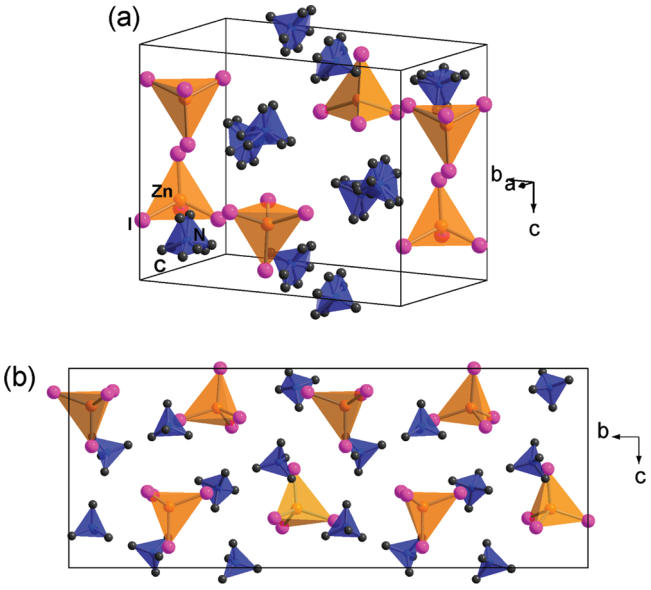

Figure 51. Crystal structures of $[(CH_3)_4N]_2[ZnI_4]$ at (a) 293 K and (b) 150 K.

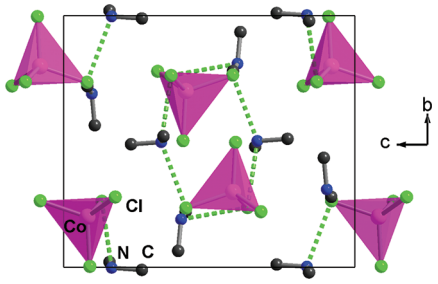

Figure 52. Crystal structures of $[(CH_3)_2NH_2]_2[CoCl_4]$ at 293 K. Green dotted lines represent hydrogen bonds.

anomaly at 279.5 K, indicating a negligibly small isotope effect on T_c.[95] This suggests a secondary role of the motion of the propionate in the mechanism of the ferroelectric phase transition of $Ca_2Sr(CH_3CH_2COO)_6$.

Furthermore, $(HCF_2CF_2COO^-)$-doped $Ca_2Sr(CH_3CH_2COO)_6$ exhibits an obvious decrease in Curie temperature but no change in spontaneous polarization when the content of the $HCF_2CF_2COO^-$ ion is between 0 and 3.42×10^{-2}. From these results, it was concluded that the motion of the propionate ions acts a trigger of the paraelectric-to-ferroelectric phase transition of $Ca_2Sr(CH_3CH_2COO)_6$.[96]

5.2. $Ca_2Ba(CH_3CH_2COO)_6$

Dicalcium barium propionate, $Ca_2Ba(CH_3CH_2COO)_6$, undergoes two low-temperature phase transitions, i.e., a first-order one at 267 K and a second-order one at 204 K.[97,98] Above 267 K, the compound adopts cubic space group $Fd3m$. The ferroelectricity in $Ca_2Ba(CH_3CH_2COO)_6$ is induced under high pressure (9.0×10^7 Pa).[99,100] In this case, the compound changes from the paraelectric $P4_12_12$ to the ferroelectric $P4_1$ at 267 K.

In the structure, the Ba^{2+} ion is octahedrally surrounded by six propionate ligands, i.e., there are 12 O atoms closest to and equidistant from the Ba^{2+} ion, forming an eight-face coordination polyhedron.[101] The Ca^{2+} ion is six-coordinated by O atoms from six different propionates to form a trigonal antiprism. The Ca−O bond is very short with a value of 2.253 Å. The terminal group of the propionate suffers an amount of disorder. A structural analysis indicates that it is the whole propionate that should be considered to be disordered. The driving force for the phase transitions in this type of compound may be the steric interactions. The observed disorder gives an average space group $Fd3m$ in which the microdomain adopts either $P4_12_12$ or $P4_32_12$ symmetry. Growth of electric domains results in a drastic phase transition at 267 K. The dielectric constant of $Ca_2Ba(CH_3CH_2COO)_6$ shows an anomaly at 267 K and 1 kHz under a high pressure of 9.0×10^7 Pa (Figure 38).

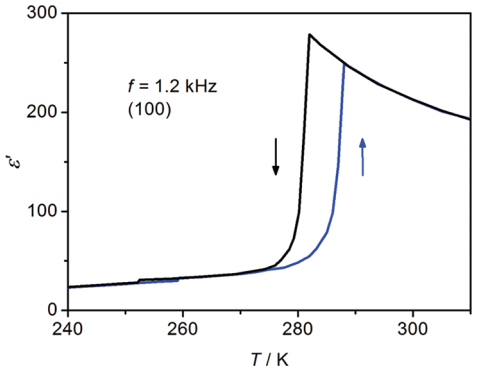

Figure 53. Temperature dependence of dielectric constant of $[(CH_3)_2NH_2]_3[CuCl_4]Cl$.

5.3. $Ca_2Pb(CH_3CH_2COO)_6$

Dicalcium lead propionate, $Ca_2Pb(CH_3CH_2COO)_6$, is a room-temperature ferroelectric.[102,103] It undergoes a second-order phase transition at 333 K between the paraelectric space group $P4_12_12$ and the ferroelectric space group $P4_1$, and then a first-order ferroelectric-to-ferroelectric phase transition at 191 K. It is isomorphous to the Sr analogue. For the above three cases, the symmetry-breaking process follows the Curie symmetry principle, that is, the subgroups of the paraelectric space group $P4_12_12$ (No. 92) include $P4_1$, $C222_1$, and $P2_12_12_1$ (Figure 39).

The crystal structures determined at various temperatures above and below the ferroelectric phase transition temperature show that the ionic Pb, Ca, and O atoms exhibit no disordered characters in both phases whereas the methyl groups exhibit a disordered characteristic (Figure 40).[104] The phase transition is essentially of order−disorder type.[105] Dielectric properties of the as-grown crystal are different from the annealed one (Figure 41). The P_s is along the c direction.

6. SULFATE FAMILY

6.1. $[C(NH_2)_3][M(H_2O)_6](XO_4)_2$ (M = Al, V, Cr, Ga, X = S, Se)

In 1955, a new family of ferroelectrics was found by Holden and co-workers.[106,107] These compounds have the general formula $[C(NH_2)_3][M(H_2O)_6](XO_4)_2$ where $C(NH_2)_3$ is guanidinium, M is trivalent Al, V, Cr or Ga, and X is S or Se. These findings rapidly expanded the ferroelectric compounds, which only included certain tartrates, orthophosphates, and arsenates and a number of oxides at that time, and refreshed previous ideas about the dielectric aspects of ferroelectrics. They show no Curie points, which are expected to lie behind decomposition temperatures, similar to that found in $(NH_3CH_2COO)_2 \cdot MnCl_2 \cdot 2H_2O$.

dx.doi.org/10.1021/cr200174w |Chem. Rev. 2012, 112, 1163–1195

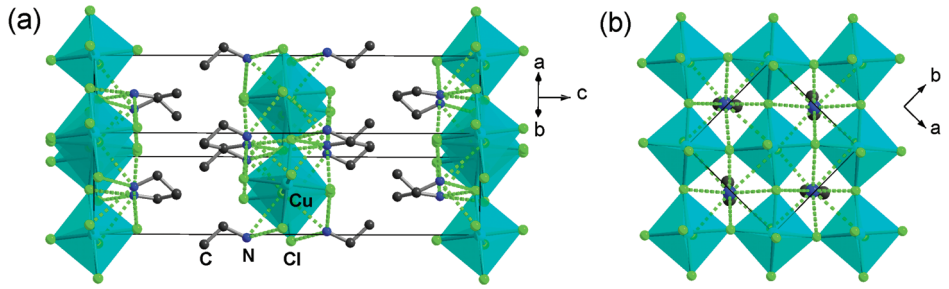

Figure 54. Crystal structure of $[C_2H_5NH_3]_2[CuCl_4]$ at 293 K. Green dotted lines represent hydrogen bonds.

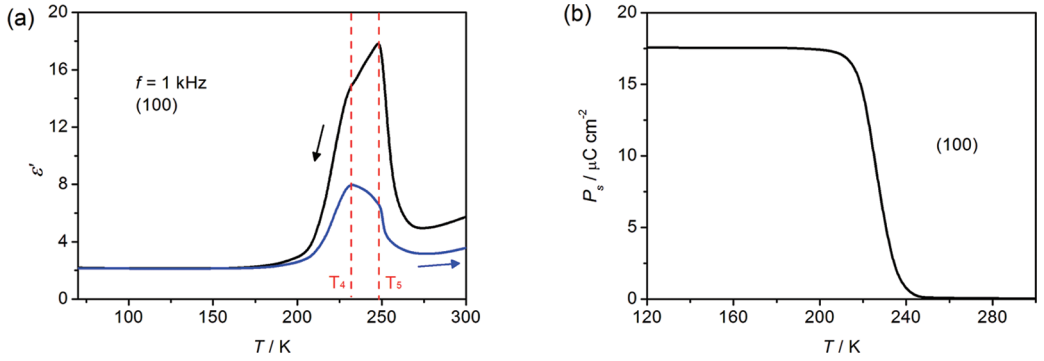

Figure 55. (a) Temperature dependence of dielectric constant, and (b) P_s versus T curve of $[C_2H_5NH_3]_2[CuCl_4]$.

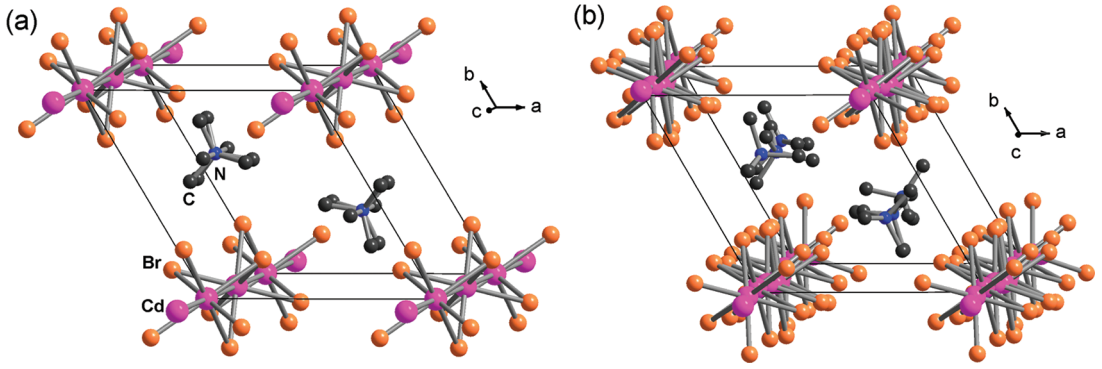

Figure 56. Crystal structure of $[(CH_3)_4N][CdBr_3]$ at (a) 293 K and (b) 133 K.

$[C(NH_2)_3][Al(H_2O)_6](SO_4)_2$, abbreviated as GASH, is such a typical compound reported first.[106] It is grown from saturated aqueous solution. At room temperature, the compound crystallizes in a trigonal space group $P31m$.[108] The guanidinium cation is planar and perpendicular to the c axis (Figure 42). The Al^{3+} ion lies on the 3-fold axes and is coordinated by six water molecules as a slightly distorted octahedron. The water molecules link the sulfate tetrahedra by hydrogen bonds. The three kinds of ions stack layer by layer along the c axis in the sequence of $-Al(H_2O)_6-SO_4-C(NH_2)_3-SO_4-$.

The dielectric constant of GASH is temperature-independent up to ~100 °C with a value of 6 along the c axis.[109] The ferroelectric-to-paraelectric phase transition does not occur up to the decomposition temperature of ~200 °C. The P_s is along the c axis with a value of 0.35 $\mu C \cdot m^{-2}$ at 293 K. It is found that the sulfates show relatively smaller P_s than the selenates (Table 1).

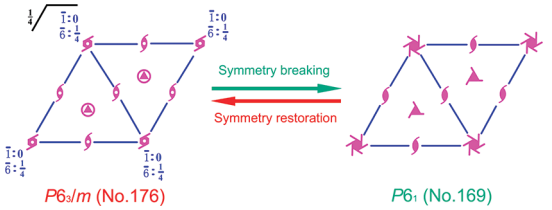

Figure 57. Transformation of the space group of $[(CH_3)_4N][CdBr_3]$ from paraelectric phase to ferroelectric phase with a change of symmetry elements from 12 (E, $2C_6$, $2C_3$, C_2, i, $2S_3$, $2S_6$, σ_h) to 6 (E, $2C_6$, $2C_3$, C_2).

6.2. $[(CH_3)_2NH_2][M(H_2O)_6](SO_4)_2$ (M = Al, Ga)

The dimethylammonium-substituted compound $[(CH_3)_2NH_2][Al(H_2O)_6](SO_4)_2$ shows some differences from the GASH analogue. Its ferroelectricity was found by Kirpichnikova and co-workers

dx.doi.org/10.1021/cr200174w |Chem. Rev. 2012, 112, 1163–1195

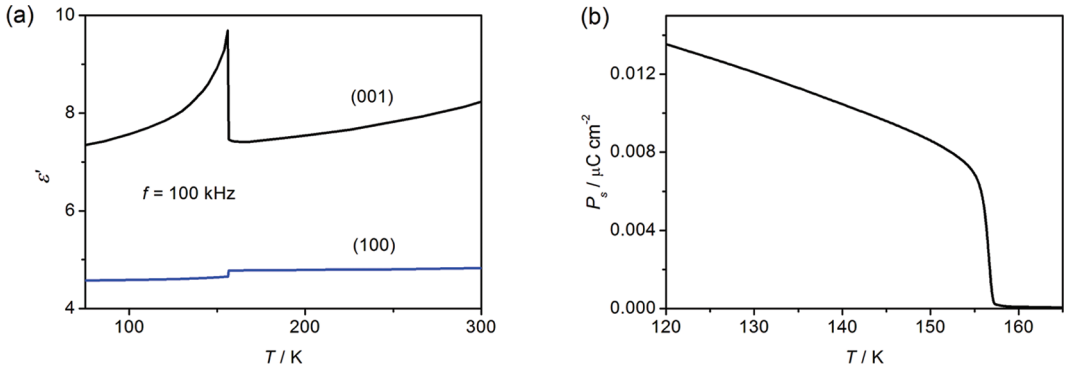

Figure 58. (a) Temperature dependence of dielectric constant, and (b) P_s versus T curve of $[(CH_3)_4N][CdBr_3]$.

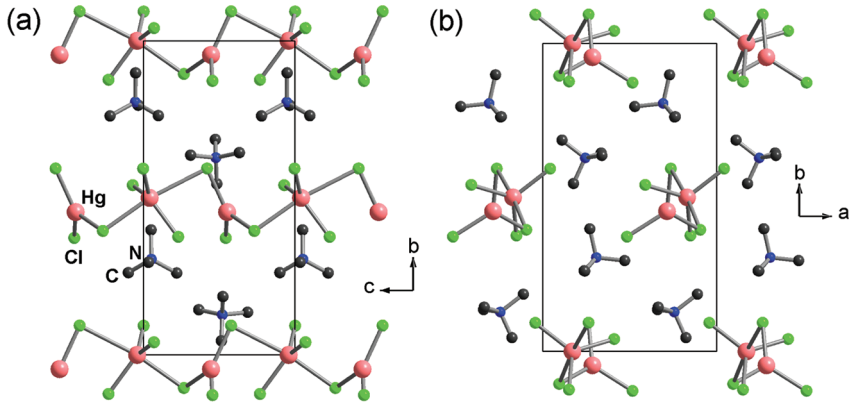

Figure 59. Crystal structure of $[(CH_3)_4N][HgCl_3]$ at 293 K.

in 1988.[110] This compound undergoes a phase transition at 152 K between the paraelectric space group $P2_1/n$ and the ferroelectric space group Pn. The symmetry-breaking process is simply like the change from the paraelectric $P2_1/c$ to the ferroelectric Pc. The maximal nonisomorphic subgroups of $P2_1/c$ include Pc, $P2_1$, and $P\bar{1}$ (Figure 43).

In the crystal structure the Al^{3+} cation coordinates with six water molecules to form a regular octahedron (Figure 44).[111] Each water molecule exhibits two hydrogen bonds with the oxygen atoms of the SO_4 tetrahedron, forming a rather complicated H-bond network. The dimethylammonium cation is located in the channel formed by the $Al(H_2O)_6-SO_4$ sublattice. It is disordered due to a rotation around the axis defined by two carbon atoms, resulting in four equilibrium positions of the NH_2 groups. This rotation is hampered by the O···H−N hydrogen bonds between the NH_2 and SO_4 groups.

At 1 MHz, the peak value of the dielectric constant is ∼700 at 160 K (Figure 45a). The P_s is ∼1.4 $\mu C \cdot m^{-2}$ at 120 K with an E_c of 7 $kV \cdot cm^{-1}$ (Figure 45b).

The ferroelectric phase transition is considered as an order−disorder type and is connected with the ordering of the dimethylammonium cation. Below the T_c the cations freeze in one position and the P_s occurs in the m plane. The direction of the P_s is parallel to the vector joining the nitrogen atoms of the two cations in the unit cell. The cation thus represents the basic reversible electric dipole, and its ordering creates the P_s below the T_c. NMR studies demonstrate that the dimethylammonium rotation freezing-out is indeed the prime reason for the ferroelectric transition in $[(CH_3)_2NH_2][Al(H_2O)_6](SO_4)_2$.[112] The ferroelectric phase transition at the T_c is most probably evoked indirectly by slowing down of rotation and reorientation of the H_2O units.[113]

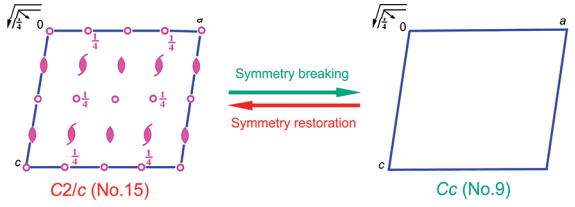

Figure 60. Transformation of the space group of $[4\text{-}NH_2PyH][SbCl_4]$ from paraelectric phase to ferroelectric phase with a change of symmetry elements from 4 (E, C_2, i, σ_h) to 2 (E, σ_h).

Ferroelectricity in $[(CH_3)_2NH_2][Ga(H_2O)_6](SO_4)_2$ was reported in 1991.[114] Like its isomorphic $[(CH_3)_2NH_2][Al(H_2O)_6](SO_4)_2$, the Ga analogue also undergoes an order−disorder phase transition between the paraelectric space group $P2_1/n$ and the ferroelectric space group $P2_1$ at 134 K.[115] The symmetry-breaking process is similar to that found in $[(CH_3)_2NH_2][Al(H_2O)_6](SO_4)_2$. Additionally, it experiences additional phase transitions, i.e., a nonferroelectric intermediate phase below 116 K and an antiferroelectric phase below ∼60 K.

ESR studies confirm the order−disorder characteristic of the ferroelectric phase transition and demonstrate freezing-out of the dimethylammonium reorientations, which is a primary reason for this transition.[116] There is a unit cell doubling in the antiferroelectric phase below 60 K.

dx.doi.org/10.1021/cr200174w |Chem. Rev. 2012, 112, 1163–1195

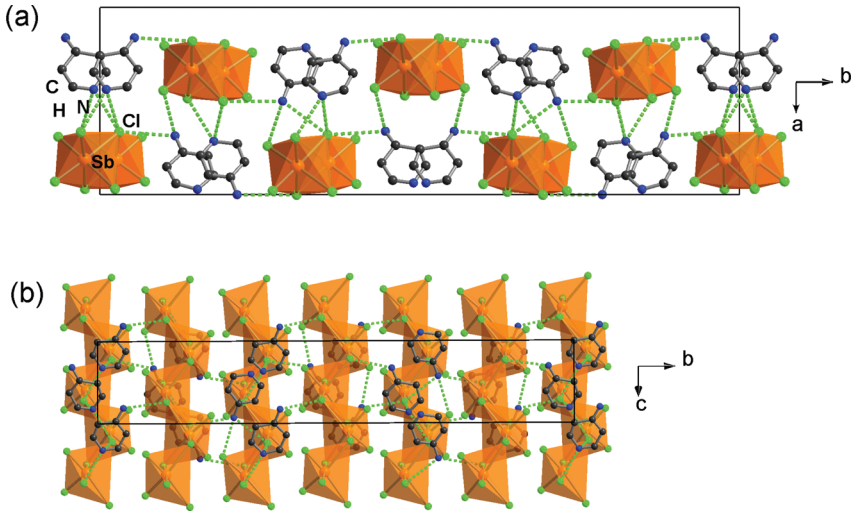

Figure 61. Crystal structure of $[4\text{-}NH_2PyH][SbCl_4]$ at 258 K. Green dotted lines represent hydrogen bonds.

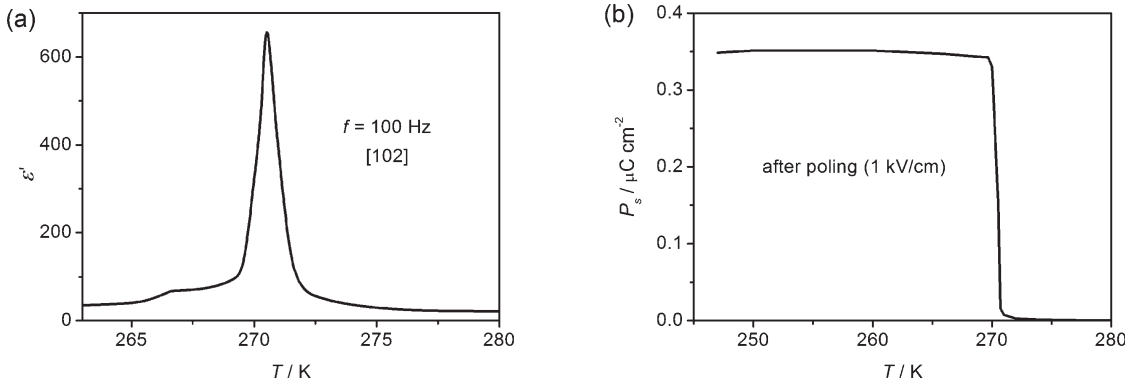

Figure 62. (a) Temperature dependence of dielectric constant, and (b) P_s versus T curve of $[4\text{-}NH_2PyH][SbCl_4]$.

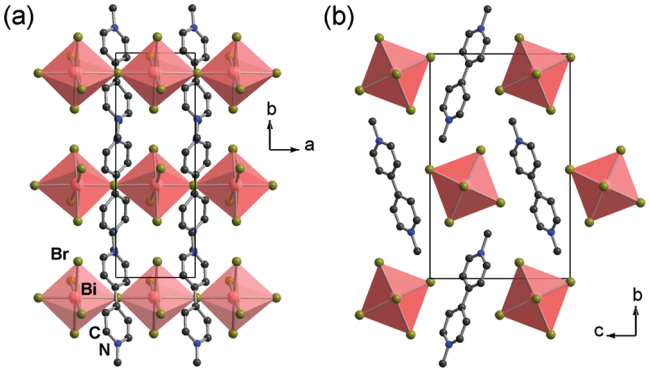

Figure 63. Crystal structure of $[MV][BiBr_5]$ at 233 K.

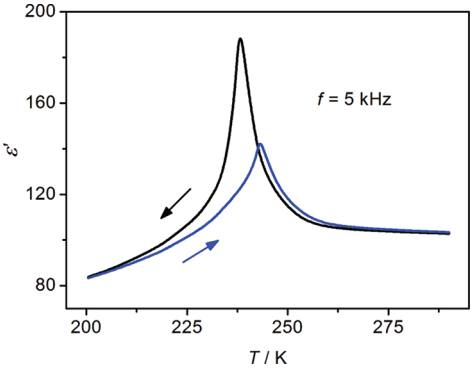

Figure 64. Temperature dependence of dielectric constant of $[MV][BiBr_5]$.

At 1 MHz, the peak value of dielectric constant is ~500 at 136 K. The P_s shows a thermal lag at ~116 K (Figure 46).[117]

6.3. $[CH_3NH_3][M(H_2O)_6](RO_4)_2\cdot 6H_2O$

Organic−inorganic hybrid alum ferroelectrics have the general formula $A[M(H_2O)_6](RO_4)_2\cdot 6H_2O$ (A = methylammonium; M = trivalent Al, V, Cr, Fe, Ga, or In; R = S or Se). The alum family compounds can be easily prepared from aqueous solutions. All of the crystals have cubic symmetry at room temperature. They show phase transitions at low temperatures. In the review, the inorganic alum ferroelectrics are not included.

Ferroelectricity of $[CH_3NH_3][Al(H_2O)_6](SO_4)_2\cdot 6H_2O$ was reported by Pepinsky and co-workers in 1956.[118] It undergoes a phase transition from the paraelectric cubic $P2_13$ space group to the ferroelectric monoclinic $P2_1$ at 177 K.[2] An alternative space

dx.doi.org/10.1021/cr200174w |*Chem. Rev.* 2012, 112, 1163–1195

Table 4. Properties of ferroelectric $A_3[M_2X_9]$

A/M/X	symmetry change upon cooling	phase transition temperatures/K	$P_s/\mu C \cdot cm^{-2}$	ref
$(CH_3)_2NH_2$/Sb/Cl	$P2_1/c \rightarrow Pc$ (ferroelectric)	242	0.66 (210 K)	153
$(CH_3)_2NH_2$/Sb/Br	$P2_1/c \rightarrow$? (ferroelectric)	164	0.07 (170 K)	154, 155
$(CH_3)_3NH$/Sb/Cl	? → ? → Pc (ferroelectric) → Pc → Pc	364, 363, 203, 127	2.0 (320)	156
CH_3NH_3/Sb/Br	$P\bar{3}m1 \rightarrow$? (ferroelastic) → ? (ferroelectric)	168, 134	0.13 (100 K)	157
CH_3NH_3/Bi/Br	$P\bar{3}m1 \rightarrow$? (ferroelastic) → ? (ferroelastic) → ? (ferroelectric)	188, 140, 104	0.06 (100 K)	158
$(CH_3)_4P$/Sb/Cl	? → $P31c$ →? (ferroelastic)	534 (continuous), 135 (discontinuous)	0.050 (just below 135 K)	159
$(CH_3)_4P$/Bi/Cl	? → $P31c$ →? (ferroelastic)	550 (continuous), 151 (discontinuous)	0.012 (just below 151 K)	159
$(CH_3)_4P$/Sb/Br	? → $P31c$ →? (ferroelastic)	540 (continuous), 193 (discontinuous)	0.003 (just below 193 K)	159
$(CH_3)_4P$/Bi/Br	? → $P31c$ →? (ferroelastic)	550 (continuous), 205 (discontinuous)	0.001 (just below 205 K)	159

group change was proposed, that is, from the paraelectric cubic $Pa\bar{3}$ to the ferroelectric orthorhombic $Pca2_1$.[119]

The symmetry-breaking process can be described as follows: the space group $P2_13$ (No. 198) in the paraelectric phase includes two maximal nonisomorphic subgroups, $R3$ and $P2_12_12_1$, while the maximal nonisomorphic subgroups of $P2_12_12_1$ include $P2_1$ only. Therefore, the symmetry-breaking process abides by the Curie symmetry principle (Figure 47a). Alternatively, the paraelectric $Pa\bar{3}$ (No. 205) covers three subgroups, $P2_13$, $R\bar{3}$, and $Pbca$. The maximal nonisomorphic subgroups of $Pbca$ include $Pca2_1$, $P2_12_12_1$, and $P2_1/c$. Thus, the Curie symmetry principle is also obeyed (Figure 47b).

In the crystal structure, the Al^{3+} ion is coordinated with six water molecules in a nearly octahedral arrangement (Figure 48). The other six water molecules link the sulfate tetrahedron, the $Al(H_2O)_6$ octahedron, and the methylammonium.

The dielectric constant of $[CH_3NH_3][Al(H_2O)_6](SO_4)_2 \cdot 6H_2O$ at T_c shows a sharp discontinuity, indicating a first-order transition (Figure 49a). Fitting the Curie−Weiss law in a narrow temperature interval (6 K) affords the T_0 of 168.5 K and the C_{para} of 500 K. It is found that the alums exhibit relatively small values of dielectric constants at the Curie points.

The E_c increases rapidly with decreasing temperature so that the saturated hysteresis loop can be only observed in the temperature range of ~15 K (Figure 49b). There is no isotope effect. The selenates show higher transition temperatures than the sulfates (Table 2).

6.4. $[H_2dbco][Cu(X_2O)_6](SeO_4)_2$ (X = H or D)

Recently, Xiong and co-workers reported a new ferroelectric compound, $[H_2dbco][Cu(X_2O)_6](SeO_4)_2$ (H_2dbco = diprotonated 1,4-diazabicyclo[2.2.2]octane, X = H or D).[120] A paraelectric-to-ferroelectric phase transition was found at ~133 K by DSC and dielectric constant measurements.

At room temperature, the crystal adopts a centrosymmetric space group $P2_1/c$. The H_2dbco cation is seriously disordered whereas the $Cu(H_2O)_6$ cation is an octahedron (Figure 50). Below 133 K, a new phase appears. The crystal structural discloses the disappearance of the mirror plane and results in a polar space group $P2_1$. It is a continuous second-order phase transition. The symmetry-breaking process is similar to the cases of $[Ag(NH_3CH_2COO)(NO_3)]$ and $[(CH_3)_2NH_2][Ga(H_2O)_6](SO_4)_2$.

From electric hysteresis loop measurement, the P_r is 1.02 $\mu C \cdot cm^{-2}$ and the P_s is 1.51 $\mu C \cdot cm^{-2}$, recorded approximately along the b axis. The E_c is 1.5 $kV \cdot cm^{-1}$. No isotope effect was observed in this case, suggesting the ferroelectricity in the alum analogue may originate not from the hydrogen bond but from the order−disorder changes of the H_2dbco cation.

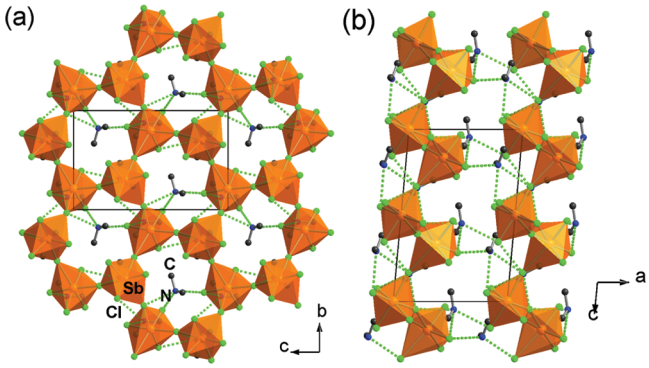

Figure 65. Crystal structure of $[(CH_3)_2NH_2]_3[Sb_2Cl_9]$ at 100 K. Green dotted lines represent hydrogen bonds.

7. HALOGENOMETALLATE FAMILY

Halogenometallate compounds, $A_y[M_mX_n]$ where A is protonated amine or its analogues, M is metal ion, and X is Cl, Br, or I anion, constitute a large family of organic−inorganic hybrid ferroelectrics with diverse structures and phase transition properties.[121]

7.1. $A_2[MX_4]$ Family

$A_2[MX_4]$ type crystals (A = organic cation, M = metal ion, X = halide) were grown by evaporation methods from the aqueous solutions of AX and MX_2 compounds in an appropriate molar ratio. To discrete $[(CH_3)_4N]_2[MX_4]$ type compounds (M = divalent Mn, Fe, Co, Cu or Zn; X = Cl, Br or I), they belong to the orthorhombic K_2SO_4 (II)-type structure with the space group $Pmcn$ in their high-temperature normal (prototype) phases. Upon cooling, they exhibit first an incommensurate phase and then ferroelectric and/or ferroelastic commensurate phases (Table 3). In the crystals, the $(CH_3)_4N$ and MX_4 ions adopt tetrahedral geometries. In the case of $[(CH_3)_4N]_2[ZnI_4]$, the $N(CH_3)_4$ cation suffers disorder in the paraelectric phase and becomes ordered in the ferroelectric phase (Figure 51).

$[(CH_3)_4N]_2[FeCl_4]$ and $[(CH_3)_4N]_2[MnCl_4]$ exhibit ferroelectricity in narrow temperature ranges at high pressures.[122] $[(CH_3)_4N]_2[CuCl_4]$ undergoes a ferroelastic phase transition at ~291 K and atmospheric pressure.[123,124]

dx.doi.org/10.1021/cr200174w |Chem. Rev. 2012, 112, 1163–1195

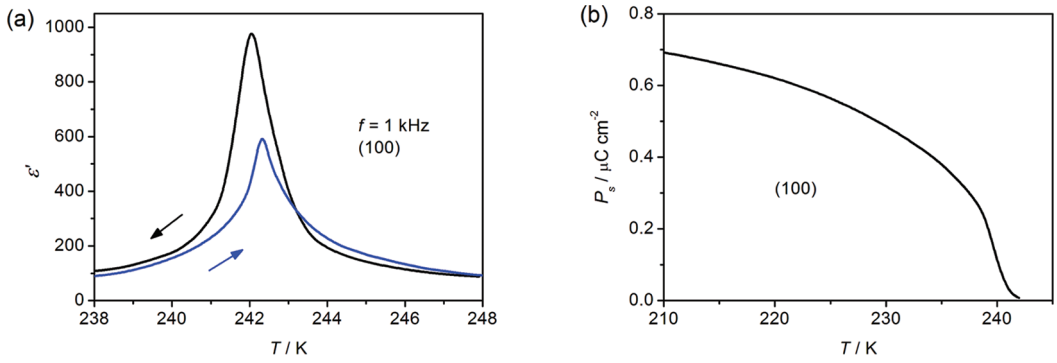

Figure 66. (a) Temperature dependence of dielectric constant, and (b) P_s versus T curve of $[(CH_3)_2NH_2]_3[Sb_2Cl_9]$.

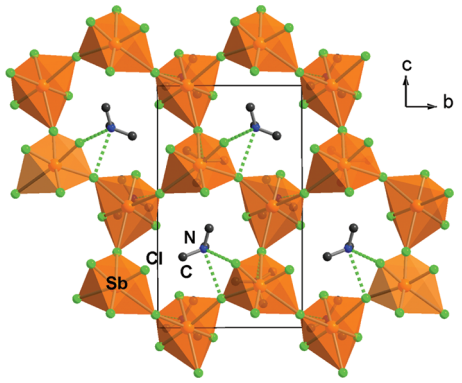

Figure 67. Crystal structure of $[(CH_3)_3NH]_3[Sb_2Cl_9]$ at 165 K. Green dotted lines represent hydrogen bonds.

When the protonated amine is dimethylammonium, there appear two compounds, $[(CH_3)_2NH_2]_2[CoCl_4]$ and $[(CH_3)_2NH_2]_2[ZnCl_4]$. Ferroelectricity in $[(CH_3)_2NH_2]_2[CoCl_4]$ was mentioned by Vasil'ev and co-workers in 1987.[130] It is grown from the aqueous solution containing a stoichiometric molar ratio of $[(CH_3)_2NH_2]Cl$ and $CoCl_2$ as hygroscopic dark blue crystals. At room temperature, the compound crystallizes in the monoclinic space group $P2_1/n$ (Figure 52). However, symmetry of the ferroelectric phase is not well-defined. It undergoes several phase transitions in the temperature range of 200−430 K. The similar compound $[(CH_3)_2NH_2]_2[ZnCl_4]$ crystallized in the monoclinic space group $P112_1/n$ at room temperature. Its phase sequence has not been established.[131]

Dimethylammonium copper chloride shows richer structural variations than its counterparts. It was reported first as $[(CH_3)_2NH_2]_2[CuCl_4]$ but later corrected as $[(CH_3)_2NH_2]_3[CuCl_4]Cl$.[132,133] The crystal structure of $[(CH_3)_2NH_2]_3[CuCl_4]Cl$ at room temperature shows that the chloride ions and anions are disordered. Dielectric constant measurements exhibit successive first-order phase transitions at 279 and 253 K with thermal hystereses of 6 and 7 K, respectively (Figure 53). The steplike shape of the dielectric constant probably suggests it is an improper ferroelectric. The high-temperature phase has the orthorhombic space group *Pnam*. The intermediate-temperature phase is ferroelectric with a P_s of 3.4 $\mu C \cdot cm^{-2}$.

Compound $[CH_3NH_3]_2[ZnCl_4]$ crystallizes in a monoclinic system with a space group of $P2_1/c$ at room temperature.[134,135] DSC and dielectric studies reveal the presence of successive phase transitions at ~483 and 555 K. The high value of the dielectric constant indicates the potential ferroelectricity of this compound.[136]

$[C_2H_5NH_3]_2[CuCl_4]$ belongs to a family of $[C_nH_{2n+1}NH_3]_2[MCl_4]$ where M is divalent Mn, Cd, Fe, or Cu.[137−140] Depending on the length of the organic chains, different structures and chain packings can be realized. These compounds recently have attracted attention because of their great varieties of structural and magnetic phases, which bring up an opportunity to explore multiferroic properties.

$[C_2H_5NH_3]_2[CuCl_4]$ shows a perovskite-type layer structure. In the crystal structure, there are infinite layers of corner-sharing Jahn−Teller distorted $CuCl_6$ octahedra with layers of ethylammonium groups attached to each side (Figure 54).[141] The ethylammonium heads form strong hydrogen bonds to all of the eight chloride ions. The hydrogen-bonding interaction exerts an effect on the temperature evolution of the structural phase transitions in the compound.

$[C_2H_5NH_3]_2[CuCl_4]$ undergoes a series of structural phase transitions: triclinic (T_4 = 232 K) → *Pbca* (T_3 = 330 K) → rhombic (T_2 = 356 K) → $P2/c$ (T_1 = 364 K) → *Bbcm*. A dielectric anomaly is found around T_5 = 247 K, accompanied with a color change. Both the broad shape and the maximum value of ε' at 247 K indicate the characteristic of an improper ferroelectric phase transition (Figure 55a). The phase transition at 247 K is of second-order type. The P_s develops below 247 K and is 18 $\mu C \cdot cm^{-2}$ at 200 K (Figure 55b). Ferroelectric origin may be ascribed to ordering of the organic $[C_2H_5NH_3]^+$. It is a common feature in $[C_nH_{2n+1}NH_3]_2[MCl_4]$ perovskites that the organic chain of the $-NH_3$ group flips among four equivalent orientations inside the cavity formed by the $CuCl_6$ octahedra.

Interestingly, $[C_2H_5NH_3]_2[MCl_4]$ shows ferromagnetic interactions with a magnetic phase transition at T_c =10.2 K. In a wide temperature range, it shows characteristics of a 2D Heisenberg ferromagnet with a dominant intralayer exchange coupling J/k_B = 18.6 K for spins at the nearest-neighbor Cu sites.[142,143]

7.2. A[MX$_3$] Family

Ferroelectricities in the family of $A[MX_3]$ were reported where A is $[(CH_3)_4N]$ or $[(CH_3)_4P]$ cation, M is divalent Cd or Hg, and X is Cl, Br, or I anion. Ferroelectricity in $[(CH_3)_4N][CdBr_3]$ was found by Gesi in 1990.[144] The compound crystallizes in the hexagonal space group $P6_3/m$ at room temperature. In the structure the 1D chains of $[CdBr_3]$ are along the *c* axis and the $[(CH_3)_4N]^+$ tetrahedra are orientationally disordered (Figure 56). $[(CH_3)_4N][CdBr_3]$ undergoes a structural phase transition from a disordered room-temperature phase to an ordered

dx.doi.org/10.1021/cr200174w |*Chem. Rev.* 2012, 112, 1163–1195

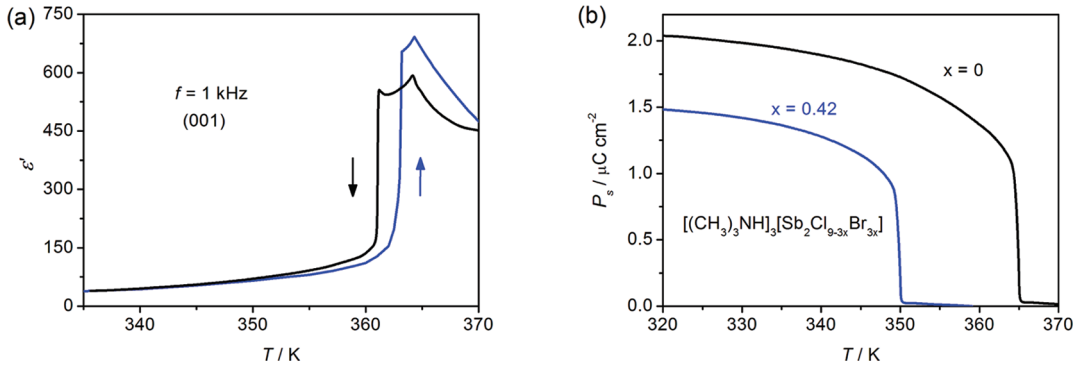

Figure 68. (a) Temperature dependence of the dielectric constant of $[(CH_3)_3NH]_3[Sb_2Cl_9]$, and (b) P_s versus T curve of $[(CH_3)_3NH]_3[Sb_2Cl_{9-3x}Br_{3x}]$ (x = 0 and 0.42).

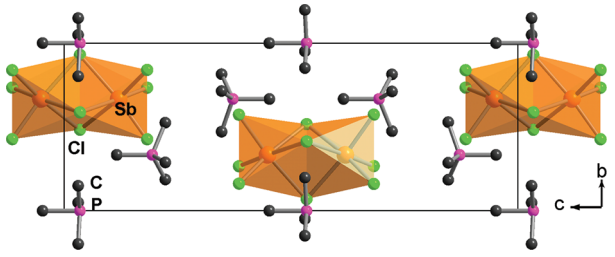

Figure 69. Crystal structure of $[(CH_3)_4P]_3[Sb_2Cl_9]$ at 293 K.

low-temperature phase with a ferroelectric space group $P6_1$ below 156 K.[145,146] The $[(CH_3)_4N]^+$ tetrahedra are ordered in the ferroelectric phase. The symmetry-breaking process here does not abide by the Curie principle because the maximal nonisomorphic subgroups of the paraelectric $P6_3/m$ (No. 167) include $P\bar{6}$, $P6_3$, $P\bar{3}$, and $P2_1/m$ but without $P6_1$, suggesting this phase transition is probably complex (Figure 57).

The temperature dependence of the dielectric constant of $[(CH_3)_4N][CdBr_3]$ shows a slight λ-type maximum along the c direction and a discontinuity along the a direction at 156 K. The change of the dielectric constant at the T_c is only ~20%. Ferroelectricity develops below the T_c. The P_s is 0.10 $\mu C \cdot cm^{-2}$ at 135 K (Figure 58). The ferroelectric transition is closely related to an orientational order−disorder process of the $[(CH_3)_4N]^+$ tetrahedra. The analogue compound $[(CH_3)_4N][CdCl_3]$, however, exhibits no ferroelectricity down to liquid nitrogen temperature.

The mercury counterparts, $[(CH_3)_4N][HgX_3]$ (X = Cl, Br, or I) and $[(CH_3)_4P][HgBr_3]$, were found to show ferroelectricities up to their decomposition temperatures.[147,148] They crystallized in polar space groups such as $P2_1$ or $Pb2_1m$ at room temperature. In the crystal structures, the 1D HgX_3 chains are separated by the discrete $[(CH_3)_4N]^+$ or $[(CH_3)_4P]^+$ ions (Figure 59). Their dielectric constants are between 10 and 60 at room temperature and almost independent of the temperature. The P_s values for these compounds are in the range 1−3 $\mu C \cdot cm^{-2}$. To $[(CH_3)_4N][HgBrI_2]$, it undergoes a paraelectric-to-ferroelectric phase transition at 375 K.[149] The dielectric constant shows a striking anomaly along the c axis with a peak value of 63 at the T_c.

7.3. $A_m[M_nX_{3n+m}]$

Halogenoantimonates(III) and halogenobismuthates(III), $A_m[M_nX_{3n+m}]$ where A is organic cation, M is Sb^{3+} or Bi^{3+}, and X is Cl, Br, or I anion, constitute an attracting family of ferroelectric and/or ferroelastic compounds, showing multiple structural phase transitions. They are ionic crystals with anionic sublattices that are composed of deformed MX_6 octahedra either isolated or connected with neighboring octahedra by corners, edges, or faces. The organic cations locate in the anionic cavities and are believed to be responsible for the ferroelectric ordering in most cases.

7.3.1. $[4\text{-}NH_2PyH][SbCl_4]$. 4-Aminopyridinium tetrachloroantimonate(III), $[4\text{-}NH_2PyH][SbCl_4]$, is a ferroelectric compound.[150] It was prepared from the aqueous solution of $[4\text{-}NH_2PyH]Cl$ and Sb_2O_3 in an equimolar ratio and excessive HCl.

$[4\text{-}NH_2PyH][SbCl_4]$ undergoes a complex sequence of phase transitions. A brief phase diagram can be shown as $P2_1/c$ (<240 K) → Cc → $C2/c$ (>271 K). In the temperature region of 240−271 K, it is in the ferroelectric phase with a monoclinic space group Cc. The symmetry-breaking process obeys the Curie principle in the temperature range: the maximal nonisomorphic subgroups of the paraelectric $C2/c$ include Cc, $C2$, and $P\bar{1}$ (Figure 60).

Its structure is composed of 1D $SbCl_4$ chains via chloride linkages along the c axis (Figure 61). The organic cation $[4\text{-}NH_2PyH]^+$ is disordered and distributed between two positions with equal occupation factors at room temperature. It becomes ordered and occupies only one position in the ferroelectric phase.

Dielectric constant measurement shows that a striking anomaly with a peak value of ~650 appears in the [102] direction at the T_c and 100 Hz (Figure 62). According to the Curie−Weiss law, the fitted T_0 is 270.5 K and the C_{para} is 48 K. The P_s keeps almost constant with a value of 0.35 $\mu C \cdot cm^{-2}$ in the temperature region of 250−270 K.

Replacement of the Cl ions by the Br ones greatly changes the physical properties of the mixed crystal $[4\text{-}NH_2PyH][SbCl_{4(1-x)}Br_{4x}]$ (x = 0−1).[151] The ferroelectric properties are preserved when the x is <0.30. However, the substitution significantly lowers the temperature of the structural phase transition, i.e., from 240 K for the pure $[4\text{-}NH_2PyH][SbCl_4]$ to ~185 K for the mixed crystal.

7.3.2. [MV][BiBr$_5$]. Compound $[MV][BiBr_5]$ (MV = methylviologen dication) was reported to show ferroelectric and semiconducting properties.[152] $[MV][BiBr_5]$ was synthesized by solvothermal method from a mixture of $BiBr_3$, 4,4′-bipyridine, and concentrated HBr in methanol. The MV^{2+} cation is in situ formed.

The compound crystallizes in the monoclinic space group $P2_1/c$ at room temperature. At 233 K, the space group turns to polar $P2_1$. The symmetry-breaking process is similar to the cases of $[Ag(NH_3CH_2COO)(NO_3)]$, $[(CH_3)_2NH_2][Ga(H_2O)_6](SO_4)_2$, and $[H_2dbco][Cu(X_2O)_6](SeO_4)_2$ (X = H or D). In the crystal

dx.doi.org/10.1021/cr200174w |Chem. Rev. 2012, 112, 1163–1195

Table 5. Properties of Ferroelectric $A_5[M_2X_{11}]$

A/M/X	symmetry change upon cooling	phase transition temperatures/K	$P_s/\mu C\cdot cm^{-2}$	ref
CH_3NH_3/Bi/Cl	$Pcab \rightarrow Pca2_1 \rightarrow P2_1 \rightarrow P2_1$	307, 250, 170	0.86 (285 K)	164, 165
CH_3NH_3/Bi/Br	$Pcab \rightarrow Pca2_1 \rightarrow P2_1$	312, 77	0.70 (285 K)	166
imidazolium/Sb/Br	$P\bar{4}n2$ (?) $\rightarrow P2_1/n \rightarrow Pn \rightarrow Pn$	353, 145, 120	0.18 (137 K)	167
imidazolium/Bi/Cl	$P\bar{4}n2 \rightarrow P2_1/n \rightarrow P2_1$	360, 165	0.6 (100 K)	168
imidazolium/Bi/Br	$? \rightarrow P2_1/n \rightarrow Pn$	355, 155	0.26 (130 K)	169
pyridinium/Bi/Br	$P2_1/n \rightarrow P2_1$	118	0.3 (105 K)	170

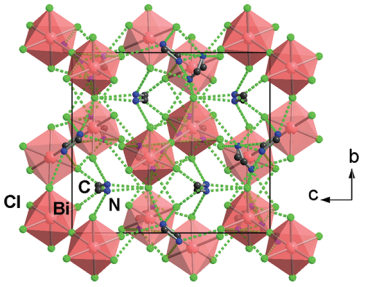

Figure 70. Crystal structure of $[CH_3NH_3]_5[Bi_2Cl_{11}]$ at 293 K. Green dotted lines represent hydrogen bonds.

structure, the 1D $BiBr_5$ regular chain adopts an unprecedented trans-connected mode and propagates along the *a* axis (Figure 63). The chains are separated by planar methylviologen dications.

Dielectric constant measurements clearly show anomalies at 243 K (Figure 64), confirming the occurrence of a phase transition. However, further evidence is needed to confirm the real ferroelectricity in this compound.

7.3.3. $A_3[M_2X_9]$. $A_3[M_2X_9]$ type compounds exhibit interesting ferroic properties such as ferroelectricity and ferroelasticity (Table 4). It is found that ferroelectric properties are strictly connected with the crystals having 2D layers of polyanionic M_2X_9 units, which may be inhibited by large bulky cations. Structural phase transitions in these crystals are governed by ordering of the organic cations.

Ferroelectric activity in $[(CH_3)_2NH_2]_3[Sb_2Cl_9]$ was reported by Jakubas in 1986.[153] It crystallizes in a monoclinic space group $P2_1/c$ at room temperature and adopts a ferroelectric space group *Pc* below 242 K. The symmetry-breaking process is similar to the case of $[(CH_3)_2NH_2][Al(H_2O)_6](SO_4)_2$. In the crystal structure the deformed $[SbCl_6]^{3-}$ octahedra connect with each other by corners to form 2D anionic layers parallel to the *bc* plane (Figure 65). There are two crystallographically nonequivalent, disordered $[(CH_3)_2NH_2]^+$ cations in the asymmetric unit cell. One is located at the center of symmetry inside the polyanionic cavities whereas the other is located at the general position between the layers. They form hydrogen bonds with the chloride ions. Low-temperature structure studies reveal that the phase transition is accompanied by distinct deformation of both the hydrogen-bond system and the polyanionic layers, which is probably one of the main reasons for the appearance of the ferroelectricity in $[(CH_3)_2NH_2]_3[Sb_2Cl_9]$.

Dielectric constant of $[(CH_3)_2NH_2]_3[Sb_2Cl_9]$ near the T_c at low frequency displays a classic critical slowing down characteristic of a second-order phase transition (Figure 66). The ferroelectric phase transition at 242 K is of order−disorder type and associated with changes in the dynamics of the $[(CH_3)_2NH_2]^+$ cations.[160]

The Br analogue $[(CH_3)_2NH_2]_3[Sb_2Br_9]$ is isomorphous to the Cl one. It undergoes a ferroelectric phase transition at 164 K, showing characteristics of first-order type.[155] Its ferroelectric-to-paraelectric phase transitions is also due to the freezing of one type of the $[(CH_3)_2NH_2]^+$ cations.

Ferroelectric activity of $[(CH_3)_3NH]_3[Sb_2Cl_9]$ was reported by Jakubas and co-workers in 1986.[156] The compound undergoes various phase transitions. Below 363 K, it is a ferroelectric down to the liquid helium with a space group of *Pc*.[160]

$[(CH_3)_3NH]_3[Sb_2Cl_9]$ shows a 2D layer structure where the 2D anionic layers are parallel to the *bc* plane (Figure 67). The cations are disordered in the paraelectric phase and ordered in the ferroelectric phase. There are hydrogen bonds between the N atoms of the cations and the chloride ions.

There are two dielectric anomalies at 363 and 364 K. The latter is independent of the direction of temperature changes, but the former exhibits an appreciable thermal hysteresis (Figure 68a). The P_s versus T curve of $[(CH_3)_3NH]_3[Sb_2Cl_9]$ is typical of a first-order phase transition. At the T_c an almost stepwise change in the polarization is observed. The replacement of chloride ions by bromide ions in the lattice of $[(CH_3)_3NH]_3[Sb_2Cl_9]$ causes a reduction of the P_s value, i.e., from $\sim 2\ \mu C\cdot cm^{-2}$ for the pure $[(CH_3)_3NH]_3[Sb_2Cl_9]$ to 1.5 $\mu C\cdot cm^{-2}$ for $[(CH_3)_3NH]_3[Sb_2Cl_{9-3x}Br_{3x}]$ ($x = 0.42$) (Figure 68b).[162] For the pure Br analogue $[(CH_3)_3NH]_3[Sb_2Br_9]$, its structure is built up by discrete Sb_2Br_9 bioctahedra and disordered trimethylammonium cations. This means the 2D polyanionic layers are indispensable for the ferroelectricity in these compounds.

Compounds $[(CH_3)_4P]_3[M_2X_9]$ (M = trivalent Sb or Bi cation; X = Cl or Br anion) belong to weak ferroelectrics.[159] In the structure the asymmetric unit consists of one discrete bioctahedral $[M_2X_9]^{3-}$ anion and three symmetrically inequivalent disordered $[(CH_3)_4P]^+$ cations (Figure 69). They undergo two phase transitions, and the low-temperature phases are ferroelectric (Table 4). Dielectric constants show very small changes at the phase transition points. The P_s values are of the order of $1 \times 10^{-2}\ \mu C\cdot cm^{-2}$, being characteristic of weak ferroelectric crystals.

When A is methylammonium in $A_3[M_2X_9]$, there are two ferroelectric compounds, $[CH_3NH_3]_3[Sb_2Br_9]$ and $[CH_3NH_3]_3[Bi_2Br_9]$.[157,158] Both compounds undergo transitions from high-temperature paraelectric phases to intermediate-temperature ferroelastic phases to low-temperature ferroelectric phases (Table 4). They crystallize in the trigonal space group $P\bar{3}m1$ at room temperature. In the crystal structures, the 2D anionic layers are parallel to the *bc* plane.

Change in dynamic state of the methylammonium cations corresponds to the phase transitions. In $[CH_3NH_3]_3[Sb_2Br_9]$, freezing of rotational motion of the cations in the C−N axis at 168 and 134 K leads to a stepwise decrease of the dielectric

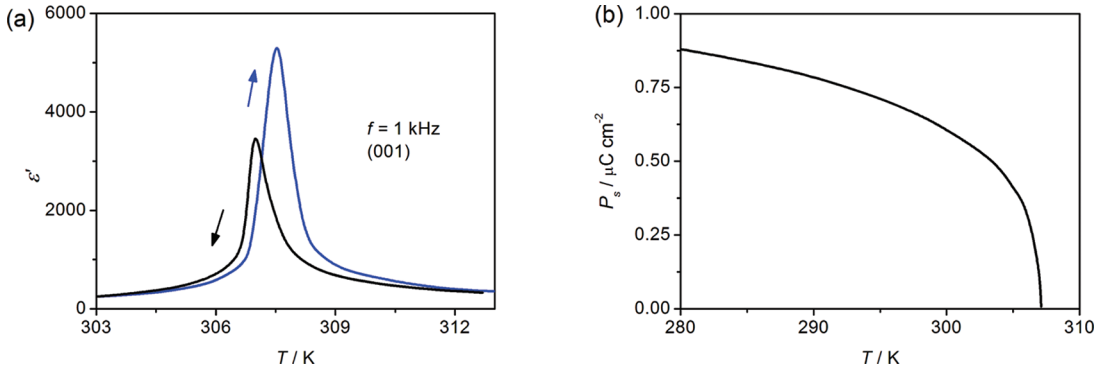

Figure 71. (a) Temperature dependence of dielectric constant, and (b) P_s versus T curve of $[CH_3NH_3]_5[Bi_2Cl_{11}]$.

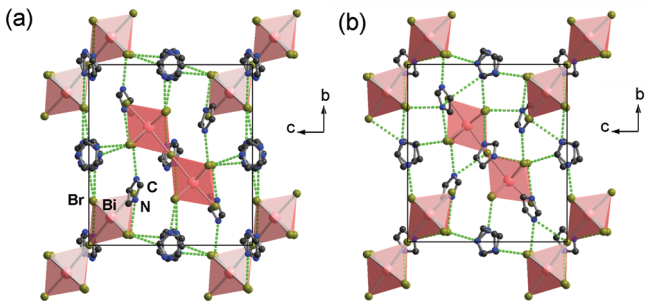

Figure 72. Crystal structures of $[Im]_5[Bi_2Br_{11}]$ at (a) 170 K and (b) 100 K. Green dotted lines represent hydrogen bonds.

constant when the phase transition is crossed. A mechanism of the phase transition at 134 K is suggested to include both order−disorder and displacive contributions.[163]

7.3.4. $A_5[M_2X_{11}]$. In contrast to $A_3[M_2X_9]$ compounds, ferroelectric system $A_5[M_2X_{11}]$ shows completely different structural changes (Table 5). Instead of polyanionic structure, there appear isolated M_2X_{11} bioctahedra. In the discrete bimetallate anions, two octahedra are connected with each other by one bridging halogen atom, showing high structural flexibility. Dynamics of the organic cations governs the order−disorder-type ferroelectric phase transitions in $A_5[M_2X_{11}]$. The M_2X_{11} counterions may also play a role in generation of ferroelectric properties due to an enhanced polarizability of the anionic sublattice or effect of lone-pair electrons of the M^{3+} ion.

$[CH_3NH_3]_5[Bi_2Cl_{11}]$ and $[CH_3NH_3]_5[Bi_2Br_{11}]$ are isomorphous ferroelectric compounds.[164,166] In the crystal structures, the bioctahedral units Bi_2Cl_{11} or Bi_2Br_{11} build the anionic sublattices (Figure 70). At room temperature, $[CH_3NH_3]_5[Bi_2Cl_{11}]$ crystallizes in the orthorhombic space group $Pca2_1$. There are three types of organic cations. The phase transition is of second-order and related to ordering of one type of the methylammonium cations. Crystal structure analysis reveals that the phase transition is accompanied by a distinct distortion of the $[Bi_2Cl_{11}]^{5-}$ anions.

The dielectric constant of $[CH_3NH_3]_5[Bi_2Cl_{11}]$ along the c axis exhibits a great anomaly with a peak value of $\sim 5 \times 10^3$ at 307 K and 1 kHz (Figure 71). The Curie−Weiss law is well obeyed in the narrow range of the T_c. The C_{para} and C_{ferro} are equal to 1.38×10^3 and 0.36×10^3 K, respectively, to give a C_{para}/C_{ferro} ratio of 3.83, suggesting this phase transition is of second order. $[CH_3NH_3]_5[Bi_2Br_{11}]$ shows similar dielectric behaviors. $[CH_3NH_3]_5[Bi_2Cl_{11}]$ is ferroelectric below 307 K, and $[CH_3NH_3]_5[Bi_2Br_{11}]$ is ferroelectric below 311 K. Phase transitions in both crystals are of order−disorder type.[165] Their P_s values are 0.86 and 0.70 $\mu C \cdot cm^{-2}$ at 285 K, respectively.

When A is imidazolium (Im), there are three ferroelectric compounds, $[Im]_5[Bi_2Cl_{11}]$, $[Im]_5[Bi_2Br_{11}]$, and $[Im]_5[Sb_2Br_{11}]$. Taking $[Im]_5[Bi_2Br_{11}]$, for example, it crystallizes in a monoclinic space group $P2_1/n$ at room temperature.[169] There are four kinds of nonequivalent imidazolium cations (Figure 72). Two cations are in general positions and ordered, and the other three are on an inversion center and show significant dynamic disorders. Quite weak N−H···Cl hydrogen bonds exist between the imidazolium cations and the distorted $[Bi_2Br_{11}]^{5-}$ bioctahedra.

$[Im]_5[Bi_2Cl_{11}]$ undergoes two phase transitions, that is, a first-order paraelastic-to-ferroelastic one at 360 K and a second-order one at 165 K to the ferroelectric phase.[171] The dielectric constant of $[Im]_5[Bi_2Cl_{11}]$ shows an anomaly with a value of ~450 along the b axis at 166 K and 100 Hz (Figure 73). The ratio of C_{para}/C_{ferro} equals 2.6 and is characteristic of the second-order ferroelectric transition. The P_s value is 0.6 $\mu C \cdot cm^{-2}$ at 100 K. The polarization predominately originates from ordering of the strongly dipolar imidazolium cations.

The Br analogues $[Im]_5[Bi_2Br_{11}]$ and $[Im]_5[Sb_2Br_{11}]$ are isostructural to $[Im]_5[Bi_2Cl_{11}]$ and show similar phase transition behaviors.[167,169] For example, the dielectric constant of $[Im]_5[Bi_2Br_{11}]$ reaches a peak value of ~420 at T_c = 155 K with a C_{para}/C_{ferro} value of 1.8, indicating the phase transition is also of second order. The P_s value is ~0.26 $\mu C \cdot cm^{-2}$ at 130 K. In both $[Im]_5[Bi_2Cl_{11}]$ and $[Im]_5[Bi_2Br_{11}]$, there is a process of dielectric critical slowing down over the paraelectric phases, which is characteristic of order−disorder ferroelectric phase transitions.[172] This is also found in $[Im]_5[Sb_2Br_{11}]$ and $[PyH]_5[Bi_2Br_{11}]$ (PyH = pyridinium).[173]

$[PyH]_5[Bi_2Br_{11}]$ is a similar compound to the Im analogues.[170] In the crystal structure there are isolated Bi_2Br_{11} units and four independent disordered pyridinium cations. It undergoes a phase transition at 118 K from the paraelectric space group $P2_1/n$ to the ferroelectric space group $P2_1$. Dielectric dispersion studies in the radio frequency region disclosed two relaxational modes in the paraelectric phase. The P_s is 0.3 $\mu C \cdot cm^{-2}$ at 100 K.

7.4. Miscellaneous Compounds

7.4.1. $[H_2dbco]_2[CuCl_3(H_2O)_2]Cl_3 \cdot H_2O$. $[H_2dbco]_2[CuCl_3(H_2O)_2]Cl_3 \cdot H_2O$ undergoes a paraelectric-to-ferroelectric phase transition at 235 K.[174]

It crystallizes in the orthorhombic space group $Pnma$ at room temperature. There are two $[H_2dbco]^{2+}$ cations, a discrete

dx.doi.org/10.1021/cr200174w |Chem. Rev. 2012, 112, 1163–1195

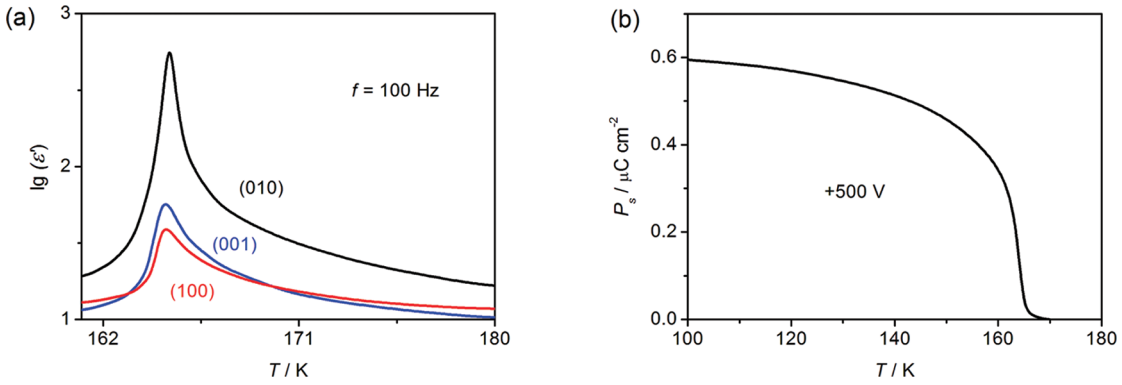

Figure 73. (a) Temperature dependence of dielectric constant, and (b) P_s versus T curve from the pyroelectric effect of $[Im]_5[Bi_2Cl_{11}]$.

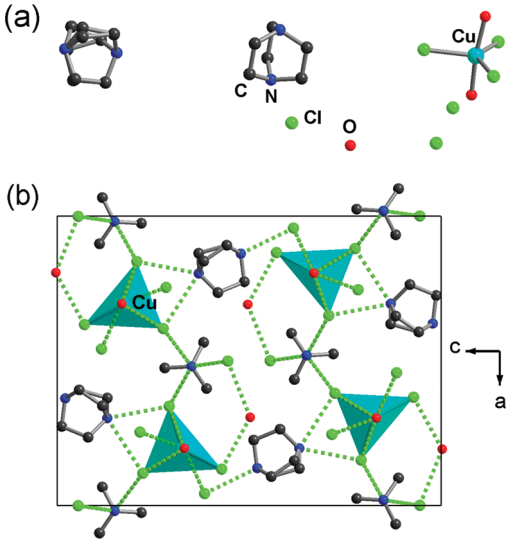

Figure 74. (a) Asymmetric unit and (b) packing structure of $[H_2dbco]_2[CuCl_3(H_2O)_2]Cl_3 \cdot H_2O$ at 293 K. Green dotted lines represent hydrogen bonds.

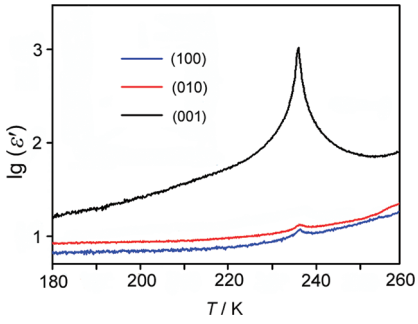

Figure 75. Temperature dependence of dielectric constant of $[H_2dbco]_2[CuCl_3(H_2O)_2]Cl_3 \cdot H_2O$.

distorted trigonal bipyramidal $[CuCl_3(H_2O)_2]^-$ anion, three Cl^- anions, and one lattice H_2O molecule in the asymmetric unit (Figure 74). Hydrogen bonds exist among these groups. It is notable that one of the two $[H_2dbco]^{2+}$ cations is disordered. At 193 K, the crystal still belongs to an orthorhombic crystal system but with the noncentrosymmetric space group $Pna2_1$. The disordered

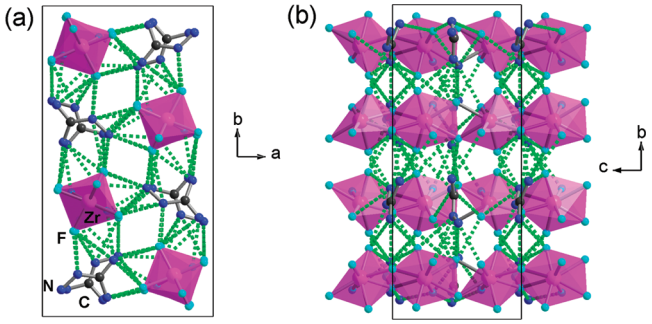

Figure 76. Crystal structure of $[CN_4H_8]ZrF_6$ at 293 K. Green dotted lines represent hydrogen bonds.

$[H_2dbco]^{2+}$ cation becomes ordered. The symmetry-breaking process is similar to the case of $[Ca(CH_3NH_2CH_2COO)_3X_2]$ (X = Cl, Br) where the maximal nonisomorphic subgroups of the paraelectric *Pnma* include $Pna2_1$, $Pmn2_1$, $Pmc2_1$, $P2_12_12_1$, $P2_1/c$, and $P2_1/m$, abiding by the Curie symmetry principle.

Temperature-dependent dielectric constant measurement along the polar axis shows a pronounced anomaly with a peak value >2000 at 1 kHz (Figure 75). Fitted with the Curie–Weiss law, the C_{para}/C_{ferro} ratio is 0.81 and the T_0 is equal to the T_c, indicating a typical feature of a second-order phase transition. The dielectric hysteresis loop of the compound is clearly observed with a P_s of 1.0 $\mu C \cdot cm^{-2}$ and an E_c of 5 $kV \cdot cm^{-1}$ at 153 K. The isotopic effect is apparent, that is, after deuteration, the value of P_s displays an enhancement of 30% from 1.0 to 1.3 $\mu C \cdot cm^{-2}$.

7.4.2. $[CN_4H_8][ZrF_6]$. Aminoguanidinium hexafluorozirconate, $[CN_4H_8]ZrF_6$, was predicted and confirmed as a ferroelectric compound.[175,176] Pure $[CN_4H_8]ZrF_6$ was prepared from the starting materials of aminoguanidine bicarbonate, $ZrF_4 \cdot 3H_2O$, and 51% HF aqueous solution.

At room temperature, the compound crystallizes in an orthorhombic space group *Pba*2. In the crystal structure, there are 1D chains of slightly distorted edge-sharing ZrF_8 dodecahedra along the *c* axis (Figure 76). Multiple hydrogen bonds connect the $[CN_4H_8]^{2+}$ cations and the dodecahedra. Displacements of the cations are expected as the origin of the ferroelectricity.

C_p and dielectric anomalies reveal a phase transition at T_c = 383 K. Entropy change is 0.7 $J \cdot mol^{-1} \cdot K^{-1}$. Dielectric anomaly at the T_c is observed only at the lowest measuring frequency (0.1 kHz). The dielectric hysteresis loop is well recorded at 295 K

dx.doi.org/10.1021/cr200174w |*Chem. Rev.* 2012, 112, 1163–1195

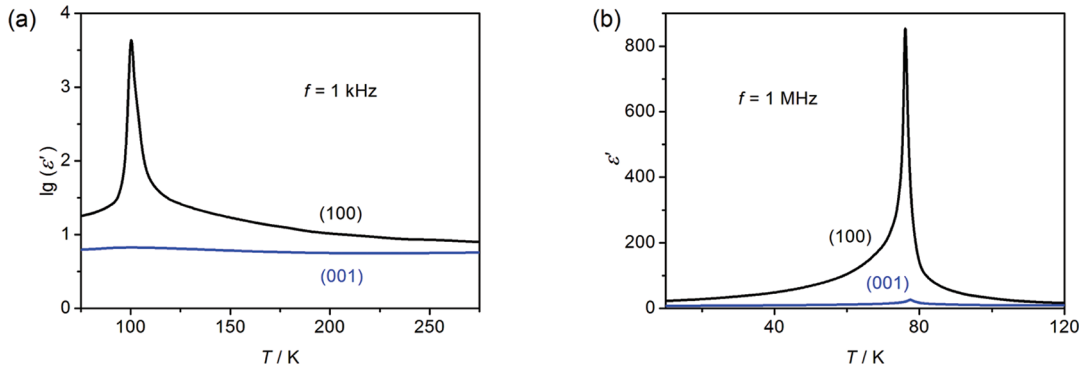

Figure 77. Temperature dependence of dielectric constants of (a) $[CH_3NH_3]_2[Al(H_2O)_6]Cl_5$ and (b) $[CH_3NH_3]_2[Al(H_2O)_6]Br_5$.

with a P_s of ~0.45 $\mu C \cdot cm^{-2}$. It remains observable below T_c but not above T_c, confirming the ferroelectricity.

7.4.3. $[CH_3NH_3]_2[Al(H_2O)_6]X_5$ (X = Cl, Br). The two compounds had been believed to be $[CH_3NH_3][AlX_4]$ (X = Cl, Br) and later were revised to be $[CH_3NH_3]_2[Al(H_2O)_6]X_5$ (X = Cl, Br).[177,178] $[CH_3NH_3]_2[Al(H_2O)_6]Cl_5$ crystallizes in the tetragonal space group $I4$ at room temperature.[179] It undergoes a paraelectric-to-ferroelectric phase transition at T_c = 100 K. The dielectric constant shows a sharp λ-type peak at the T_c along the a axis (Figure 77a). It obeys the Curie−Weiss law above the T_c with a C_{para} of 700 K. P_s is measured along the a axis with a value of 0.6 $\mu C \cdot cm^{-2}$ at 80 K. These results indicate the phase transition is of second order.

$[CH_3NH_3]_2[Al(H_2O)_6]Br_5$ is isostructural to the Cl analogue.[180] It crystallizes in the tetragonal space group $I4/mmm$ at room temperature. It undergoes a paraelectric-to-ferroelectric phase transition at T_c = 76.6 K. Besides the ferroelectric transition, a first-order structural phase transition is found at ~250 K. The Br compound exhibits very similar dielectric behaviors to the Cl analogue (Figure 77b). The dielectric constant obeys the Curie−Weis law with a C_{para} of 370 K. The P_s approaches a value of 0.65 $\mu C \cdot cm^{-2}$ at 64 K along the a axis.

8. CONCLUSIONS AND PERSPECTIVES

After decades of development, the field of ferroelectric MOFs blossoms out again nowadays due to chemists' participation. There are some practical synthetic strategies for construction of ferroelectric MOFs, though the search for new ferroelectrics is now still an empirics-driven activity. From the perspective of origin of ferroelectricity, one can utilize hydrogen transfer, motions of polar components, or chiral centers to introduce electric polarizations. Taking hydrogen transfer, for example, its role has been seen in design and construction of organic ferroelectrics and dielectrics.[27,181−185] Hydrogen bonds are widespread in MOFs. In certain cases, aggregates linked by hydrogen bonds may undergo phase transitions due to proton transfers, which lead to structural polarizations. Order−disorder motions of polar components in MOFs are another major source of ferroelectricity. Model compounds include host−guest compounds or inclusion compounds.[54,57−59] Guest molecules or ions are loosely confined in the porous space, and therefore they are subject to external stimuli such as temperature and electric field. This is similar to molecular rotators, which can be used as polarization rotation units in ferroelectric compounds.[186] Dynamics of the guest molecules or ions may arouse complex structural phase transitions that reflect details of interactions between the host and the guest.[187] Once the guest molecules or ions and the host frameworks match each other well so that long-range interactions develops, ferroelectricity will eventually occur.

In spite of great progress being made, research and applications of ferroelectric MOFs are still restricted by lack of basic understanding of ferroelectricity that needs extensive exploration. Future studies of ferroelectric MOFs will include development of high-performance ferroelectrics such as high operating temperatures and strong polarization properties. Fine tuning of the different anionic and cationic components in MOFs is one approach to solve this problem, together with well developed synthetic strategies in coordination chemistry. For this purpose, investigation of the origin of ferroelectricity is urgently necessary. This is a tough but interesting task to chemists. Assistance from physicists and materials scientists is indispensable because these studies need various analytical and theoretical tools. It should be noted that ferroelectricity is a topic involved in interdisciplinary fields of chemistry, physics, materials science, electronics, crystallography, and mechanics.

Meanwhile, multifunctional ferroelectric MOFs have been drawing great attention. Coexistence or coupling between ferroelectricity and other physical (or chemical) properties such as magnetism, porosity, chirality, photoresponse, and optical properties may afford new types of materials and physical phenomena. These target compounds can be largely designed and realized in MOFs, that is, one component possesses one property and another component possesses the other. Multiferroic host−guest compounds are such an example in which the metal-containing frameworks and the guest molecules or ions show magnetic and ferroelectric order, respectively. However, in the reported multiferroic MOFs, the two properties only coexist rather than being coupled.[48−59] For potential applications, it requires coupling between the two types of order so that local magnetization can be changed by applying an electric field or the local electric polarization by a magnetic field.[188,189] Realization of such multiferroic MOFs remains challenging, although Stroppa, Jain, and co-workers just reported a possibly true multiferroic MOF $[(CH_3)_2NH_2][Cu(HCOO)_3]$ in which Jahn−Teller effect and antiferro-distortions cooperate to induce a ferroelectric polarization that is coupled to a weak ferromagnetism of the framework.[190,191] Furthermore, once ferroelectricity in MOFs is controlled by guest molecules or light, various novel materials would appear, e.g., guest-tuned ferroelectrics and photoresponsive ferroelectrics. These studies, undoubtedly, will enrich the field of MOFs and future advanced ferroelectric materials.[192]

dx.doi.org/10.1021/cr200174w |*Chem. Rev.* 2012, 112, 1163–1195

AUTHOR INFORMATION

Corresponding Author

*E-mail: zhangwen@seu.edu.cn; xiongrg@seu.edu.cn.

BIOGRAPHIES

Ren-Gen Xiong was born in 1961 in Jiangxi Province, P. R. China. He received his Ph.D. in 1994 from the University of Logistical Engineering. He then pursued research, firstly at the Coordination Chemistry Institute at Nanjing University (1994−1996), then at the Department of Chemistry at Puerto Rico University (1996−1997), and finally at the Chemistry Department, Brandeis University (1997−1998). He has been a professor at the Coordination Chemistry Institute at Nanjing University since 1998. In 1999 and 2006, he was a visiting scholar at Boston College and Kyoto University as well as Hokkaido University. In 2007, he was appointed as the head of the Ordered Matter Science Research Center, Southeast University. His research interests mainly cover the exploration of molecule-based ferroelectric, piezoelectric, and dielectric materials.

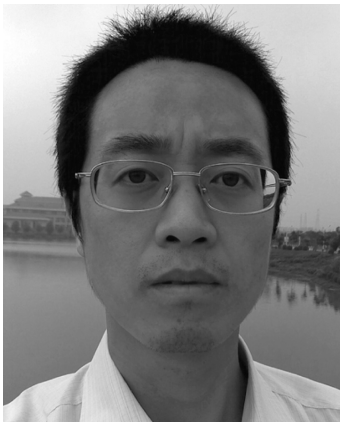

Wen Zhang was born in 1973 in Zhejiang Province, P. R. China. He received his M.Sc. from Nanjing University in 2000 and his Ph.D. degree from Institute of Chemistry, CAS, in 2004. He held postdoctoral positions at Peking University (2004−2006) and Kyushu University (2006−2008). He then joined the Ordered Matter Science Research Center, Southeast University, and became a professor in 2010. His research interests cover the catalytic, magnetic, dielectric, and ferroelectric properties in metal−organic hybrid compounds.

ACKNOWLEDGMENT

We thank National Natural Science Foundation of China (20931002, 20973037, 21071030, and 90922005), and 973 project (Grant 2009CB623200) as well as Jiangsu Province NSF (BK2010425 and BK2008029) for financial support.

REFERENCES

(1) Nye, J. F. *Physical Properties of Crystals*; Oxford University Press: Oxford, U.K., 1957.
(2) Jona, F.; Shirane, G. *Ferroelectric Crystals*; Pergamon Press: New York, 1962.
(3) Lines, M. E.; Glass, A. M. *Principles and Applications of Ferroelectrics and Related Materials*; Clarendon Press: Oxford, U.K., 1977.
(4) Smolenskii, G. A.; Bokov, V. A.; Isupov, V. A.; Krainik, N. N.; Pasinkov, R. E.; Sokolov, I. A. *Ferroelectrics and Related Materials*; Gordon and Breach Science Publishers: New York, 1984.
(5) Valasek, J. *Phys. Rev.* **1921**, *17*, 475.
(6) Busch, G.; Scherrer, P. *Naturwissenschaften* **1935**, *23*, 737.
(7) Cross, L. E.; Newnham, R. E. *History of Ferroelectrics*, Vol. III; American Ceramic Society: Westerville, OH, 1987.
(8) Martienssen, W., Warlimont, H., Eds. *Springer Handbook of Condensed Matter and Materials Data*; Springer: Berlin, Heidelberg, New York, 2005.
(9) Shiozaki, Y., Nakamura, E., Mitsui, T., Eds. *Ferroelectrics and Related Substances*; Landolt-Börnstein New Series, Vol. III/36; Springer-Verlag: Berlin, 2006.
(10) Scott, J. F. *Ferroelectric Memories*; Springer: Berlin, 2000.
(11) Waser, R., Ed. *Nanoelectronics and information technology*; Wiley-VCH: Weinheim, Germany, 2003.
(12) Ye, Z. G., Ed. *Handbook of advanced dielectric, piezoelectric and ferroelectric materials: Synthesis, properties and applications*; Woodhead Publishing: Cambridge, U.K., 2008.
(13) Scott, J. F. *Science* **2007**, *315*, 954.
(14) Grindlay, J. *An Introduction to the Phenomenological Theory of Ferroelectricity*; Pergamon Press: Oxford, U.K., 1970.
(15) Blinc, R.; Žekš, B. *Soft Modes in Ferroelectrics and Antiferroelectrics*; North Holland: Amsterdam, The Netherlands, 1974.
(16) Kristoffel, N.; Konsin, P. *Phys. Status Solidi B* **1988**, *149*, 11.
(17) Cohen, R. E., Ed. In *First-Principles Calculations for Ferroelectrics*; American Institute of Physics: New York, 1998.
(18) Cohen, R. E. *J. Phys. Chem. Solids* **2000**, *61*, 139.
(19) Mitsui, T.; Tatsuzaki, I.; Nakamura, E. *An Introduction to the Physics of Ferroelectrics*; Gordon and Breach Science Publishers: New York, 1976.
(20) Izyumov, Y. A.; Syromyatnikov, V. N. *Phase Transitions and Crystal Symmetry*; Kluwer Publishers: Dordrecht, The Netherlands, 1990.
(21) Kadau, K.; Germann, T. C.; Lomdahl, P. S.; Lee Holian, B. *Science* **2002**, *296*, 1681.
(22) Collet, E.; Lemée-Cailleau, M.-H.; Cointe, M. B.-L.; Cailleau, H.; Wulff, M.; Luty, T.; Koshihara, S.; Meyer, M.; Toupet, L.; Rabiller, P.; Techert, S. *Science* **2003**, *300*, 612.
(23) Lund, A.; Shiotani, M.; Shimada, S. *Principles and Applications of ESR Spectroscopy*; Springer-Verlag: New York, 2010.
(24) Stevens, J. G., Shenoy, G. K., Eds. *Mössbauer Spectroscopy and Its Chemical Applications*; American Chemical Society: Washington, DC, 1981.
(25) Soergel, E. *Appl. Phys. B: Laser Opt.* **2005**, *81*, 729.
(26) Steiner, T. *Angew. Chem., Int. Ed.* **2002**, *41*, 48.
(27) Horiuchi, S.; Tokura, Y. *Nat. Mater.* **2008**, *7*, 357.
(28) Solans, X.; Gonzalez-Silgo, C.; Ruiz-Pérez., C. *J. Solid State Chem.* **1997**, *131*, 350.
(29) Shiozaki, Y.; Shimizu, K.; Suzuki, E.; Nozaki, R. *J. Korean Phys. Soc.* **1998**, *32*, S192.
(30) Frazer, B. C.; Mc Keown, M.; Pepinsky, R. *Phys. Rev.* **1954**, *94*, 1435.

(31) Jona, F.; Pepinsky, R. *Phys. Rev.* **1953**, *92*, 1577.
(32) Matthias, B. T.; Hulm, J. K. *Phys. Rev.* **1951**, *82*, 108.
(33) Merz, W. J. *Phys. Rev.* **1951**, *82*, 562.
(34) Kambay, S.; Březina, B.; Petzelt, J.; Schaack, G. *J. Phys.: Condens. Matter* **1996**, *8*, 8669.
(35) Abe, R.; Matsuda, M. *J. Phys. Soc. Jpn.* **1974**, *37*, 437.
(36) Abe, R.; Matsuda, M. *J. Phys. Soc. Jpn.* **1973**, *34*, 686.
(37) Maeda, M.; Suzuki, I.; Abe, R. *J. Phys. Soc. Jpn.* **1975**, *38*, 592.
(38) Maeda, M.; Suzuki, I.; Abe, R. *J. Phys. Soc. Jpn.* **1975**, *39*, 1319.
(39) Fousek, J.; Cross, L. E.; Seely, K. *Ferroelectrics* **1970**, *1*, 63.
(40) Sawaguchi, E.; Cross, L. E. *Ferroelectrics* **1971**, *2*, 37.
(41) Kamba, S.; Schaack, G.; Petzelt, J.; Březina, B. *J. Phys.: Condens. Matter* **1996**, *8*, 4631.
(42) Deguchi, K.; Iwata, Y. *J. Phys. Soc. Jpn.* **2000**, *69*, 135.
(43) Wang, X.-Y.; Wang, Z.-M.; Gao, S. *Chem. Commun.* **2008**, 281.
(44) Wang, Z.-M.; Zhang, Y.-J.; Liu, T.; Kurmoo, M.; Gao, S. *Adv. Funct. Mater.* **2007**, *17*, 1523.
(45) Okada, K. *Phys. Rev. Lett.* **1965**, *15*, 252.
(46) Makita, Y.; Suzuki, S. *J. Phys. Soc. Jpn.* **1973**, *34*, 278.
(47) Kay, M. I.; Kleinburg, R. *Ferroelectrics* **1972**, *4*, 147.
(48) Matsuo, T.; Kume, Y.; Suga, H.; Seki, S. *J. Phys. Chem. Solids* **1976**, *37*, 499.
(49) Kobayashi, H.; Haseda, T. *J. Phys. Soc. Jpn.* **1963**, *18*, 541.
(50) Burger, N.; Fuess, H.; Burlet, P. *Solid State Commun.* **1980**, *34*, 883.
(51) Cornia, A.; Caneschi, A.; Dapporto, P.; Fabretti, A. C.; Gatteschi, D.; Malavasi, W.; Sangregorio, C.; Sessoli, R. *Angew. Chem., Int. Ed.* **1999**, *38*, 1780.
(52) Wang, Z.-M.; Zhang, B.; Fujiwara, H.; Kobayashi, H.; Kurmoo *Chem. Commun.* **2004**, 416.
(53) Cui, H.; Takahashi, K.; Okano, Y.; Kobayashi, H.; Wang, Z.; Kobayashi, A. *Angew. Chem., Int. Ed.* **2005**, *44*, 6508.
(54) Cui, H.; Wang, Z.-M.; Takahashi, K.; Okano, Y.; Kobayashi, H.; Kobayashi, A. *J. Am. Chem. Soc.* **2006**, *128*, 15074.
(55) Wang, X.-Y.; Gan, L.; Zhang, S.-W.; Gao, S. *Inorg. Chem.* **2004**, *43*, 4615.
(56) Wang, Z.-M.; Zhang, B.; Otsuka, T.; Inoue, K.; Kobayashi, H.; Kurmoo, M. *Dalton Trans.* **2004**, 2209.
(57) Xu, G.-C.; Ma, X.-M.; Zhang, L.; Wang, Z.-M.; Gao, S. *J. Am. Chem. Soc.* **2010**, *132*, 9588.
(58) Jain, P.; Dalal, N. S.; Toby, B. H.; Kroto, H. W.; Cheetham, A. K. *J. Am. Chem. Soc.* **2008**, *130*, 10450.
(59) Jain, P.; Ramachandran, V.; Clark, R. J.; Zhou, H. D.; Toby, B. H.; Dalal, N. S.; Kroto, H. W.; Cheetham, A. K. *J. Am. Chem. Soc.* **2009**, *131*, 13625.
(60) Wang, Z.-M.; Zhang, B.; Kurmoo, M.; Fujiwara, H.; Otsuka, T.; Kobayashi, H. *Inorg. Chem.* **2005**, *44*, 1230.
(61) Xiong, R.-G.; et al. *Angew. Chem., Int. Ed.* **2011**, in press.
(62) Lee, J. H.; Fang, L.; Vlahos, E.; Ke, X.; Jung, Y. W.; Kourkoutis, L. F.; Kim, J.-W.; Ryan, P. J.; Heeg, T.; Roeckerath, M.; Goian, V.; Bernhagen, M.; Uecker, R.; Chris Hammel, P.; Rabe, K. M.; Kamba, S.; Schubert, J.; Freeland, J. W.; Muller, D. A.; Fennie, C. J.; Schiffer, P.; Gopalan, V.; Johnston-Halperin, E.; Schlom, D. G. *Nature* **2010**, *466*, 954.
(63) Sánchez-Andújar, M.; Presedo, S.; Yáñez-Vilar, S.; Castro-García, S.; Shamir, J.; Señarís-Rodríguez, M. A. *Inorg. Chem.* **2010**, *49*, 1510.
(64) Pepinsky, R.; Vedam, K.; Hoshino, S.; Okaya, Y. *Phys. Rev.* **1958**, *111*, 430.
(65) Pepinsky, R.; Okaya, Y.; Eastman, D. P.; Mitsui, T. *Phys. Rev.* **1957**, *107*, 1538.
(66) Launer, S.; Le Maire, M.; Schaack, G.; Haussuhl, S. *Ferroelectrics* **1992**, *132*, 257.
(67) Rao, J. K. M.; Viswamitra, M. A. *Acta Crystallogr., B* **1972**, *28*, 1481.
(68) Choudhury, R. R.; Panicker, L.; Chitra, R.; Sakuntala, T. *Solid State Commun.* **2008**, *145*, 407.
(69) Pepinsky, R.; Vedam, K.; Oakaya, Y. *Phys. Rev.* **1958**, *110*, 1309.
(70) Lee, M.; Okaya, Y.; Pepinsky, R. *Bull. Am. Phys. Soc.* **1962**, *7*, 177.
(71) Pepinsky, R.; Makita, Y. *Bull. Am. Phys. Soc.* **1962**, *7*, 241.
(72) Mishima, N.; Itoh, K.; Nakamura, E. *Acta Crystallogr., Sect. C* **1984**, *40*, 1824.
(73) Makita, Y. *J. Phys. Soc. Jpn.* **1965**, *20*, 2073.
(74) Haga, H.; Onodera, A; Yamashita, H; Shiozaki, Y. *J. Phys. Soc. Jpn.* **1993**, *62*, 1857.
(75) Prokhorova, S. D.; Smolensky, G. A.; Siny, I. G.; Kuzminov, E. G.; Mikvabia, V. D.; Arndt, H. *Ferroelectrics* **1980**, *25*, 629.
(76) Sugo, M.; Kasahara, M.; Tokunaga, M.; Tatsuzaki, I. *J. Phys. Soc. Jpn.* **1984**, *53*, 3234.
(77) Kozlov, G. V.; Volkov, A. A.; Scott, J. F.; Feldkamp, G. E.; Petzelt, J. *Phys. Rev. B* **1983**, *28*, 255.
(78) Fujimoto, S.; Yasuda, N.; Fu, S. *J. Phys. D: Appl. Phys.* **1982**, *15*, 1469.
(79) Fujimoto, S.; Yasuda, N.; Takagi, K.; Narayanan, P. S.; Bhat, H. L. *J. Phys. D: Appl. Phys.* **1980**, *13*, L217.
(80) Fujimoto, S.; Yasuda, N.; Kashiki, H. *J. Phys. D: Appl. Phys.* **1982**, *15*, 487.
(81) Hikita, T.; Maruyama, T. *J. Phys. Soc. Jpn.* **1992**, *61*, 2840.
(82) Fujimoto, S.; Yasuda, N.; Kawamura, A.; Hachigai, T. *J. Phys. D: Appl. Phys.* **1984**, *17*, 1019.
(83) Rother, H. J.; Albers, J.; Klöpperpieper, A. *Ferroelectrics* **1984**, *54*, 107.
(84) Brill, W.; Schildkamp, W.; Spilker, J. *Z. Kristallogr.* **1985**, *172*, 281.
(85) Ezpeleta, J. M.; Zúniga, F. J.; Pérez-Mato, J. M.; Paciorek, W.; Breczcwski, T. *Acta Crystallogr., B* **1992**, *48*, 261.
(86) Chaves, M. R.; Almeida, A.; Carvalho, P. S.; Ribeiro, J. L.; Müser, H. E.; Albers, J.; Klöpperpieper, A. *Phys. Rev. B* **1991**, *43*, 11162.
(87) Brill, W.; Ehses, K. H. *Jpn. J. Appl. Phys. Suppl.* **1983**, *24−2*, 826.
(88) Cui, H. B.; Zhou, B.; Long, L. S.; Okano, Y.; Kobayashi, H.; Kobayashi, A. *Angew. Chem., Int. Ed.* **2008**, *47*, 3376.
(89) Zhou, B.; Kobayashi, A.; Cui, H. B.; Long, L.-S.; Fujimori, H.; Kobayashi, H. *J. Am. Chem. Soc.* **2011**, *133*, 5736.
(90) Ren, Y. P.; Long, L. S.; Mao, B. W.; Yuan, Y. Z.; Huang, R. B.; Zheng, L. S. *Angew. Chem., Int. Ed.* **2003**, *42*, 532.
(91) Zhao, H.-X.; Kong, X.-J.; Li, H.; Jin, Y.-C.; Long, L.-S.; Zeng, X. C.; Huang, R.-B.; Zheng, L.-S. *Proc. Natl. Acad. Sci. U. S. A.* **2011**, *108*, 3481.
(92) Matthias, B. T.; Remeika, J. P. *Phys. Rev.* **1957**, *107*, 1727.
(93) Mishima, N. *J. Phys. Soc. Jpn.* **1984**, *53*, 1062.
(94) Itoh, K.; Mishima, N.; Nakamura, E. *J. Phys. Soc. Jpn.* **1981**, *50*, 2029.
(95) Yagi, T. *J. Phys. Soc. Jpn.* **1986**, *55*, 1822.
(96) Yano, S.; Yamada, K.; Shimizu, H. *J. Phys. Soc. Jpn.* **1987**, *56*, 3338.
(97) Seki, S.; Momotani, M.; Nakatsu, K.; Oshima, T. *Bull. Chem. Soc. Jpn.* **1955**, *28*, 411.
(98) Nakamura, N.; Suga, H.; Chihara, H.; Seki, S. *Bull. Chem. Soc. Jpn.* **1968**, *41*, 291.
(99) Gesi, K.; Ozawa, K. *J. Phys. Soc. Jpn.* **1975**, *38*, 467.
(100) Sawada, A.; Kikugawa, T.; Ishibashi, Y. *J. Phys. Soc. Jpn.* **1979**, *46*, 871.
(101) Stadnicka, K.; Glazer, A. M. *Acta Crystallogr., Sect. B* **1980**, *36*, 2977.
(102) Nakamura, N.; Suga, H.; Chihara, H.; Seki, S. *Bull. Chem. Soc. Jpn.* **1965**, *38*, 1779.
(103) Takashige, M.; Iwamura, K.; Hirotsu, S.; Sawada, S. *J. Phys. Soc. Jpn.* **1975**, *38*, 1217.
(104) Itoh, K.; Niwata, A.; Abe, W.; Kasatani, H.; Nakamura, E. *J. Phys. Soc. Jpn.* **1992**, *61*, 3593.
(105) Deguchi, K.; Takeuchi, M.; Nakamura, E. *J. Phys. Soc. Jpn.* **1992**, *61*, 1362.
(106) Holden, A. N.; Matthias, B. T.; Merz, W. J.; Remeika, J. P. *Phys. Rev.* **1955**, *98*, 546.
(107) Remeika, J. P.; Merz, W. J. *Phys. Rev.* **1956**, *102*, 295.

(108) Schein, J. B.; Lingafelter, E. C.; Stewart, J. M. *J. Chem. Phys.* **1967**, *47*, 5183.
(109) Holden, A. N.; Merz, W. J.; Remeika, J. R.; Matthias, B. T. *Phys. Rev.* **1956**, *101*, 962.
(110) Kirpichnikova, L. F.; Andreev, E. F.; Ivanov, N. R.; Shuvalov, L. A.; Varikash, V. M. *Kristallografiya* **1988**, *33*, 1437. *Sov. Phys. Crystallogr. (English Transl.)* **1988**, *33*, 855.
(111) Kirpichnikova, L. F.; Pietraszko, A.; Lukaszewich, K.; Shuvalov, L. A.; Dolbinina, V. V.; Yakovleva, L. M. *Crystallogr. Rep.* **1994**, *39*, 990. *Kristallografiya* **1994**, *39*, 1078.
(112) Dolinšek, J.; Klanjšek, M.; Arčon, D.; Kim, H. J.; Seliger, J.; Žagar, V.; Kirpichnikova, L. F. *Phys. Rev. B* **1999**, *59*, 3460.
(113) Bednarski, W.; Waplak, S.; Kirpichnikova, L. F. *J. Phys.: Condens. Matter* **1999**, *11*, 1567.
(114) Andreev, E. F.; Varikash, V. M.; Shuvalov, L. A. *Izv. Akad. Nauk SSSR, Ser. Fiz.* **1991**, *55*, 572. *Bull. Acad. Sci. USSR, Phys. Ser. (English Transl.)* **1991**, *55*, 154.
(115) Pietraszko, A.; Łukaszewicz, K.; Kirpichnikova, L. F. *Pol. J. Chem.* **1993**, *67*, 1877. **1995**, *69*, 922.
(116) Hrabański, R.; Janiec-Mateja, M.; Czapla, Z. *Phase Transitions* **2007**, *80*, 163.
(117) Sobiestianskas, R.; Grigas, J.; Andreev, E. F.; Varikash, V. M. *Phase Transitions* **1992**, *40*, 85.
(118) Pepinsky, R.; Jona, F.; Shirane, G. *Phys. Rev.* **1956**, *102*, 1181.
(119) Flecher, R. O.; Steeple, H. *Acta Crystallogr.* **1964**, *17*, 290.
(120) Zhang, W.; Chen, L.-Z.; Xiong, R.-G.; Nakamura, T.; Huang, S. D. *J. Am. Chem. Soc.* **2009**, *131*, 12544.
(121) Kałuża, S.; Suchańska, M.; Belka, R.; Leśniewski, S. *Ferroelectrics* **2002**, *273*, 143.
(122) Shimizu, H.; Abe, N.; Kokubo, N.; Yasuda, N.; Fujimoto, S.; Yamaguchi, T.; Sawada, S. *Solid State Commun.* **1980**, *34*, 363.
(123) Sawada, A.; Sugiyama, J.; Wada, M.; Ishibashi, Y. *J. Phys. Soc. Jpn.* **1980**, *48*, 1773.
(124) Gesi, K.; Iizumi, M. *J. Phys. Soc. Jpn.* **1980**, *48*, 775.
(125) Mashiyama, H.; Tanisaki, S. *J. Phys. Soc. Jpn.* **1981**, *50*, 1413.
(126) Sawada, S.; Shiroishi, Y.; Yamamoto, A.; Takashige, M.; Matsuo, M. *Phys. Lett. A* **1978**, *67*, 56.
(127) Wada, M.; Suzuki, M.; Sawada, A.; Ishibashi, Y.; Gesi, K. *J. Phys. Soc. Jpn.* **1981**, *50*, 1813.
(128) Sawada, S.; Shiroishi, Y.; Yamamoto, A.; Takashige, M.; Matsuo, M. *J. Phys. Soc. Jpn.* **1978**, *44*, 687.
(129) Gesi, K.; Perret, R. *J. Phys. Soc. Jpn.* **1988**, *57*, 3698.
(130) Vasil'ev, V. E.; Rudyak, V. M.; Bobrova, Z. A.; Varikash, V. M. *Fiz. Tverd. Tela* **1987**, *29*, 1539. *Sov. Phys. Solid State (English Transl.)* **1987**, *29*, 882.
(131) Bobrova, Z. A.; Varikash, V. M. *Dokl. Akad. Nauk BSSR* **1986**, *30*, 510.
(132) Bobrova, Z. A.; Varikash, V. M.; Baranov, A. I.; Shuvalov, L. A. *Kristallografiya* **1987**, *32*, 255. *Sov. Phys. Crystallogr. (English Transl.)* **1987**, *32*, 148.
(133) Czapla, Z.; Eliyashevskyy, Yu.; Dacko, S. *Ferroelectr., Lett. Sect.* **2006**, *33*, 1.
(134) Daoud, A. *J. Appl. Crystallogr.* **1977**, *10*, 133.
(135) Perez-Mato, J. M.; Manes, J. L.; Fernandez, J.; Zuniga, J.; Tello, M. J.; Socias, C.; Arriandiaga, M. A. *Phys. Status Solidi A* **1981**, *68*, 29.
(136) Priya, R.; Krishnan, S.; Bhagavannarayana, G.; Jerome Das, S. *Physica B* **2011**, *406*, 1345.
(137) Knorr, K.; Jahn, I. R.; Heger, G. *Solid State Commun.* **1974**, *15*, 231.
(138) Kind, R.; Blinc, R.; Žekš, B. *Phys. Rev. B* **1979**, *19*, 3743.
(139) Chapuis, G.; Arend, H.; Kind, R. *Phys. Status Solidi A* **1975**, *31*, 449.
(140) Steadman, J. P.; Willett, R. D. *Inorg. Chim. Acta* **1970**, *4*, 367.
(141) Kundys, B.; Lappas, A.; Viret, M.; Kapustianyk, V.; Rudyk, V.; Semak, S.; Simon, C.; Bakaimi, I. *Phys. Rev. B* **2010**, *81*, 224434.
(142) De Jongh, L. J.; Botterman, A. C.; de Boer, F. R.; Miedema, A. R. *J. Appl. Phys.* **1969**, *40*, 1363.
(143) De Jongh, L. J.; Van Amstel, W. D.; Miedema, A. R. *Physica (Amsterdam)* **1972**, *58*, 277.
(144) Gesi, K. *J. Phys. Soc. Jpn.* **1990**, *59*, 432.
(145) Aguirre-Zamalloa, G.; Madriage, G.; Couzi, M.; Breczewski, T. *Acta Crystallogr., Sect. B* **1993**, *49*, 691.
(146) Asahi, T.; Hasebe, K.; Gesi, K. *Acta Crystallogr., Sect. C* **1991**, *47*, 1208.
(147) Fatuzzo, E. *Proc. Phys. Soc. (London)* **1960**, *76*, 797.
(148) Fatuzzo, E.; Nitsche, R.; Roetschi, H.; Zingg, S. *Phys. Rev.* **1962**, *125*, 514.
(149) Arend, H.; Ehrensperger, M.; Muralt, P.; Chapuis, G.; Zuniga, J. F. *Ferroelectrics Lett.* **1982**, *44*, 147.
(150) Jakubas, R.; Ciunik, Z.; Bator, G. *Phys. Rev. B* **2003**, *67*, 024103.
(151) Wojtaś, M.; Jakubas, R.; Zaleski, J.; Bator, G.; Baran, J. *J. Mol. Struct.* **2008**, *887*, 262.
(152) Bi, W.; Leblanc, N.; Mercier, N.; Auban-Senzier, P.; Pasquier, C. *Chem. Mater.* **2009**, *21*, 4099.
(153) Jakubas, R. *Solid State Commun.* **1986**, *60*, 389.
(154) Jakubas, R.; Sobczyk, L.; Matuszewski, J. *Ferroelectrics* **1987**, *74*, 339.
(155) Zaleski, J.; Pawlaczyk, Cz.; Jakubas, R.; Unruh, H.-G. *J. Phys.: Condens. Matter* **2000**, *12*, 7509.
(156) Jakubas, R.; Czapla, Z.; Galewski, Z.; Sobczyk, L. *Ferroelectrics Lett.* **1986**, *5*, 143.
(157) Jakubas, R.; Bator, G.; Sobczyk, L.; Mróz, J. *Ferroelectrics* **1994**, *158*, 43.
(158) Jakubas, R.; Krzewska, U.; Bator, G.; Sobczyk, L. *Ferroelectrics* **1988**, *77*, 129.
(159) Wojtas, M.; Jakubas, R. *J. Phys.: Condens. Matter* **2004**, *16*, 7521.
(160) Latanowicz, L.; Medycki, W.; Jakubas, R. *J. Phys. Chem. A* **2005**, *109*, 3097.
(161) Bujak, M.; Zaleski, J. *J. Solid State Chem.* **2004**, *117*, 3202.
(162) Wojtaś, M.; Bator, G.; Jakubas, R.; Zaleski, J. *J. Phys.: Condens. Matter* **2003**, *15*, 5765.
(163) Pawlaczyk, C.; Jakubas, R. *Z. Naturforsch.* **2003**, *58a*, 189.
(164) Jakubas, R.; Sobczyk, L.; Lefebvre, J. *Ferroelectrics* **1989**, *100*, 143.
(165) Szklarz, P.; Gałązka, M.; Zieliński, P.; Bator, G. *Phys. Rev. B* **2006**, *74*, 184111.
(166) Jakubas, R. *Solid State Commun.* **1989**, *69*, 267.
(167) Piecha, A.; Pietraszko, A.; Bator, G.; Jakubas, R. *J. Solid State Chem.* **2008**, *181*, 1155.
(168) Jakubas, R.; Piecha, A.; Pietraszko, A.; Bator, G. *Phys. Rev. B* **2005**, *72*, 104107.
(169) Piecha, A.; Białońska, A.; Jakubas, R. *J. Phys.: Condens. Matter* **2008**, *20*, 325224.
(170) Jozkow, J.; Jakubas, R.; Bator, G. *J. Chem. Phys.* **2001**, *114*, 7239.
(171) Przesławski, J.; Kosturek, B.; Dacko, S.; Jakubas, R. *Solid State Commun.* **2007**, *142*, 713.
(172) Piecha, A.; Bator, G.; Jakubas, R. *J. Phys.: Condens. Matter* **2005**, *17*, L411.
(173) Piecha, A.; Jakubas, R. *J. Phys.: Condens. Matter* **2007**, *19*, 406225.
(174) Zhang, W.; Ye, H.-Y.; Cai, H.-L.; Ge, J.-Z.; Xiong, R.-G.; Huang, S. P. D. *J. Am. Chem. Soc.* **2010**, *132*, 7300.
(175) Abrahams, S. C.; Mirsky, K.; Nielson, R. *Acta Crystallogr., B* **1996**, *52*, 806.
(176) Bauer, M. R.; Pugmire, D. L.; Paulsen, B. L.; Christie, R. J.; Arbogast, D. J.; Gallagher, C. S.; Raveane, W. V.; Nielson, R. M.; Ross, C. R., II; Photinos, P.; Abrahams, S. C. *J. Appl. Crystallogr.* **2001**, *34*, 47.
(177) Onoda-Yamamura, N.; Ikeda, R.; Yamamura, O.; Matsuo, T. *Solid State Commun.* **1997**, *101*, 647.
(178) Gesi, K. *J. Phys. Soc. Jpn.* **1999**, *68*, 3095.

(179) Czapla, Z.; Czupiński, O.; Ciunik, Z. *Solid State Commun.* **1986**, *58*, 383.
(180) Gesi, K. *J. Phys. Soc. Jpn.* **1996**, *65*, 703.
(181) Katrusiak, A.; Szafrański, M. *Phys. Rev. Lett.* **1999**, *82*, 576.
(182) Szafrański, M.; Katrusiak, A.; McIntyre, G. J. *Phys. Rev. Lett.* **2002**, *89*, 215507.
(183) Horiuchi, S.; Tokunaga, Y.; Giovannetti, G.; Picozzi, S.; Itoh, H.; Shimano, R.; Kumai, R.; Tokura, Y. *Nature* **2010**, *463*, 789.
(184) Akutagawa, T.; Takeda, S.; Hasegawa, T.; Nakamura, T. *J. Am. Chem. Soc.* **2004**, *126*, 291.
(185) Katrusiak, A.; Szafrański, M. *J. Am. Chem. Soc.* **2006**, *128*, 15775.
(186) (a) Akutagawa, T.; Koshinaka, H.; Sato, D.; Takeda, S.; Noro, S.-I.; Takahashi, H.; Kumai, R.; Tokura, Y.; Nakamura, T. *Nat. Mater.* **2009**, *8*, 342. (b) Fu, D.-W.; Zhang, W.; Cai, H.-L.; Zhang, Y.; Ge, J.-Z.; Xiong, R.-G.; Huang, S. D. *J. Am. Chem. Soc.* **2011**, *133*, 12780.
(187) Zhang, W.; Cai, Y.; Xiong, R.-G.; Yoshikawa, H.; Awaga, K. *Angew. Chem., Int. Ed.* **2010**, *49*, 6608.
(188) Fiebig, M. *J. Phys. D: Appl. Phys.* **2005**, *38*, R123.
(189) Eerenstein, W.; Mathur, N. D.; Scott, J. F. *Nature* **2006**, *442*, 759.
(190) Stroppa, A.; Jain, P.; Barone, P.; Marsman, M.; Perez-Mato, J. M.; Cheetham, A. K.; Kroto, H. W.; Picozzi, S. *Angew. Chem., Int. Ed.* **2011**, *50*, 5847.
(191) Hu, K.-L.; Kurmoo, M.; Wang, M.; Gao, S. *Chem.—Eur. J.* **2009**, *15*, 12050.
(192) (a) Hang, T.; Zhang, W.; Ye, H.-Y.; Xiong, R.-G. *Chem. Soc. Rev.* **2011**, *40*, 3577. (b) Guo, M.; Cai, H.-L.; Xiong, R.-G. *Inorg. Chem. Commun.* **2010**, *13*, 1590.

NOTE ADDED IN PROOF

During the publication of the paper, there appeared some new results of the ferroelectric MOFs. One is the work done by Wang, Gao, and co-workers (including Xiong) that is just published in *J. Am. Chem. Soc.* (**2011**, doi: 10.1021/ja206891q) with the title "Coexistence of Magnetic and Electric Orderings in the Metal—Formate Frameworks of $[NH_4][M(HCOO)_3]$". The work is an extension of the one reported in ref 57. The authors summarized that the 3D chiral metal—formate frameworks, $[NH_4][M(HCOO)_3]$ (M = divalent Mn, Fe, Co, Ni, and Zn), display paraelectric to ferroelectric phase transitions between 191 and 254 K due to the disorder—order transitions of the NH_4^+ cations. The magnetic members show spin-canted antiferromagnetic orderings within 8—30 K, indicating they are a new class of multiferroic MOFs. Meanwhile, Zhang, Xiong, and co-workers reported their study on "Multiferroic perdeutero metal—organic framework $[(CD_3)_2ND_2]Co(DCOO)_3$" (*Angew. Chem., Int. Ed.* **2011**, in press [anie.201103265]) as a related work to ref 59. They successfully demonstrated that the perdeutero-MOF undergoes two phase transitions, i.e., one above room temperature, which is unprecedented in the known metal—formate, and the other paraelectric-to-ferroelectric phase transition at 151 K while its symmetry breaking from centrosymmetric (*R-3c, No. 167*) to acentric (*Cc*) structure is unambiguously confirmed by temperature-dependence of SHG (second harmonic generation) effect from zero to sharp signal appearance. The complex dielectric constant measurements show that this compound is a MOF-based relaxor ferroelectric with the coexistence of magnetic and electric orderings.